STRUCTURAL DAMAGE DETECTION UTILIZING EXPERIMENTAL MODE SHAPES

A Thesis

presented to

the Faculty of California Polytechnic State University,

San Luis Obispo

In Partial Fulfillment

of the Requirements for the Degree

Master of Science in Architecture with a Specialization in Architectural Engineering

by

Evan Jamison Gerbo

June 2014

COMMITTEE MEMBERSHIP

TITLE:	Structural Damage Detection Utilizing Experimental Mode Shapes
AUTHOR:	Evan Gerbo, EIT
DATE SUBMITTED:	June 2014
COMMITTEE CHAIR:	Graham Archer, PhD, P.E., Associate Professor, Architectural Engineering
COMMITTEE MEMBER:	Cole McDaniel, PhD, P.E., Associate Professor, Architectural Engineering
COMMITTEE MEMBER:	Peter Laursen, PhD, P.E., Assistant Professor, Architectural Engineering

ABSTRACT

Structural Damage Detection Utilizing Experimental Mode Shapes

Evan Gerbo

A method of locating structural damage is developed and tested to aid in the evaluation of structural health. This method will help minimize the cost of structural inspection and repair by informing engineers of where damage, due a seismic event, has occurred before the removal of finishes for visual inspection. This thesis begins to answer the question "can structural damage be detected solely through analysis of experimentally measured mode shapes?"

The work encompasses construction of a test structure, with three braces that can be repeatedly engaged or dis-engaged, thus allowing for testing of a variety of braced configurations. For this thesis, damage is assumed to cause a change in stiffness. Experimental testing is conducted to acquire mode shapes and frequencies for the 6 dominant modes of the test structure. Lastly, the data is analyzed to identify the configuration of braces engaged on the structure. The accuracy of the method is assessed by the number of configurations that it correctly predicts and the confidence of the predictions.

Keywords: damage detection, structural, mode shapes, frequency, stiffness

ACKNOWLEDGMENTS

There are many people that have contributed to the inspiration of this thesis. I would like to thank Graham Archer, Cole McDaniel and Peter Laursen for serving on my committee as well as contributing their time and expertise. I would like to thank Ray Ward for aiding in the construction process more times than I can count. I would like to thank Matthew Kidd and Jason Cerda for completing the welding on the project, as they are certified welders and did a great job.

This would not have been possible without my mother, Peggy Gerbo. She has always supported my drive in engineering disciplines and has made me the person I am today, thank you for your continual support and motivation.

TABLE OF CONTENTS

LIST OF TABLES

LIST OF FIGURES

1.0 INTRODUCTION

This thesis uses analysis of modal behavior, collected through forced vibration testing, to detect and locate changes in the stiffness of a structure. These changes in stiffness represent damage to the structure. The use of this research is to aid in quick analysis of structural damage.

1.1 Topic of the Thesis

This thesis will improve upon structural damage detection techniques that have been previously researched. The improvement upon previous research comes in the application to real structures, rather than theoretical models. The analysis method will be applied to a test structure that is constructed in a laboratory. The hypothesis is that analysis of mode shapes for the location of structural damage can accurately detect and locate damage to a structure.

A novel aspect of this thesis will be to detect where this damage has occurred to precisely inform the location of repair efforts. There has been some work done in this field, but it is still in development and requires further research before it can be implemented commercially. Xu et al detected damage based on inter-story stiffness, limiting the accuracy of damage location to a floor by floor basis (Xu et al 2005). While

technology to detect structural damage has existed for several years, it has been limited by the precision of its results to theoretical experiments.

1.2 Purpose

Modern technology has revolutionized the efficiency of structural analysis. The concept is to have a method of testing and analysis that can be quickly completed after a seismic event to aid in rehabilitation efforts. The technique produced by this thesis will allow for quicker damage detection and location than visual inspection in cases where the damage is hidden by finishes such as drywall. Widespread implementation of this technique would lead to a vast database of structural damage data, which could aid in furthering the understanding of how damage occurs. This deeper comprehension of the concepts behind damage occurrence allows for more efficient seismic retrofits in future rehabilitation efforts.

There are many possible sources of error when modeling a building such as foundation interaction, architectural component interaction and connection assumptions. These sources of error make it difficult to accurately model a building's behavior, and thus assumptions are typically conservative. While this approach works well for design, it can significantly affect the accuracy of an analytical model. The goal of this thesis is to improve upon previous techniques to allow for greater accuracy of damage detection,

while achieving a level of robustness that can handle typical inaccuracies due to assumptions in the analytical model. This combination of durability and accuracy will help in furthering this area of research toward commercial application.

Once fully developed and proved, this technology can be used for rapid assessment of damage after an earthquake. This benefits the occupants and the owner by giving earlier warning of impending collapse as well as information to help limit the extent of required seismic repairs.

Utilizing a non-destructive testing based approach to locate structural damage is more advantageous than manual structural inspections because it does not require the removal of finishes, and can be done quickly after a seismic event, saving money and time. The ability to automatically detect damage will allow for structural damage to be located quickly after an earthquake in a wide array of structures. This will quicken the process of investigation and reduce disruption to occupants.

This use of the method will allow people to go back to their normal lives quicker than current techniques, by not requiring a structural inspection if the building is not showing signs of damage. Christchurch, New Zealand is an example of where this technology could have been of assistance. Since the earthquake in 2011 many structures have been considered potentially damaged and uninhabitable until further structural inspection can be completed. This puts businesses on hold and greatly affects the

economy of the local area. This technique to locate structural damage could have been applied to allow many non-damaged buildings to be re-opened many months, if not years, earlier. This would have allowed society to return to normal much faster than relying solely on visual structural inspection.

1.3 Concept

There are two fundamental approaches to implementing this technique, relative changes and absolute comparisons.

1.3.1 Relative Changes in Modal Behavior

The ideal way is to have data from a test performed before the structure has been damaged. This allows for relative, rather than absolute, comparisons and leads to greater accuracy. The issue with this method is that it requires extensive preparatory testing before a seismic event to allow the approach to be applicable to a large number of buildings.

1.3.2 Absolute Changes

The more practical approach is to use an absolute comparison between the analytical model and the physical structure. This requires the model to be more accurate than having pre-damage data, but it allows for more universal application. Due to the

impractical nature of testing many buildings beforehand, this thesis investigates the absolute approach.

1.4 Scope

For simplicity and time constraints the scope of this thesis is limited in the following ways. Damage is assumed to have a correlation with a decrease in stiffness. The exact relationship between damage and stiffness change is not within the scope of this thesis. This thesis is only evaluating the effectiveness of the analysis approach on the test structure detailed in chapter 4. This was chosen as a compromise between a full size building and a small scale experiment. Mirrored configurations were not tested due to the expectation of essentially duplicate results.

2.0 BACKGROUND

2.1 Structural Health Monitoring

Structural health monitoring is an area of research focused on evaluating the structural integrity of structures using performance data. This method produces information to inform owners of damage that has occurred to their buildings. The building's behavior changes when damage occurs, and this change can be detected in data recorded from accelerometers installed in the structure. There are other methods of structural health monitoring such as the use of strain gauges on structural members. This thesis will focus on aiding structural health monitoring utilizing accelerometer data due to the relatively low cost and ease of installation compared to alternative methods.

The idea of finding structural damage from accelerometer data is not a new concept. The technique has been studied for years, yet it still requires more refinement and study before being applied commercially. This is due to the high amount of performance validation required before the technique is applied to scenarios where people's lives are depending on the accuracy of this system.

2.2 Quality of Data

One of the crucial considerations in testing is the quality of the data that is collected. The factors that can influence this quality include noise from outside influences, how settled the structure is during shaking, and most crucially how accurately

the mode shape excitation is completed. The accuracy of the mode shape measurement is influenced by the location of the shaker placed on the structure. Without proper placement, the mode shapes that are measured will not be orthogonal and can lead to issues in analysis.

3.0 LITERATURE REVIEW

Structural damage detection research is not in its infancy. For almost two decades engineers have been working on techniques to accomplish this seemingly simple task. Previous research has looked at both global and local damage detection techniques.

3.1 Global Techniques

Global techniques measure the overall damage to the structure and represent it as one number. This was done successfully on the Imperial County Services Building by analyzing the overall system frequencies (Todorovska and Trifunac 2006). The authors analyzed the frequency of the building at various times during the Imperial Valley Earthquake. Through this examination they discovered that the frequency of the structure changed significantly both temporarily as well as permanently. It is theorized that the frequency was at its lowest when the damage occurred. This technique looked at the primary modal frequencies of the building in the east and west direction to detect damage. They found that while the frequency dropped during the shaking, it also went back up after the shaking had subsided. This shows that structural damage is not the only factor influencing frequency change and the other sources of interference need to be properly examined before this technique can be confirmed and used commercially.

3.2 Local Techniques

Local techniques break the building down into a series of components and represent the damage in each component with one number. This type of technique was utilized by analyzing inter-story stiffness to look for local signs of damage (Wu, Xu, Yokohama 2002). The authors' research utilized trained neural networks to evaluate the damage of local portions of a structure. The neural network was trained by measuring healthy behavior and creating an elastic model to replicate that behavior. During a seismic event the network would compare the performance of the elastic model to the measured response. The difference between the two was used to estimate the degree of non-linearity of the structure and represent damage. This technique has benefits in that it can be implemented without complex model data due to the application on a local scale. The downside is that this technique relies on the healthy structure behaving elastically. While this is a common assumption in design, it is not always the case. This assumption prevents the technique from properly capturing behavior such as non-linear soil structure interaction and any geometric non-linearity the structure might exhibit.

3.3 Noise

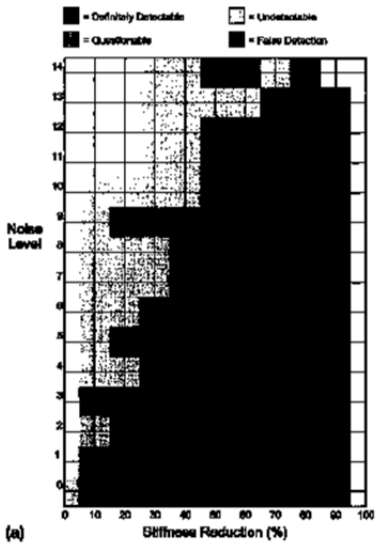

Figure 3.1 Impact of Noise Level on Damage Detection Technique

One of the main areas that could benefit from further investigation is the reduction of noise in the data to allow for greater accuracy of results. This will allow smaller amounts of damage to be detected and make the technique a more viable commercial option. Previous research has analyzed the effect noise has on damage detection and presented the results shown in Figure A to the right (Hou, Noori and Amand 2000). The amount of damage is shown on the x axis while the noise level in the sample is on the y axis. The damage and noise levels that allowed for clear detection are shown in black. Their results show that the noise level does have a significant impact on the feasibility of the use of damage detection software. The results of attempted noise reduction techniques can be presented in a similar way to these graphics to show the effect of noise reduction software

4.0 TEST STRUCTURE

For the testing of this technique a test structure was constructed as shown below in figure 4.1. This structure is located in the Engineering West Seismic Laboratory (Room 21-18), Cal Poly, San Luis Obispo, CA.

Figure 4.1 Test Structure

4.1 Test Structure Description

This technique is tested on a medium scale structure constructed of reinforced concrete slabs with a steel moment frame and temporary steel. The test structure can be changed by altering the braces to represent damage. This allows for a well-behaved model that will be easier to work with in the beginning stages of the investigation. This structure will be well-behaved because it will provide data will low levels of interference. This is due to the fact that it does not have architectural components and will be tested in a laboratory setting, thus eliminating interference from wind and large temperature changes. This removes the main sources of noise and allows for precision data collection.

This structure provides an avenue to test the technique on a simple physical structure and show that detecting changes to the structure is possible using modal behavior analysis. Once the proof of concept is completed on this simplified structure, the same approach can be applied to larger structures. It must then be refined to account for all of the variables the test structure eliminated such as architectural damping, wind, and noise from outside sources.

The structure's diaphragms are composed of concrete slabs that are 18 inches thick. 6" tall shear studs are welded to the beams and encased within the slab. These ensure that the slab stays solidly connected to the frame through all the vibratory testing. The prolonged vibration that the structure would be subjected to called for this extra connection strength according to Verco, the sponsor of the metal decking.

4.2 Test Structure Design

There were several f actors that influenced the design of the test structure. The degrading performance of the shaker at high frequency led to thick slabs that would lower the modal frequencies. The base plates were originally only 3/8" thick, this flexible connection would have presented complex modeling requirements to capture the behavior accurately. To reduce this possible source of error, new 1" thick base plates were installed to minimize this flexibility as shown in figure 4.2.

Figure 4.2 Modified Base Plates

4.2.1 Slab Design

Triangular portions were created in the edges of the bottom slab to allow for braces to be installed in these bays in the future. This allows the slab to expand all the way to the edge of the beams and maintain a solid connection to the frame.

The thickness of the slab was chosen by finding a compromise between economy of construction and optimal performance of the shaker. 18" was chosen because it

brought the six modes of interest into a frequency range where the shaker can perform well, and was not unreasonable for construction.

4.2.2 Manufacturer Rated Shaker Performance

The shaker used for this testing is rated by the manufacturer to produce a 30lbs peak sine force at a maximum of 20Hz. No performance data is provided by the manufacturer beyond this range. It was estimated that to pull all six modes of interest down to this frequency range would have required 36" slabs. This thickness was not deemed feasible for construction, so the performance of the shaker at higher frequencies was investigated further to learn its true capabilities.

4.2.3 Measured Shaker Performance

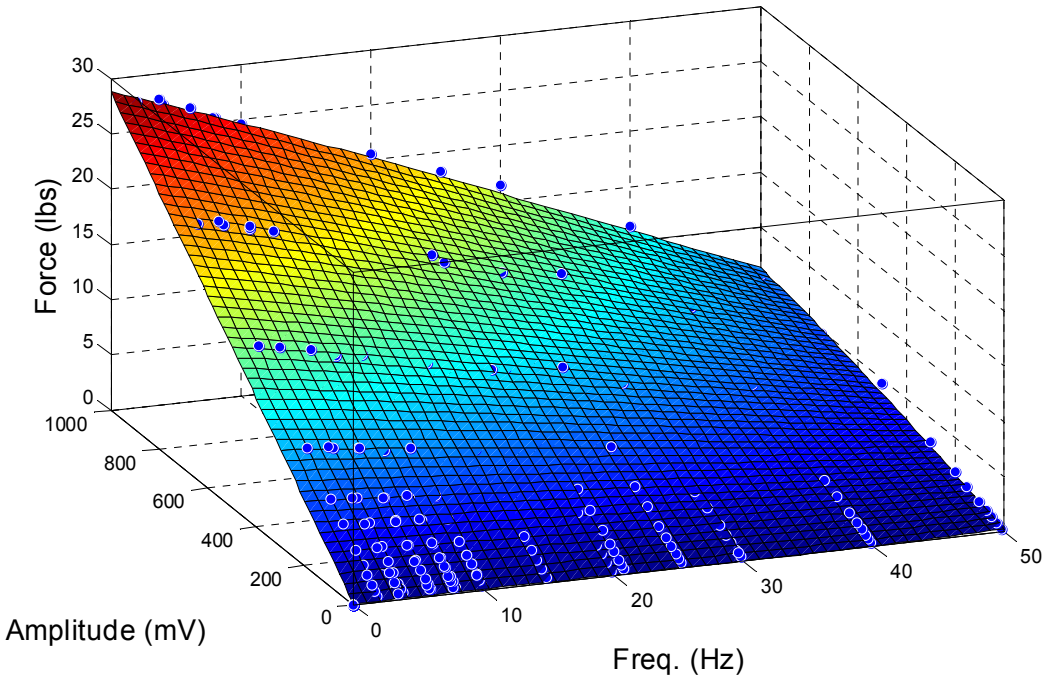

Figure 4.3 Shaker Performance

The force output of the shaker was measured at a variety of frequencies and amplitudes. The collected data points are displayed in Figure 4.3 above by the blue dots, and the general trend is displayed by the overlaid surface. The relationship between input voltage and output force was as expected, with a direct linear correlation. The trend with regard to frequency shows that at high frequencies the output of the shaker is diminished. This meets original expectations of performance because the shaker is only rated to 20 Hz by the manufacturer. The 30lbs rated output was found to be greater than the measured maximum force output of the shaker, however for this study the maximum force output was not a limiting factor. The collected data is summarized in Table 8.4. Regular intervals of frequencies were tested from 2 Hz to 50 Hz, as well as additional frequencies that correspond with early estimates of modal frequency of the base structure. These were taken to provide more information on the shaker's performance at the modal frequencies.

Shaker Force Performance (lbs)

	Voltage (mV)											
Freq.	10	20	30	50	70	100	150	200	300	500	750	1000
2 Hz	.33	.58	.94	1.54	2.01	2.87	4.33	5.76	8.63	14.31	15.22	19.71
3.65 Hz	.35	.59	.96	1.55	1.89	2.87	4.20	5.69	8.56	14.03	21.01	27.65
4 Hz	.36	.57	.80	1.44	2.09	2.95	4.18	5.58	8.32	13.64	20.7	27.14
6 Hz	.40	.66	.87	1.37	1.93	2.77	4.10	5.39	8.04	13.24	20.02	26.26
6.06 Hz	.39	.72	.98	1.46	2.01	2.85	4.19	5.38	8.08	13.43	20.23	26.55
7.87 Hz	.33	.69	.97	1.47	2.01	2.76	4.10	5.35	7.72	12.86	19.52	25.46
8 Hz	.29	.65	.94	1.42	1.91	2.62	3.90	5.08	7.65	12.63	19.10	25.42
10 Hz	.28	.55	.84	1.42	1.93	2.62	3.75	4.94	7.37	11.79	18.39	24.37
10.03 Hz	.30	.57	.89	1.48	1.93	2.64	3.76	5.00	7.61	12.46	18.55	24.55
15 Hz	.25	.49	.72	1.17	1.66	2.38	3.51	4.58	6.8	11.03	16.89	22.04
20 Hz	.24	.45	.63	1.07	1.49	2.09	3.05	4.02	6.24	9.84	15.8	20.54
20.99 Hz	.27	.48	.69	1.11	1.53	2.14	3.14	4.11	6.06	9.82	15.07	19.19
25.39 Hz	.27	.48	.67	1.05	1.42	1.98	2.89	3.79	5.71	9.38	13.53	18.28
30 Hz	.22	.38	.50	.78	1.07	1.50	2.14	2.77	4.44	7.24	12.78	16.4
40 Hz	.17	.31	.43	.68	.94	1.30	1.90	2.50	3.62	5.88	8.43	11.37
50 Hz	.13	.24	.34	.55	.74	1.03	1.50	1.97	2.88	4.62	4.80	5.74

Table 4.1 Shaker Performance Data

This performance was considered in the choice of slab thickness to ensure a balance between all 6 modes and the usable range of the equipment. The 18" thick slab provides a reasonable compromise and chosen for the slab thickness.

4.3 Test Structure Construction

4.3.1 Frame

Figure 4.4 Steel Frame of Test Structure

The frame in figure 4.4 above was obtained from the High Bay Lab in Engineering West. It is composed of W6x8.5 members and is 9' tall. There are two levels with approximately equal story heights. All connections were welded after placement in the lab. This helped reduce required assumptions in the analytical model by preventing any flexibility or nonlinearity in the bolted connection.

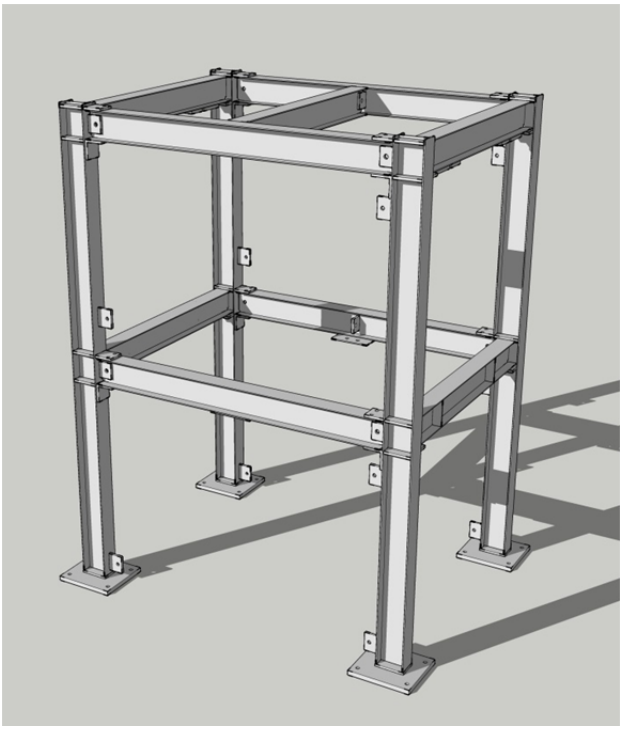

Figure 4.5 Steel Frame of Test Structure

A digital model of the frame was created in Sketchup as seen in figure 4.5 above. This model was used to facilitate the construction process. Slab size and formwork was laid out using the digital model. This allowed for the construction process to be carried out digitally before it was physically performed to check for compatibility issues between the formwork and the structure.

4.3.2 Base Plates

Figure 4.6 Frame Base Plate

The existing base plates were only 3/8” thick, and the bolt holes were several inches away from the edge of the column. This was believed to have a significant amount of flexibility that would be difficult to accurately capture in the analytical model, as it is not very close fixed or pinned. To reduce the possible error from this flexibility, the old base plates were removed via an oxy-acetylene torch to allow for new 1” thick base plates to be welded on in their place. This process was completed with the structure placed on cinder blocks to allow for precise leveling with the use of shims under each base plate.

4.3.3 Core Drilling

To fix the structure to the slab 16 anchor bolts were installed; four in each base plate. The previous installation of this frame had issues with alignment of the anchor bolts and the structure. These issues prevented several of the anchor bolts from being

installed. To ensure this installation did not experience similar issues core drilling was implemented. The hole locations were drawn on the slab through the structure's base plates, and this allowed for precision drilling and proper alignment of the anchor bolts.

Once the holes were drilled they were cleaned out and the structure was moved on top of the holes. Each anchor bolt was then epoxied to the slab through the base plate. This ensures that every bolt is properly aligned and prevented the structure from needing to be lifted on top of the anchor bolts.

4.3.4 Decking and Shear Studs

Figure 4.7 Decking and Shear Studs

The decking chosen for the structure is 16 ga 3" deep W-Formlock. This was chosen through consultation with Verco, the sponsor and provider of the decking. They recommended the use of shear studs due to the vibratory testing that the structure would

be undergoing. Nelson Stud Welding consulted on the design of the shear studs. ½" diameter 6" tall shear studs were chosen and placed in each valley of the decking. This was deemed sufficient to provide a solid connection between the slab and the frame.

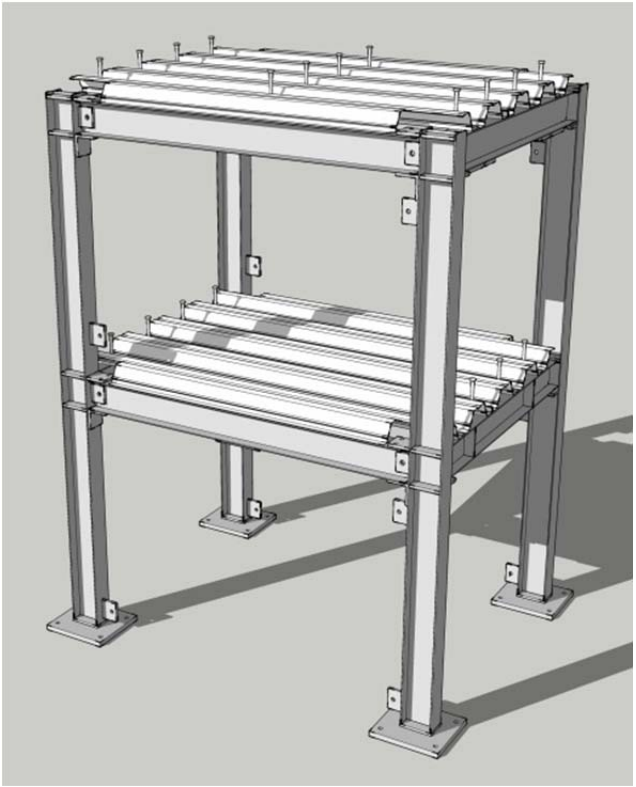

Figure 4.8 Decking Sketchup Model

Figure 4.8 above shows the decking and shear studs placed in the Sketchup model. This model provided dimensions for cutting the decking to size and drilling holes for the shear studs.

4.3.5 Slabs

Figure 4.9 Concrete Pour

The day the concrete was poured is shown in figure 4.9 above. A forklift was used with a cage attachment to provide a work platform for the top slab. Ladders and scaffolding were also used for the workers who were operating the vibrators and ensuring the concrete was properly consolidated. A concrete truck and pump were used to facilitate the pouring of the slabs. This was chosen partially because of the height of the 2nd level and partly because of the large volume (4 yd^3) of concrete required.

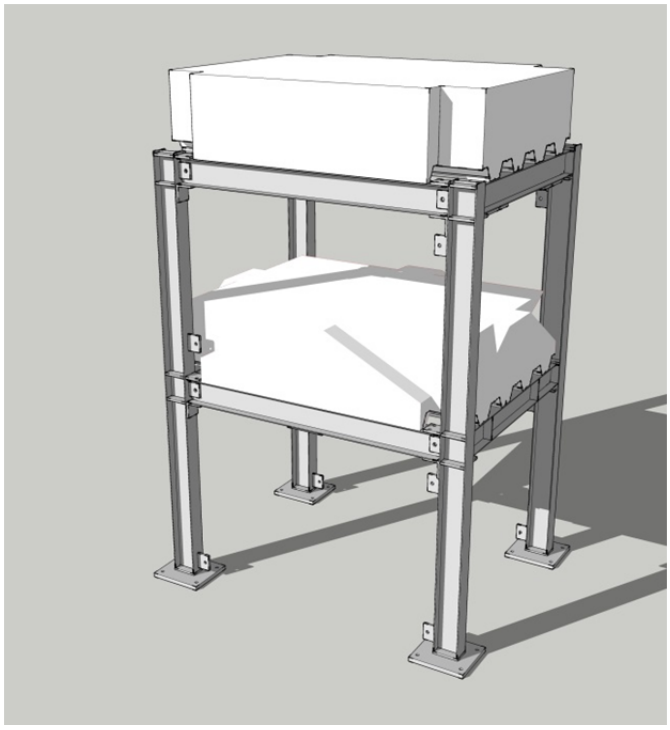

Figure 4.10 Slab in Sketchup Model

The model of the finished structure is shown in figure 4.10 above. The triangular cutouts on the bottom slab are to allow for the future installation of additional braces in the second story bays. This allows for more flexibility in future study utilizing this frame.

4.4 Braces

This single structure was used to test 6 different configurations of braces, allowing for six independent tests of the proposed damage detection technique. The desired change to the structure was minimal, which led to the choice of #5 rebar for the brace section. Braces were designed such that they could easily be engaged or disengaged to alter the configuration of the structure. This was accomplished by only welding one end of the brace. The other end is attached through the use of a C-clamp. A grinder was used to flatten the contact surface between the rebar, the frame, and the C-clamp, allowing for a solid connection. The low amplitude of vibration allowed for the clamped connection to rigidly secure the brace. See figure 4.11 below for an example of this connection.

Figure 4.11 Clamped Brace Connection

The braces in the either the strong axis or the weak axis are imparting very different degrees of change to the structure's stiffness. In the weak axis the braces have a much larger effect than in the strong axis. In the strong axis, the addition of a single brae increases the structure's stiffness in that direction by 30%, but in the weak axis the addition of a single brace adds 210% to the structure's stiffness in that direction. This allows for the analysis technique to be evaluated on a variety of stiffness changes to help inform the degree of stiffness change that this approach can locate.

4.5 Complex Behavior

Figure 4.12 Column to Beam Connection

The stiffness of the columns is influenced by several factors. The interaction with the slabs on each level creates significant out of plane stiffness that contributes to the moment frame beam stiffness. This behavior is difficult to precisely model because of the tapered geometry of the slab and complex interaction near the connection. See section 7.2.1 for details on how this behavior was modeled in the analytical model.

4.5.1 Slab Interaction

The floor slab that the structure is bolted to is 6" thick. While it has sufficient strength to support the structure, the flexibility introduced by the slab is believed to play a considerable effect in the behavior of the structure. This is investigated in further detail in section 11.2.

This additional flexibility is theorized to have a more significant impact on the strong axis direction than the weak axis. The slab and the columns work in series; with the large stiffness of the strong axis direction the slab has a larger influence on the overall system stiffness.

4.5.2 Panel Zone Behavior

The connection from the column to the beam is shown in figure 4.12. The beam connection and additional plates welded to this area contribute to the stiffness of this panel zone area, but the exact behavior is difficult to quantify accurately. There is expected to be a significant increase in stiffness of this zone, the approach to modeling this behavior is discussed in further detail in section 7.2.3.

4.6 Simplifying Behavior

The structure does not have any architectural components. This allows for clearer results than a full-scale building because architectural components may cause behavior that is difficult to model accurately. The structure was constructed in a laboratory environment, which is devoid of wind, and sun, minimizing interference from these sources. These factors simplify the system compared to analysis of a full size building.

4.7 Naming Convention

The naming of the tested configurations is summarized in figure 4.13. Each digit of the name represents a brace that can be engaged on the structure. The first digit is the brace on the left side of the structure in the weak axis orientation of the moment frame. The second digit is the brace that is on the front of the structure in the strong axis direction. The third digit is the brace on the right side of the structure in the weak axis direction. A "0" in the name denotes a disengaged brace in this position, and a letter denotes that a brace is engaged.

000:

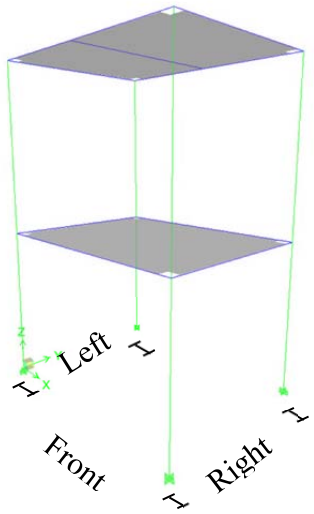

LFR:

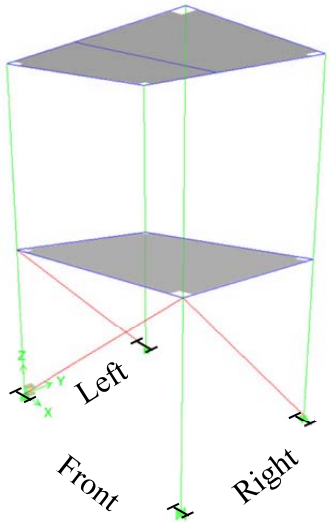

L00:

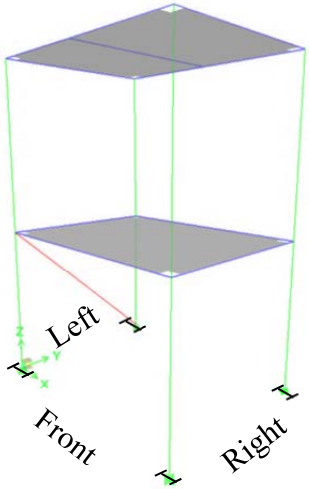

LF0:

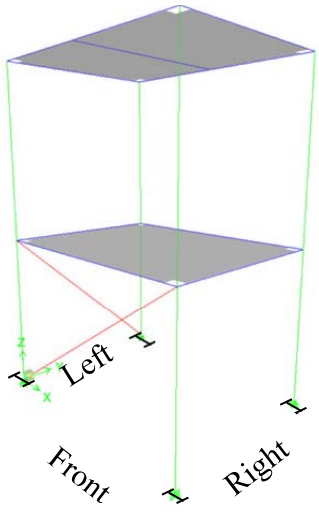

L0R:

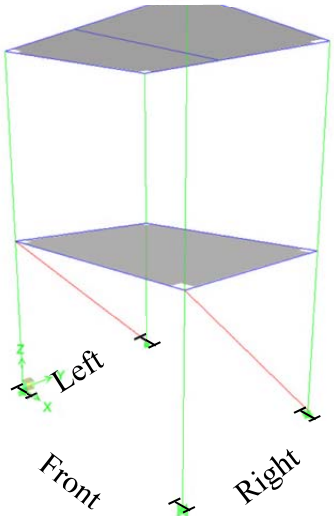

0F0:

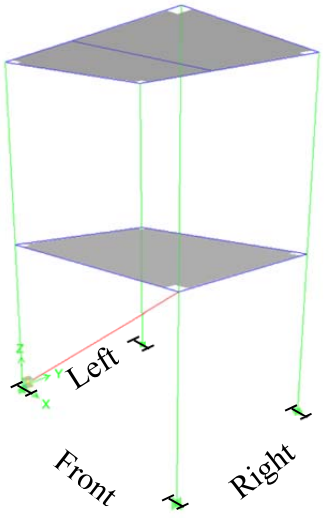

Figure 4.13 Configurations of Braces

5.0 THEORY AND METHODOLOGY

The hypothesis of this thesis is that the proposed mode shape derived damage detection technique can be accurate and reliable in application to physical structures. To test this hypothesis a method of analysis is developed using mode shapes.

The idea is to detect changes in the mode shapes when something in the physical model is different than in the analytical model. It is hypothesized that mode shapes provide an excellent way to locate where a particular element or set of elements are not performing as expected.

The measured mode shapes are susceptible to impurities from imperfections in testing. They can be cleaned using a process called modal sweeping, which removes traces of other modes that can reduce the accuracy of the analysis. Modal sweeping is discussed in further detail in section 5.1.2.

5.1 Mode Shape Analysis

The mode shape analysis uses a series of techniques to determine the correlation between the experimental and analytical models. This approach uses relative analysis because the mode shapes are normalized. This means that the analytical model must be proportionately accurate to the real structure, but overall changes in the model's stiffness do not affect this comparison. Overall changes are here meant to be even distributed changes to every member of the structure. For instance if every member's stiffness was increased by 10%, the mode shapes would be the same and the mode shape analysis

would not be impacted. This is a significant advantage over the frequency analysis that uses an absolute comparison to the analytical model and requires a higher level of accuracy than the mode shape analysis.

5.1.1 Modal Assurance Criteria (MAC)

Modal Assurance Criteria is a metric used to compare two vectors and detect how well they correlate. The resulting value has range of 0 to 1, where 0 indicates that the vectors are perfectly orthogonal to each other. A MAC of 1 indicates that the two vectors are identical. Vectors composed of random numbers yield a MAC value of .5, indicating no correlation between the modes. The equations for MAC matrix calculations are shown in Equation 5.1 below. (Pastor 2012)

Equation 5.1 Modal Assurance Criterion (MAC)

$$MAC_{ij} = \frac{(\varphi_i{}^T \varphi_j)^2}{(\varphi_i{}^T \varphi_i)(\varphi_j{}^T \varphi_j)}$$

φ_i = i^{th} mode of the first matrix used for comparison
φ_j = j^{th} mode of the second matrix used for comparison

In this study 6 modes are examined. The MAC calculation is completed as a matrix to compute the correlation between all 6 modes. The resulting 6x6 matrix contains correlation values for 36 comparisons, with the diagonal values showing the correlation of the correct mode shape comparison.

For the modal contamination matrices, this calculation is used compare the experimental mode shapes against themselves, yielding a correlation matrix that is ideally equal to the identity matrix. A result of the identity matrix indicates that the measured mode shapes are perfectly orthogonal to each other and sweeping will have no effect.

For the comparative MAC matrices, the swept experimental mode shapes are compared with the analytical mode shapes. In these matrices each column in the table represents an experimental mode shape, and each row represents an analytical mode shape. This means that the diagonal terms should be close to 1, and the off diagonal terms should be close to 0, ideally creating the identity matrix. A result of the identity matrix indicates an exact match between the experimental and analytical mode shapes.

5.1.1.1 Mass Weighted Modal Assurance Criteria (MWMAC)

The MAC metric is a universal way of comparing any two vectors, however to adapt this calculation to specific analysis of mode shapes a modification to the calculation was used. In each vector operation the Mass matrix is multiplied by the first vector to calibrate the values for units of measurement. This equalizes weighting between translational and rotational measurements by converting the value from acceleration to energy. The multiplication of acceleration by the mass of the degree of freedom balances translational and rotational measurements by negating the importance of units in the original measurement. This modified MAC calculation is used throughout the thesis in lieu of the standard MAC calculation to ensure that the particular units of

measurement do not skew the results. Without this mass weighting process the difference in units between the translational and rotational measurements would make the metric biased. The Mass Weighted Modal Assurance Criteria is calculated using equation 5.2.

Equation 5.2 Mass Weighted Modal Assurance Criterion (MWMAC)

$$MWMAC_{ij} = \frac{(\varphi_i{}^T M \varphi_j)^2}{(\varphi_i{}^T M \varphi_i)(\varphi_j{}^T M \varphi_j)}$$

φ_i = i^{th} mode of the first matrix used for comparison

φ_j = j^{th} mode of the second matrix used for comparison

M = Mass matrix

5.1.2 Modal Sweeping

Sweeping of the mode shapes is used to ensure the measured modes are orthogonal. Sweeping takes one mode shape and goes through the remaining modes to remove any contamination from the mode shape. This results in a set of modes that are all perfectly orthogonal to each other. The process starts with the first mode and continues through the remaining modes.

The raw test data had impurities due to modal mixing; sweeping the data helps reduce the effect of these impurities. This modal mixing means that certain measured modes have contamination from other modes because they were also excited during testing. This stems from two main sources, the adjacency of the modal frequencies and their damping values, and the eccentricity between the shaking location and centers of

mass and rigidity. For further detail on reduction of this issue see section 11.1. Modal sweeping is completed using equation 5.3. (Chopra 2007)

Equation 5.3 Modal Sweeping

$$\varphi_{si} = \varphi_i - (\varphi_j{}^T M \varphi_i)\varphi_j$$

φ_j = Mode shape being swept out

φ_i = Mode shape that is being swept

φ_{si} = Mode shape that has been swept

M = Mass matrix

This sweeping calculation removed any trace of mode shape j out of mode shape i. This is done by subtracting $(\varphi_j{}^T M \varphi_i)\varphi_j$ from the original mode shape. This subtracted term is composed of two vectors multiplied by each other: $(\varphi_j{}^T M \varphi_i)$ and φ_j. The first term provides a vector representing the contamination between the modes, that term is then used to scale mode shape j. The resulting term $(\varphi_j{}^T M \varphi_i)\varphi_j$ is then subtracted from the original mode shape i, providing a swept mode shape i that is orthogonal to mode shape j.

The order in which sweeping occurs can have a significant impact on the results. This is because if an impure mode is used to sweep a relatively pure mode it will contaminate it, thus reducing the accuracy of the results. To solve this issue, the order of sweeping starts from the most pure modes and works towards the least pure modes. This specific order of sweeping ensures that the accurate mode shapes will not be

compromised by any impure mode shapes. The metric used to quantify contamination is discussed in further detail in section 5.1.3.

5.1.3 Modal Contamination

To determine the contamination of each mode MAC matrices are calculated to examine the experimental mode shapes against themselves. The resulting matrix displays the degree of contamination between the modes. An ideal output is the identity matrix, which represents entirely pure modes. The off-diagonal terms show the impurities of each mode. To simplify this degree of contamination down to a single value that can be used for comparison, a one-norm of the off-diagonal terms is used. This adds the off-diagonal terms for each mode, and allows for a simple comparison to be made to determine the relative contamination level of each mode. A value of 0 represents no contamination, and a high value represents a significant degree of contamination in the mode shape.

5.1.4 Error Matrix (EM)

To produce an error matrix from the MWMAC matrix, the identity matrix is subtracted. The identity matrix is used because it is the ideal output of the MWMAC calculation. This error matrix is then used for further calculations. The ideal value in each cell of the error matrix is 0, which allows the Two-Norm metric to evaluate this data.

5.1.5 Prediction Metric: Two Norm of Error Matrix (TNEM)

The two norm of the MWMAC error matrix provides a reliable way to consolidate the 36 MWMAC error values down to a single value metric. The two-norm uses the largest singular value as a metric. Singular values of a matrix M are the square roots of the eigenvalues of the M transposed multiplied by M. This is shown in equation 5.4 below.

Equation 5.4 Singular Value

$$\sigma = \sqrt{\lambda}$$

λ is a vector of eigenvalues taken with respect to the matrix M according to equation 5.5 below.

Equation 5.5 Eigenvalue

$$\lambda = eig(M^T \mathrm{M})$$

The results were found to be very similar to the Frobenius Norm, which uses square root of the sum of the squares (SRSS). If the error matrix only contains 0, the metric will also be 0. If the error matrix has non zero terms the TNEM will be larger than 0. The optimal value of this metric is 0 which represents perfect correlation of all modes between the experimental and analytical mode shapes. This two norm provides a good metric for comparison of error matrices because it is directly correlated with how different the error matrix is from the ideal zero matrix,. This property is excellent for this style of comparison because it provides a single value that allows for ranking of computational models according to how similar they are to the measured configuration.

5.1.6 Normalization

The raw measured mode shapes are composed of acceleration measurements taken from the structure during forced vibration testing. This is dependent on the amplitude of excitation imparted by the shaker. To remove this variable from the measured mode shapes normalization is used. Normalization negates the influence of units on the mode shape and yields a unit-less mode shape that can then be properly compared with mode shapes derived from the analytical model. The calculation to perform normalization is shown in equation 5.6 below.

Equation 5.6 Normalization

$$\varphi_N = \frac{\varphi}{\sqrt{\varphi^T M \varphi}}$$

φ = Raw mode shape measurements
φ_N = Normalized mode shape
M = Mass matrix

5.2 Frequency Analysis

The measured modal frequencies are compared to the analytical model through percent error. This is an absolute style of comparison and requires a high level of accuracy in the analytical model to achieve an optimal metric value. The ideal value of this metric is 0, which represents zero error in all frequency predictions. The use of percent error prevents the frequency of each mode from unfairly weighting its importance as would occur if absolute changes were used. Using the percentage change also ensures that using either frequency or period would yield similar results. Frequency was chosen

for the error calculation because a positive percent change represents additional stiffness, which creates a convention of an increase in stiffness being associated with a positive percent change.

5.3 Dynamic Amplification Factor R_d

A dynamic amplification factor is used to estimate the resonance of a system exposed to a known cyclic load, given a known frequency and damping. This factor models the ratio of maximum dynamic displacement to static deformation versus a known ratio of the frequency of the applied load to the natural frequency of the system.

5.3.1 Derivation

The following section details the derivation of the dynamic amplification factor R_d.

u = Deformation
$\dot{u}$ = Velocity
$\ddot{u}$ = Acceleration
$\overline{\omega}$ = Circular frequency of applied load
ω = Natural circular frequency
M = Mass
K = Stiffness
C = Damping coefficient
ζ = Damping ratio
P_o = Dynamic load

The starting equation [1] is summing the forces on the system. On the left are the internal forces, on the right are the external forces.

$$M\ddot{u} + C\dot{u} + Ku = P_o \sin\left(\overline{\omega}\ t\right) \qquad [1]$$

Dividing equation [1] by M yields [2].

$$\ddot{u} + \frac{C}{M}\dot{u} + \frac{K}{M}u = \frac{P_o}{K}\sin\left(\overline{\omega}\ t\right) \qquad [2]$$

The natural frequency (ω) of the system is defined as:

$$\omega = \sqrt{\frac{K}{M}} \qquad [3]$$

Squaring equation [2] yields [4].

$$\omega^2 = \frac{K}{M} \qquad [4]$$

The critical damping coefficient (C_{cr}) is equal to:

$$C_{cr} = 2M\omega \qquad [5]$$

The damping ratio (ζ) is defined as the system's damping over critical damping.

$$\zeta = \frac{C}{C_{cr}} \qquad [6]$$

Substituting equation [5] into [6] yields [7].

$$\zeta = \frac{C}{2M\omega} \qquad [7]$$

Substituting equations [7] and [4] into [2] yields [8].

$$\ddot{u} + 2\zeta M\omega\dot{u} + \omega^2 u = \frac{P_o}{K}\sin\left(\overline{\omega}\ t\right) \qquad [8]$$

The system behavior is broken in two parts: general and particular. The general solution (u_g) describes the transient motion of the system. The particular solution (u_p) describes the steady state motion of the system.

$$u(t) = u_g(t) + u_p(t) \qquad [9]$$

The transient solution is not relevant to the Rd derivation, and therefore $u_g(t)$ is ignored.

The standard form of the particular solution is defined as:

$$u_p(t) = Asin\left(\overline{\omega}\ t\right) + Bcos\left(\overline{\omega}\ t\right) \qquad [10]$$

Taking the derivative of equation [10] yields [11].

$$\mathring{u}_p(t) = A\overline{\omega}\ cos\left(\overline{\omega}\ t\right) - B\overline{\omega}\ sin\left(\overline{\omega}\ t\right) \qquad [11]$$

Taking the derivative of equation [11] yields [12].

$$\ddot{u}_p(t) = -A\overline{\omega}^{\,2} sin\left(\overline{\omega}\ t\right) - B\overline{\omega}^{\,2} cos\left(\overline{\omega}\ t\right) \qquad [12]$$

Substituting equations [9], [10] and [11] into [8] and solving yields [13] and [14]:

$$A = \frac{P_o}{K}\frac{1 - (\frac{\overline{\omega}}{\omega})^2}{(1 - \left(\frac{\overline{\omega}}{\omega}\right)^2)^2 + (2\zeta\frac{\overline{\omega}}{\omega})^2} \qquad [13]$$

$$B = \frac{P_o}{K}\frac{-2\zeta\frac{\overline{\omega}}{\omega}}{\left(1 - \left(\frac{\overline{\omega}}{\omega}\right)^2\right)^2 + \left(2\zeta\frac{\overline{\omega}}{\omega}\right)^2} \qquad [14]$$

The alternative form of the steady state solution is:

$$u(t) = Psin\left(\overline{\omega}\ t - \theta\right) \qquad [15]$$

θ is defined as:

$$\theta = tan^{-1}\left(\frac{P}{C}\right) \qquad [16]$$

P is defined as:

$$P = \sqrt{A^2 + B^2} \qquad [17]$$

Substituting equations [13] and [14] into [17] yields [18].

$$P = \frac{\frac{P_o}{K}}{\sqrt{\left(1 - \left(\frac{\overline{\omega}}{\omega}\right)^2\right)^2 + \left(2\zeta\frac{\overline{\omega}}{\omega}\right)^2}} \qquad [18]$$

Substituting equation [18] into [15] yields [19].

$$u(t) = \frac{\frac{P_o}{K}}{\sqrt{\left(1 - \left(\frac{\overline{\omega}}{\omega}\right)^2\right)^2 + \left(2\zeta\frac{\overline{\omega}}{\omega}\right)^2}} sin\left(\overline{\omega}\ t - \theta\right) \qquad [19]$$

The static deformation is equal to:

$$u_{st} = \frac{P_o}{K} \qquad [20]$$

Substituting equation [20] into [19] and creating the dynamic amplification factor R_d yields [21]

$$u(t) = u_{st} R_d sin\left(\overline{\omega}\ t - \theta\right) \qquad [21]$$

Setting equation [21] equal to [19] yields:

Equation 5.7 Dynamic Amplification Factor R_d

$$R_d = \frac{1}{\sqrt{(1-\left(\frac{\bar{\omega}}{\omega}\right)^2)^2 + (2\xi\frac{\bar{\omega}}{\omega})^2}} \qquad [22]$$

$\bar{\omega}$ = Natural circular frequency of the system (rad/s)
ω = Natural circular frequency of the applied load (rad/s)
ξ = System damping (expressed as percentage of critical damping)

5.3.2 Importance

The u_{st} term in equation [21] is the static deformed shape of the structure under the applied load. This means that for accurate mode shape collection to occur, the shaker must be oriented such that the deformed shape will be very similar to the mode shape. For the symmetric configurations each mode tends to move primarily in one degree of freedom, which aligns with the orientation of the shaker well. This means that the mode shapes can be accurately collected with the shakers placed at the center of mass for the symmetric configurations. For the asymmetric configurations, the static deformed shape of the structure is not as similar to the mode shape, and thus the accuracy of the measured mode shape is degraded.

The force that each mode is excited with is referred to as the modal force. The modal force is equal to the dot product of the force vector and the mode shape. The placement and orientation of the shaker should be such that the modal force is greatest for the mode that is being tested, and smallest for the other modes. In most structures that are symmetric this can be achieved relatively easily, however the modes of some unique

structures may not be able to be excited independently, and this can lead to contamination between modes.

The dynamic amplification factor (R_d) shows how the frequency of an applied load will affect the excitation of a mode, and this is important to take note of when completing forced vibration testing. If two modes are similar in frequency they will tend to be excited together. The damping of each mode is directly correlated with the degree to which this blending of modal excitation will occur. High damping values will spread the structure's response out and cause this phenomenon to occur with wider frequency gaps. Figure 5.1 shows the effect of damping on the dynamic amplification factor.

The structure examined in this thesis has lower damping values than would be expected of a normal building, which is typically estimated at 5%. This means that the adjacency of the frequencies does not have as large of an impact on the accuracy of the measured mode shapes as the alignment spatial component of the applied force.

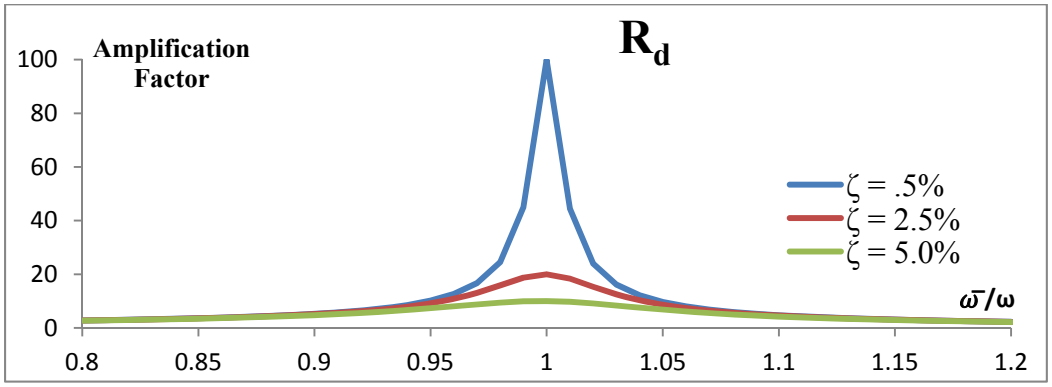

Figure 5.1 Dynamic Amplification Factor R_d

Figure 5.1 shows that high damping values reduce the peak amplification factor significantly. This allows the surrounding frequencies to more excited compared to the maximum excitation. With a less distinct peak at the maximum excitation level, the effects of modal contamination due to similar frequencies are more pronounced and the difficulty of measuring accurate orthogonal mode shapes is increased.

5.3.3 Dynamic Amplification Factors for Each Test

The Rd factor for each testing procedure was calculated from the measured results, and is summarized in the sections 5.3.3.1 through 5.3.3.6. This shows the theoretical degree to which each mode is excited from the shaking of each other mode. These are calculated using equation 5.7. See section 14.4 for the frequency sweep data that was used to calculate the damping value for each mode.

5.3.3.1 000 Configuration

000			R_d					
Excited Mode	Freq.	Damping	1WA	1SA	1T	2WA	2SA	2T
1WA	3.61	0.24%	208.3	1.6	1.3	1.2	1.0	1.0
1SA	5.92	0.34%	0.6	147.1	2.4	1.5	1.1	1.1
1T	7.72	0.41%	0.3	1.4	122.0	2.5	1.2	1.1
2WA	9.98	0.20%	0.2	0.5	1.5	250.0	1.3	1.2
2SA	20.7	0.27%	0.0	0.1	0.2	0.3	185.2	3.1
2T	25.14	0.56%	0.0	0.1	0.1	0.2	2.1	89.3

Table 5.1 000 Testing: Rd for each Mode

5.3.3.2 L00 Configuration

L00			R_d					
Excited Mode	Freq.	Damping	1WA	1SA	1T	2WA	2SA	2T
1WA	4.35	0.24%	208.3	2.2	1.4	1.1	1.0	1.0
1SA	5.92	0.34%	1.2	147.1	1.9	1.3	1.1	1.0
1T	8.5	0.31%	0.4	0.9	161.3	1.8	1.2	1.1
2WA	12.66	0.22%	0.1	0.3	0.8	227.3	1.6	1.2
2SA	20.7	0.24%	0.0	0.1	0.2	0.6	208.3	2.0
2T	29.1	0.86%	0.0	0.0	0.1	0.2	1.0	58.1

Table 5.2 L00 Testing: Rd for each Mode

5.3.3.3 L0R Configuration

L0R			R_d					
Excited Mode	Freq.	Damping	1WA	1SA	1T	2WA	2SA	2T
1WA	5.03	0.28%	178.6	3.6	1.3	1.1	1.1	1.0
1SA	5.92	0.42%	2.6	119.0	1.5	1.2	1.1	1.0
1T	10.26	0.28%	0.3	0.5	178.6	2.0	1.3	1.1
2WA	14.54	0.19%	0.1	0.2	1.0	263.2	2.0	1.3
2SA	20.68	0.23%	0.1	0.1	0.3	1.0	217.4	1.8
2T	30.9	0.55%	0.0	0.0	0.1	0.3	0.8	90.9

Table 5.3 L0R Testing: Rd for each Mode

5.3.3.4 LFR Configuration

LFR			R_d					
Excited Mode	Freq.	Damping	1WA	1SA	1T	2WA	2SA	2T
1WA	5.04	0.25%	200.0	2.4	1.3	1.1	1.1	1.0
1SA	6.56	0.38%	1.4	131.6	1.6	1.3	1.1	1.0
1T	10.58	0.25%	0.3	0.6	200.0	2.1	1.3	1.1
2WA	14.54	0.19%	0.1	0.3	1.1	263.2	1.7	1.2
2SA	22.72	0.10%	0.1	0.1	0.3	0.7	500.0	1.9
2T	32.8	0.34%	0.0	0.0	0.1	0.2	0.9	147.1

Table 5.4 LFR Testing: Rd for each Mode

5.3.3.5 LF0 Configuration

LF0			R_d					
Excited Mode	Freq.	Damping	1WA	1SA	1T	2WA	2SA	2T
1WA	4.4	0.23%	217.4	1.9	1.3	1.1	1.0	1.0
1SA	6.46	0.33%	0.9	151.5	2.0	1.4	1.1	1.0
1T	9.06	0.20%	0.3	1.0	250.0	2.0	1.2	1.1
2WA	12.68	0.23%	0.1	0.4	1.0	217.4	1.5	1.2
2SA	21.94	0.19%	0.0	0.1	0.2	0.5	263.2	2.0
2T	31	0.55%	0.0	0.0	0.1	0.2	1.0	90.9

Table 5.5 LF0 Testing: Rd for each Mode

5.3.3.6 0F0 Configuration

0F0			R_d					
Excited Mode	Freq.	Damping	1WA	1SA	1T	2WA	2SA	2T
1WA	3.61	0.36%	138.9	1.5	1.2	1.2	1.0	1.0
1SA	6.28	0.36%	0.5	138.9	2.1	1.7	1.1	1.1
1T	8.66	0.32%	0.2	1.1	156.3	4.0	1.2	1.1
2WA	9.98	0.20%	0.2	0.7	3.0	250.0	1.3	1.1
2SA	22.3	0.27%	0.0	0.1	0.2	0.3	185.2	2.7
2T	28.1	0.64%	0.0	0.1	0.1	0.1	1.7	78.1

Table 5.6 0F0 Testing: Rd for each Mode

The R_d values for the modes that are not desired to be excited are quite low because of the very low damping values of the structure as can be seen in tables 5.1 through 5.6. Due to these low levels of damping, the accidental excitation of other modes is not believed to significantly contaminate the measured mode shapes for this particular structure. In buildings with larger amounts of damping, this phenomenon would become a larger issue and would require more consideration of the shaker location to minimize the contamination caused by this effect, as discussed in section 11.1.

5.3.4 Effect of Damping vs Frequency Adjacency

To investigate whether damping or frequency adjacency has a larger effect on modal contamination, a parametric study was completed. The R_d tables for a hypothetical data set were calculated with a control, and then two altered data sets. The first has the spacing between the frequencies halved, and thus provides a factor of two increase to their frequency adjacency. The second set has the damping values increased by a factor of two, and this provides a comparable percent change to the case with altered frequencies. To properly compare the cases, the Rd values are normalized by converting them to a percentage of the maximum R_d for that data set.

Control			R_d					
Excited Mode	Freq. (Hz)	Damping	1WA	1SA	1T	2WA	2SA	2T
1WA	2	0.50%	100.0	1.3	1.1	1.1	1.0	1.0
1SA	4	0.50%	0.3	100.0	1.8	1.3	1.2	1.1
1T	6	0.50%	0.1	0.8	100.0	2.3	1.6	1.3
2WA	8	0.50%	0.1	0.3	1.3	100.0	2.8	1.8
2SA	10	0.50%	0.0	0.2	0.6	1.8	100.0	3.3
2T	12	0.50%	0.0	0.1	0.3	0.8	2.3	100.0
			Normalized					
			1WA	1SA	1T	2WA	2SA	2T
		1WA	100.0%	1.3%	1.1%	1.1%	1.0%	1.0%
		1SA	0.3%	100.0%	1.8%	1.3%	1.2%	1.1%
		1T	0.1%	0.8%	100.0%	2.3%	1.6%	1.3%
		2WA	0.1%	0.3%	1.3%	100.0%	2.8%	1.8%
		2SA	0.0%	0.2%	0.6%	1.8%	100.0%	3.3%
		2T	0.0%	0.1%	0.3%	0.8%	2.3%	100.0%

Table 5.7 Control Rd Evaluation

Freq Impact			Rd					
Excited Mode	Freq. (Hz)	Damping	1WA	1SA	1T	2WA	2SA	2T
1WA	2	0.50%	100.0	1.8	1.3	1.2	1.1	1.1
1SA	3	0.50%	0.8	100.0	2.3	1.6	1.3	1.2
1T	4	0.50%	0.3	1.3	100.0	2.8	1.8	1.5
2WA	5	0.50%	0.2	0.6	1.8	100.0	3.3	2.0
2SA	6	0.50%	0.1	0.3	0.8	2.3	100.0	3.8
2T	7	0.50%	0.1	0.2	0.5	1.0	2.8	100.0

	Normalized					
	1WA	1SA	1T	2WA	2SA	2T
1WA	100.0%	1.8%	1.3%	1.2%	1.1%	1.1%
1SA	0.8%	100.0%	2.3%	1.6%	1.3%	1.2%
1T	0.3%	1.3%	100.0%	2.8%	1.8%	1.5%
2WA	0.2%	0.6%	1.8%	100.0%	3.3%	2.0%
2SA	0.1%	0.3%	0.8%	2.3%	100.0%	3.8%
2T	0.1%	0.2%	0.5%	1.0%	2.8%	100.0%

Table 5.8 Impact of Frequency on Rd Calculation

Damping Impact			Rd					
Excited Mode	Freq. (Hz)	Damping	1WA	1SA	1T	2WA	2SA	2T
1WA	2	1.00%	50.0	1.3	1.1	1.1	1.0	1.0
1SA	4	1.00%	0.3	50.0	1.8	1.3	1.2	1.1
1T	6	1.00%	0.1	0.8	50.0	2.3	1.6	1.3
2WA	8	1.00%	0.1	0.3	1.3	50.0	2.8	1.8
2SA	10	1.00%	0.0	0.2	0.6	1.8	50.0	3.3
2T	12	1.00%	0.0	0.1	0.3	0.8	2.3	50.0

	Normalized					
	1WA	1SA	1T	2WA	2SA	2T
1WA	100.0%	2.7%	2.2%	2.1%	2.1%	2.1%
1SA	0.7%	100.0%	3.6%	2.7%	2.4%	2.2%
1T	0.2%	1.6%	100.0%	4.6%	3.1%	2.7%
2WA	0.1%	0.7%	2.6%	100.0%	5.6%	3.6%
2SA	0.1%	0.4%	1.1%	3.6%	100.0%	6.5%
2T	0.1%	0.2%	0.7%	1.6%	4.5%	100.0%

Table 5.9 Impact of Damping on Rd Calculation

Examination of tables 5.7 through 5.9 show that damping has a larger impact on modal contamination than frequency. Damping has approximately a factor of 2 larger impact on non-desirable Rd values compared to the same percent change in the frequency adjacency of the modes.

5.4 Data Collection

The acceleration of the structure is measured to yield experimental mode shapes. This is completed with the use of highly sensitive piezo-electric accelerometers and a data acquisition system.

5.4.1 Quantity of Measurements

In determining the number of measurement locations, there are two main factors to be considered. The first is the complexity of the system being tested, where a more complex building will typically require measurements at more locations. Each measurement location is a node that allows for comparison with the computational model. Additional nodes allow for more thorough comparison of experimental to computational mode shapes by including extra data from the structure.

The second factor is the desired precision of the damage detection. The damage detection technique is limited in informing the location of damage by the number of nodes in the model. For instance, in a 50 story building the complexity of the data acquisition system used for this technique can be varied. As a method of simplifying the

system, measurements could be taken at every 5th floor. Independent behavior of members between these measurement nodes is unknown, but the performance of the assembly is known. In this scenario, damage could be located with a precision level of a five floor zone. The location can be made more precise by adding additional measurement locations because it gains information about the system in those areas. This flexibility allows for system customization based on the project budget.

For this structure six measurement locations were chosen, this was driven by the desire to capture the 6 dominant modes of behavior including first and second modes of translation in each direction and rotation. The translation in plan is measured by accelerometers placed at the center of mass of each slab. Rotation is obtained by placing another accelerometer offset 20" from the center of mass. A function is then used in signal express to evaluate the difference in these accelerations and calculate rotational acceleration.

5.4.2 Data Acquisition System

The system used for data collection was composed of 7 accelerometers. 6 are used for measuring the structure's performance, and the other accelerometer is used to measure the shaker's force output. This is used during testing to ensure the shaker is performing as expected. The modules that take in the accelerometer readings are capable of recording 4 input channels, thus two collection modules were required.

Labview Signal-Express was used to communicate with the National Instruments data collection system. It was found that when using multiple modules there was a phase shift in the signals of the 2nd box of .0135 seconds. This is believed to be caused by the order in which signals are processed when using two modules. To correct for this delay a "Subset and Resample" tool was used to crop the first .0135 seconds out of the early data set.

5.4.3 Shaking Equipment

5.4.3.1 Shaker

Figure 5.2 Shaker

This machined shown in figure 5.2 above is named the "Shaker" because its purpose is to harmonically oscillate the structure by shaking a 78 lb. mass back and forth using a linear electric motor. This machine is rated by the manufacturer to output a 30 lbs peak sinusoidal force at frequencies up to 20 Hz. The performance was measured at a variety of voltages and frequencies, the results are displayed in section 8.3. This machine is powered by an amplifier, two of which are shown in figure 5.4.3.2 below.

5.4.3.2 Amplifier

Figure 5.3 Amplifier

Amplifiers are used to convert the low power signal from the signal generator, shown in figure 5.3, to a high power signal capable of powering the shaker. This is completed using APS amplifiers. For translational mode shape excitation a single shaker and amplifier is used, but for torsional mode shapes two shakers and amplifiers are used. This allows for rotational excitation to be accomplished without inducing translational force because the two shakers vibrate 180 degrees out of sync and cancel out each other's translational force.

5.4.3.3 Signal Generator

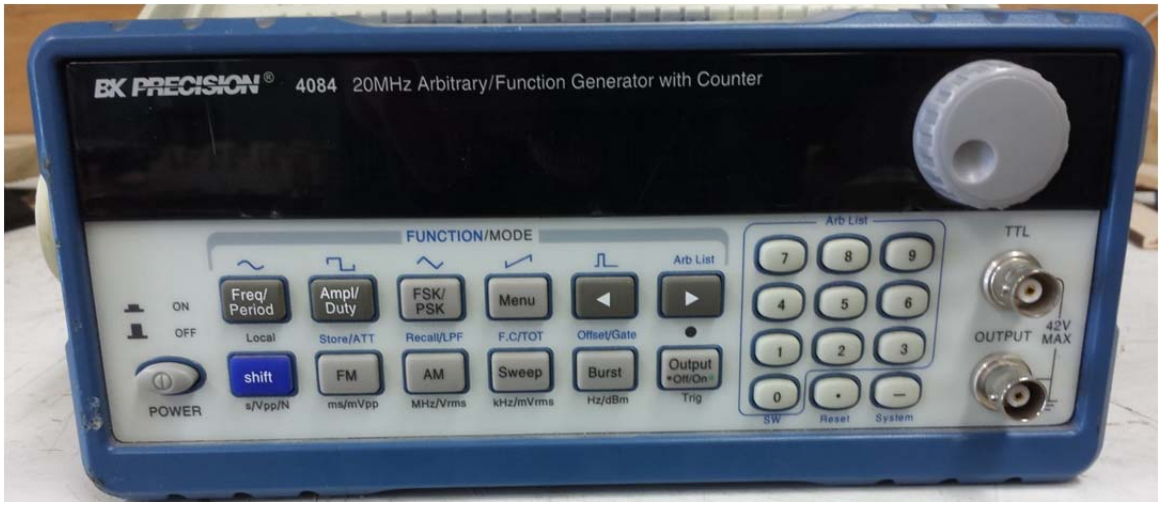

Figure 5.4 Signal Generator

A signal generator, shown in figure 5.4 above, is used to produce the sine wave to excite the structure. It allows for precisely controlled frequencies and amplitudes to be created which facilitates accurate data collection.

5.4.4 Settlement Standard

To ensure that the system has reached steady state motion a clear definition of steady state must be defined. In theory steady state means that the system is going through exactly the same motion each cycle, but in reality this does not occur. Due to ambient vibrations and interference the system will never complete the exact same motion between cycles, but the motions will be very close to the same. To ensure that consistent data readings were taken, an Excel spreadsheet was setup to evaluate the

structures settlement during testing. Three readings were taken for each data point, and the average of the set was used as the final value.

To measure the consistency of the readings the standard deviation is calculated. The amplitude of each measured mode's vibrations varies depending on the chosen amplitude of excitation; therefore a universal metric of settlement was created by dividing the standard deviation by the average. This metric represents the settlement of the structure. After initial testing it was determined that a metric of less than 1% is a reasonable value. This was a compromise between getting consistent data and maintaining a reasonable amount of time for testing. To achieve more consistent values a longer amount of time is required between changing settings and taking readings.

5.4.5 Filtering

Raw data from accelerometers is prone to low frequency noise. This is due to the piezo-electric nature of the sensors. To reduce this noise, filtering is employed during testing in Labview Signal Express. This filtering uses a 12^{th} order Buttersworth filter to drastically reduce frequency content below 2 Hz and above 100 Hz. Filtering helps ensure the collected data is of the desired mode and has low levels of noise due to equipment limitations.

6.0 TESTING PROCEDURE

This chapter details the process in which mode shape testing was completed. Frequency sweeps are completed to measure the natural frequency of each mode. Once the natural frequencies were determined the mode shapes were collected.

6.1 Forced Vibration

This test procedure involves exciting a particular mode in the structure to a chosen amplitude and letting it settle until it reaches steady state motion driven by forced vibration from the shaker. The actual modal frequencies are unknown at the beginning of this test, so initially a frequency sweep is completed to find those frequencies. Once the natural frequencies are found, the mode shapes are recorded.

6.1.1 Frequency Sweep

A frequency sweep is where the frequency of the shaker is varied in small increments around the natural frequency of the mode being examined. The amplitude at each frequency is recorded. The frequency associated with the peak amplitude is considered to be the natural frequency. This provides a fairly precise natural frequency and can also be used to calculate damping via the half power band method. As a compromise between time restrains and detail of data a minimum of 4 data points were recorded for each mode. This ensures that enough data is collected to estimate damping via the half power band method.

6.1.2 Steady State Vibration

The desired behavior of the structure forced vibration testing is steady state vibration. This means that the damping of the structure has reached equilibrium with the energy input and the structure will not resonate to a higher amplitude. This creates vibration that is constant and can be measured with a high degree of precision. The criterion to consider vibration steady state is discussed in further detail in section 5.4.4.

6.1.3 Procedure

After the frequency sweep has been completed and the natural frequency of the mode found, the mode shape can be measured. First the structure is allowed to reach stead state shaking. Readings for each measurement position are then recorded with each value representing the average cyclic peak of 30 seconds of activity. This averaging is completed through Labview Signal Express. Three points are collected and their degree of settlement is determined using the criteria in section 5.4.4. If the structure is not settled sufficiently then additional points are collected, replacing the earlier values, until the settlement criteria is satisfied. This allowed for consistent collection of data by maintaining the degree of settlement between each data value that was collected.

6.1.4 Shaker Locations

For the testing completed in this thesis, the shaker placement was determined with regard to the center of mass. The shaker positions varied for each mode, but were the same across each configuration. The testing results in section 9.1 indicate that this solely

basing the shaker location on the center of mass is not ideal and could be improved upon in future studies as detailed in section 11.1.

In the following figures the lines crossing each slab indicate the lines of symmetry which coincides with the center of mass. These are used for reference because many of the shaker locations are placed in line with the center of mass. The process of selecting a shaker location is based on the mode shape. The underlying assumption is that placing the shaker at the point and orientation of the largest deformation in the mode shape will produce optimal results.

In the following figures, the black rectangular prism represents the shaker that is used on the structure. The long orientation of this object indicates the direction of shaking. For the first weak axis (1WA) mode the shaker is placed on the top slab in line with the center of mass as shown in figure 6.1. This was chosen because this orientation is predicted to have the largest deformation in the 1WA mode.

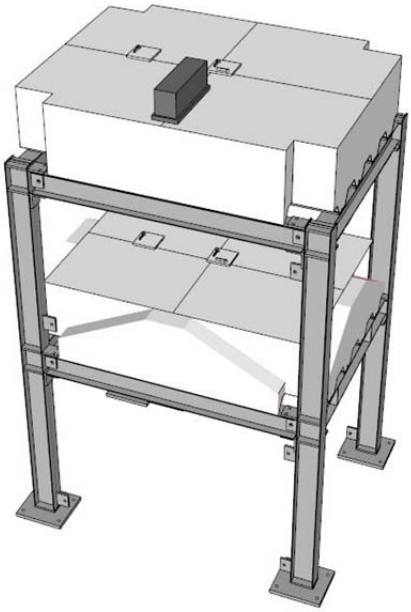

Figure 6.2 1WA Shaker Location

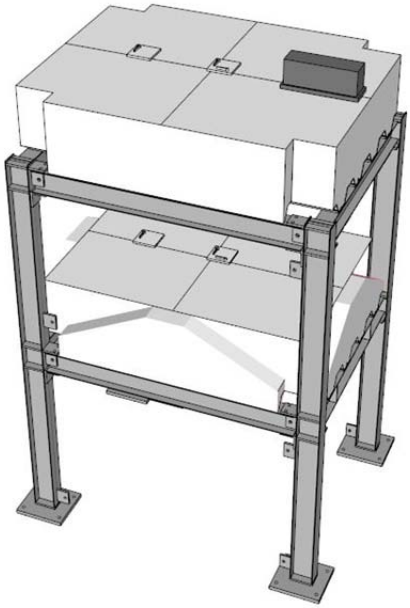

Figure 6.1 1SA Shaker Location

The shaker placement for testing of the 1SA mode is shown in figure 6.2. This direction and location were chosen because it has the largest deformation of any degree of freedom for the 1SA mode.

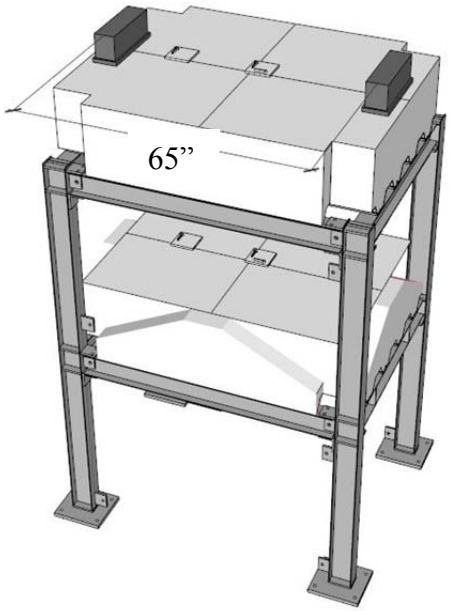

Figure 6.3 1T Shaker Locations

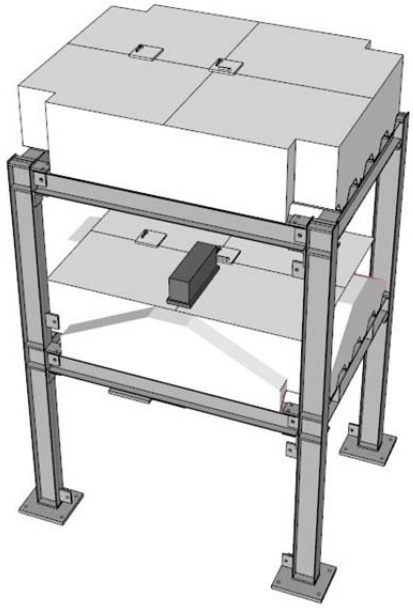

Figure 6.4 2WA Shaker Location

To properly excite the first torsional (1T) mode, a moment needs to be applied without a net translational force. To accomplish this, two shakers were used as shown in figure 6.3. The two shakers are run 180 degrees out of phase with each other by orienting them in opposite directions. This creates a force couple and imparts a moment about the center of mass without a net translational force. The shaker location for the 2WA mode was chosen because this direction and location have the largest deformation for the 2WA mode.

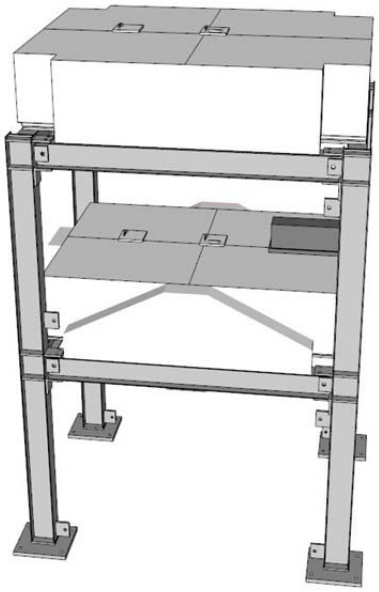

Figure 6.5 2SA Shaker Location

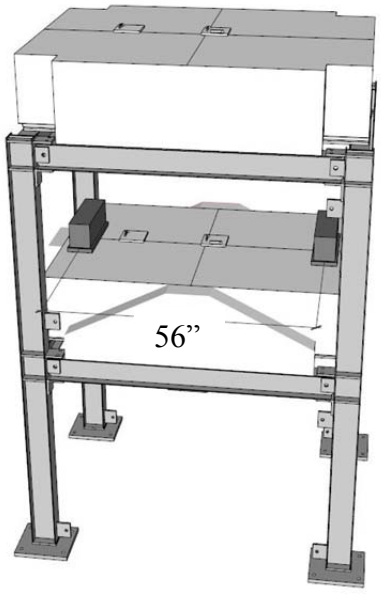

Figure 6.6 2T Shaker Locations

The shaker locations for testing of the 2SA mode and 2T mode are chosen for the same reasons discussed previously for the other modes. While these locations were found to work fine for the 000 configuration, the results show that for other configurations the shaker placement could be improved as detailed in section 11.1.

6.1.5 Shaker Amplitude

The final shaker amplitudes chosen for testing were decided based on the performance of the braces. Initial testing was completed and careful examination of the braces at various amplitudes allowed for shaker amplitudes to be chosen that minimized possible effects of buckling. The chosen shaker settings are summarized in table 6.1.

Mode	Freq	Shaker Voltage	Shaker Force
1WA	3.61 Hz	30 mV	.89 lbs
1SA	6.02 Hz	125 mV	3.39 lbs
1T	7.78 Hz	40 mV	1.11 lbs
2WA	10.04 Hz	60 mV	1.57 lbs
2SA	20.7 Hz	100 mV	2.08 lbs
2T	25.14 Hz	125 mV	2.34 lbs

Table 6.1 Shaker Amplitude and Force Output

The force shown in table 6.1 is the predicted force based on shaker testing shown in section 4.2.3. The output force is dependent on both the shaker voltage as well as frequency. The same shaker settings were used for each configuration to ensure that varying amplitudes of excitation did not impact the accuracy of the results.

6.1.6 Acceleration Measurement Locations

Six measurement locations were chosen because they allow for horizontal translation and rotation to be measured at each slab. The slabs are assumed to act as rigid bodies due to their 18" depth and stiffness. The square plates in the following figures represent the steel plates used to hold the accelerometers. The arrows on the plates indicate the location and orientation of accelerometers.

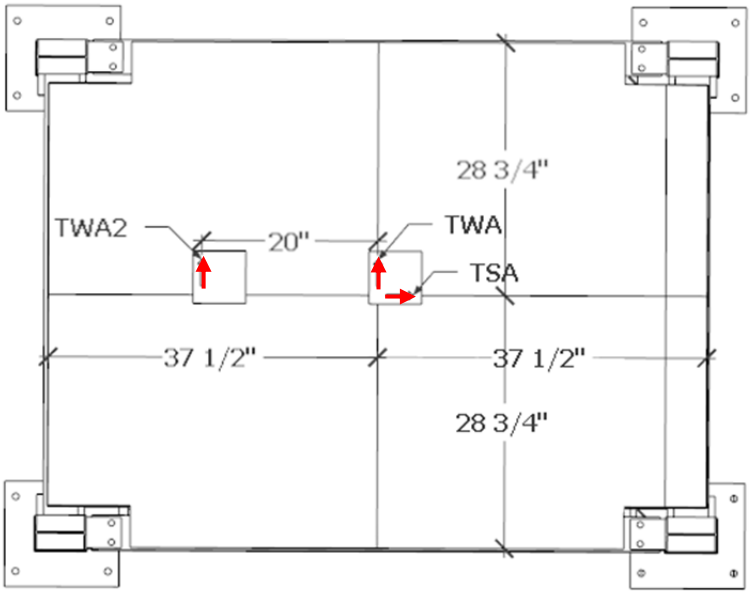

Figure 6.7 Location of Accelerometers on Top Slab

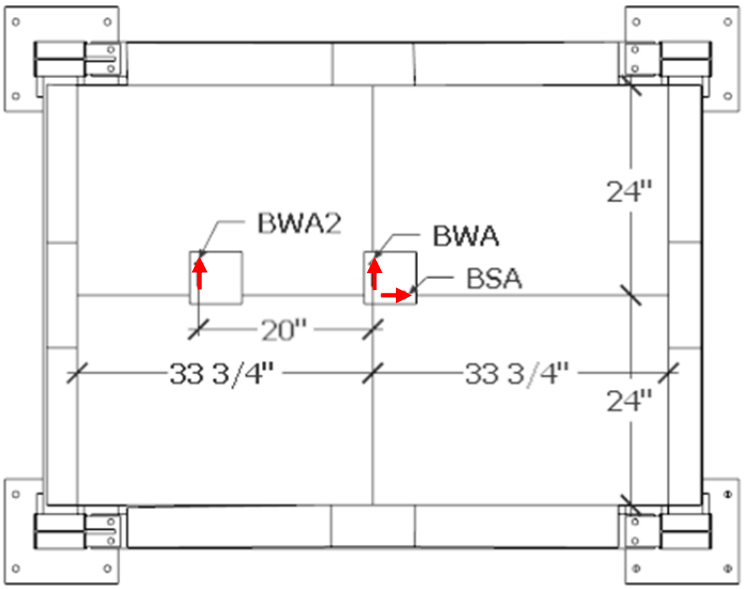

Figure 6.8 Location of Accelerometers on Bottom Slab

The accelerometers are placed in the same orientation on both the top and bottom slab as indicated in figures 6.7 and 6.8. The rotation of the levels, TTOR and BTOR, must be calculated using the difference between the acceleration at the center of mass and the acceleration at another point 20" offset from the center of mass. 20" was chosen because it was near the maximum distance feasible before interfering with the shaker placement. A long distance between the measurement locations improves the accuracy of the rotational reading because it increases the differential in acceleration between the two readings and reduces the effect of noise on the measurement.

6.2 Free Vibration

The original method of collecting modal behavior was planned to be free vibration testing. The concept is to measure the structure's performance as it settles from steady state shaking to ambient vibrations. This type of testing provides mode shapes, frequencies and damping values of the structure at a variety of amplitude levels and can detect nonlinearities in the structure. This data output provides many opportunities for intricate analysis of the structure's behavior.

6.2.1 Procedure

This free vibration testing was conducted using the following procedure. First the structure is excited to steady state motion induced by a shaker placed strategically to excite a particular mode. Next the data acquisition system is turned on the structure is monitored until it is relatively settled. The shaker is then turned off and the degradation

of the structures motion is measured in the form of a time history recording. The frequency can then be calculated by averaging the number of cycles over a window of time. The damping can be calculated using logarithmic decrement theory.

6.2.2 Complications

It was noticed during examination of the time history recordings that the damping changed unexpectedly during settlement; this is theorized to be due to the interaction with the shaker. When shut off, the shaker does not stop instantly and lock itself into one position, but instead its vibration is damped out through free vibration of the machine. The moveable mass is suspected to artificially increase the damping measurement of the structure while it is damping out in free vibration. This issue is believed to have significantly skewed the collected data and thus was not explored further.

The added complexity of the data set was another deterrent to using this method. Instead of a single value measurement of the structure, a time history recording of the measurements is produced. The method of selecting the exact value for comparison is made more complex by this overloading of data.

6.3 Test Method Selection

Forced vibration was chosen due to its reliability and clarity of the recorded data. This system was deemed overly complicated to implement for this study. This lack of ability to collect accurate data contributed to the selection of the forced vibration test method for further testing in this study.

7.0 ANALYTICAL MODEL

The structures examined in this thesis were modeled in ETABS. Modal analysis of each structure was completed for comparison with measured modes.

Figure 7.1 ETABS Model

7.1 Overview

There are two levels of the frame, each with an 18" thick concrete slab. The frame is composed of W6x8.5 sections throughout the structure. The width of the frame from centerline to centerline is 71 3/8" The length of the frame from centerline to centerline is 54". The height of the first floor from the top of the base plate to the

centerline of the beams is 48 1/2". The height of the second floor from centerline of beam to centerline of beam is 51 3/8".

7.2 Assumptions

Analytical models are simplified versions of real structures, and thus require assumptions to be made. For this study several assumptions required significant consideration as summarized in sections 7.2.1 through 7.2.3

7.2.1 Slab

The slab is modeled as area elements that provide both in plane and out of plane stiffness. This was chosen because the interaction of the slab with the moment frame is considered to be significant. The thick concrete slabs are nearly rigid compared to the steel moment frame. This provides a significant rotational restraint to the beams, and this behavior was captured by these meshed elements providing out of plane stiffness. The slab was meshed into segments approximately 6" square.

The structure's lower slab is separated from the columns to ensure that it does not alter the flexibility of the columns. This separation was incorporated into the analytical model by meshing the slab to the same distance from the columns as seen in Figure 7.2 on the next page. The corner that would overlap with the column was removed. A significant degree of flexibility is then allowed in the beams at the corners of the slab, while the majority of the beam is assisted by the thick concrete slab.

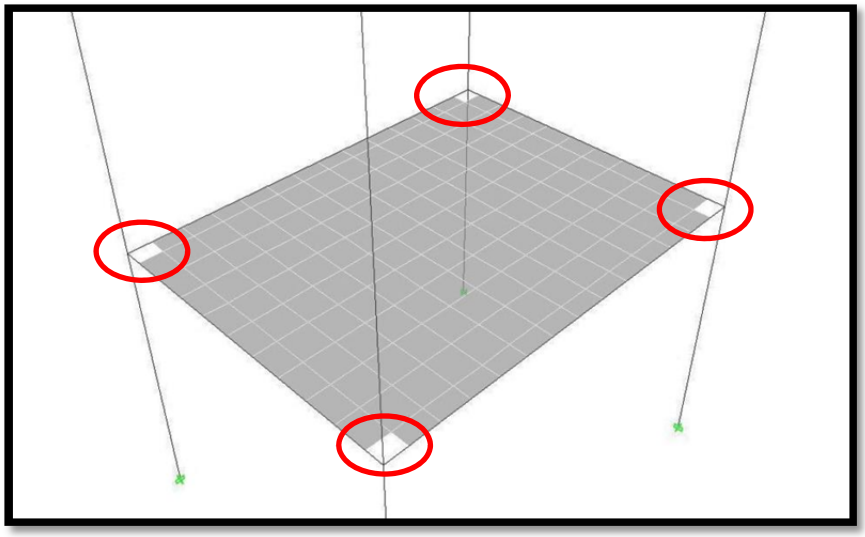

Figure 7.2 Slab Meshing

7.2.2 Base Fixity

The base plate was designed to maximize the stiffness of the connection to the slab, however it is believed that the flexibility of the slab played a considerable role in the frequency of modes in the strong axis direction. It is not believed to have played a significant role in the weak axis direction because the stiffness of the weak direction is 7 times lower than the strong direction. This phenomenon is examined in further detail in section 11.2.

For the analytical model, the decision was made to use fixed restraints at the base connection. The complexity of attempting to capture the flexibility of the slab was deemed unnecessary and overly complicated. There are many variables that would

require assumptions such as the behavior of the soil beneath the slab, and the degree of interaction with the rest of the building such as the near-by retaining wall and isolated slab. With the introduction of these approximated behaviors the performance of the technique would potentially have been considered unique to this structure.

7.2.3 Rigid End Offsets

Rigid end offsets of 3" were used with a rigidity factor of .75. This was chosen through careful examination of the beam to column connection, seen in figure 7.3 below. The length of 3" was used because it is half the member depth, which is the length from the center line of the beams to the edge of the panel zone. The plates used to stiffen this panel zone combined with the interaction of the beam resulted in this area being considered relatively rigid, but with some noticeable flexibility. For these reasons the rigidity factor of .75 was chosen.

Figure 7.3 Panel Zone

7.3 Modes

The following tables contain a summary of the six modes being examined. The frequency is displayed in the column on the left, and the mode shape is summarized on the right. These are normalized mode shapes

7.3.1 000 Configuration

		in/s/s	in/s/s	rad/s/s	in/s/s	in/s/s	rad/s/s
Freq	Mode	TWA	TSA	TTOR	BWA	BSA	BTOR
3.6 Hz	1WA	7.423	0.000	0.000	3.844	0.000	0.000
7.53 Hz	1SA	0.000	7.580	0.000	0.000	3.544	0.000
9.21 Hz	1T	0.041	-0.002	0.294	-0.091	0.001	0.144
9.25 Hz	2WA	-3.728	0.000	0.003	7.323	0.000	0.002
22.12 Hz	2SA	0.000	-3.429	0.000	0.000	7.460	0.000
25.58 Hz	2T	0.002	0.007	-0.148	0.000	0.015	0.298

Table 7.1 Analytical Modal Summary of 000

In this symmetric configuration one can see that each mode is exciting discrete measurements. This is shown by the values close to 0 in measurement locations that are orthogonal to the primary shaking direction. This discrete excitation allows for each mode to be independently measured without significant impurities from the other modes.

7.3.2 L00 Configuration

		in/s/s	in/s/s	rad/s/s	in/s/s	in/s/s	rad/s/s
Freq	Mode	TWA	TSA	TTOR	BWA	BSA	BTOR
4.46 Hz	1WA	8.015	0.040	0.034	2.242	0.014	0.026
7.53 Hz	1SA	-0.051	7.579	-0.001	0.050	3.544	-0.001
9.22 Hz	1T	-2.152	-0.002	0.242	4.171	0.001	0.118
13.46 Hz	2WA	-1.320	-0.045	-0.173	6.795	-0.062	-0.012
22.08 Hz	2SA	-0.001	-3.431	-0.002	0.021	7.459	0.002
28.65 Hz	2T	0.071	0.053	-0.112	-1.649	-0.044	0.307

Table 7.2 Analytical Modal Summary of L00

In this configuration the weak axis is asymmetric, this results in a significant weak axis measurements in the torsional mode shapes as can be seen by the highlighted values -2.152 and -1.649 in Table 7.2 above. These values have changed significantly from .041 and .000 in the base 000 configuration. This type of change to the structure is quantified through the use of the mode shape derived metrics.

7.3.3 L0R Configuration

		in/s/s	in/s/s	rad/s/s	in/s/s	in/s/s	rad/s/s
Freq	Mode	TWA	TSA	TTOR	BWA	BSA	BTOR
4.93 Hz	1WA	8.341	0.000	0.000	1.059	0.000	0.000
7.53 Hz	1SA	0.000	7.579	-0.004	0.000	3.544	-0.002
11.36 Hz	1T	-0.006	0.083	0.313	-0.001	0.073	0.092
16.45 Hz	2WA	-1.014	0.000	0.000	8.110	0.000	0.000
22.08 Hz	2SA	0.000	-3.432	-0.002	0.000	7.458	0.003
30.86 Hz	2T	0.002	0.072	-0.096	0.000	-0.065	0.320

Table 7.3 Analytical Modal Summary of L0R

In this symmetric configuration it can be seen that each mode is exciting particular measurement locations without impacting the other measurements. This is

similar to the 000 configuration with values close to 0 at all measurements not in the orientation of shaking.

7.3.4 LFR Configuration

		in/s/s	in/s/s	rad/s/s	in/s/s	in/s/s	rad/s/s
Freq	Mode	TWA	TSA	TTOR	BWA	BSA	BTOR
4.93 Hz	1WA	8.341	-0.034	0.000	1.059	-0.023	0.000
8.25 Hz	1SA	0.041	7.712	-0.042	-0.020	3.035	-0.024
11.71 Hz	1T	0.013	1.375	0.312	-0.033	0.014	0.081
16.45 Hz	2WA	-1.014	0.045	0.001	8.109	-0.038	0.000
23.7 Hz	2SA	0.002	-2.908	0.030	0.050	7.532	-0.049
32.68 Hz	2T	0.005	-0.248	-0.082	0.022	1.653	0.316

Table 7.4 Analytical Modal Summary of LFR

In this configuration the strong axis direction is asymmetric and this results in significant participation of the strong axis measurements in the torsional modes as can be seen by the highlighted values 1.375 and 1.653 in table 7.4 above. These values indicate contamination between the translational excitation in the strong axis direction and the torsion of the structure. This agrees with expectations about the asymmetric configuration's behavior.

7.3.5 LF0 Configuration

		in/s/s	in/s/s	rad/s/s	in/s/s	in/s/s	rad/s/s
Freq	Mode	TWA	TSA	TTOR	BWA	BSA	BTOR
4.5 Hz	1WA	8.057	-0.324	0.028	2.144	-0.241	0.022
8.08 Hz	1SA	1.014	7.232	-0.085	-1.263	2.989	-0.049
9.99 Hz	1T	-1.698	3.051	0.226	4.184	0.593	0.095
13.46 Hz	2WA	-1.305	-0.187	-0.178	6.720	-0.018	-0.012
23.58 Hz	2SA	-0.032	-2.893	0.039	0.600	7.432	-0.062
30.49 Hz	2T	0.058	-0.417	-0.093	-1.385	2.149	0.302

Table 7.5 Analytical Modal Summary of LF0

Due to the asymmetry in both directions, all of the directions of measurement have significant contributions to the mode shapes in this configuration. This makes measuring pure modes a difficult task because it requires iteration on the location of the shaker as detailed in section 11.1.

7.3.6 0F0 Configuration

		in/s/s	in/s/s	rad/s/s	in/s/s	in/s/s	rad/s/s
Freq	Mode	TWA	TSA	TTOR	BWA	BSA	BTOR
3.6 Hz	1WA	7.423	-0.010	0.000	3.844	-0.007	0.000
8.01 Hz	1SA	-0.002	7.229	-0.100	0.026	3.039	-0.058
9.25 Hz	1T	0.041	3.171	0.281	-0.067	0.529	0.112
10.22 Hz	2WA	-3.730	0.006	0.003	7.322	0.002	0.001
23.26 Hz	2SA	0.003	-2.835	0.070	0.001	7.028	-0.106
27.93 Hz	2T	0.009	-0.888	-0.109	-0.008	3.488	0.279

Table 7.6 Analytical Modal Summary of 0F0

The 0F0 configuration has clear contamination between the strong axis direction and rotation as can be seen by the highlighted values of 3.171 and 3.488 in Table 7.6 above. These show that the strong axis direction is participating in the torsional modes.

The highlighted values of -.100 and -.106 show that there is a torsional component to the strong axis modes as well.

7.4 Dynamic Vibration Modeling

ETABS was used to complete time history analyses of each forced vibration test. This provides information on the maximum shaker amplitude that is safe to excite the structure in each direction. The structure was found to have damping that varied with respect to amplitude, see appendix 14.2 for this relationship. Damping for each mode was decided in a conservative manner, with the lowest recorded damping being utilized for time history analysis in ETABS of the applied sinusoidal load. The chosen damping values are shown in table 7.7.

Mode	Damping
1WA	0.19%
1SA	0.30%
1T	0.28%
2WA	0.09%
2SA	0.18%
2T	0.11%

Table 7.7 Modal Damping Values

These values are used in ETABS to specify the damping for each mode. An applied sinusoidal load at the natural frequency is applied to the ETABS model for each mode that is tested. This allows a time history analysis to be completed to estimate the maximum allowable force output of the shaker. An initial force was estimated, the maximum accelerations were then compared with the allowable strength of the frame. A

capacity to demand ratio was applied to the initial guessed force. This yielded a theoretical maximum force output of the shaker for testing of each mode. A safety factor of 2 is then applied to yield the following safe shaker settings shown in table 7.8.

7.4.1 Safe Amplitudes of Excitation

In determining safe levels of excitation the strength capacity of the frame was determined with a load pattern derived from the particular mode shape. Accelerations were measured during testing, so the maximum theoretical accelerations that the frame could withstand before yielding was determined for each mode. These maximum theoretical accelerations were then divided in half to provide a factor of safety of 2 as seen in the table below.

The red highlighted values indicate cases where the maximum force is greater than the capability of the shaker, thus the maximum voltage of 1000mV is recommended as the maximum shaker setting.

First Yield					
Freq	Accel Location	Max Force (lbs)	Shaker Setting (mV)	Acceleration	Hand Calculation
3.61 Hz	**Top Slab**	4.35lbs	**156mV**	**168 mg**	**161 mg**
6.02 Hz	**Top Slab**	30.79lbs	**1000mV**	**1863 mg**	**1721 mg**
7.78 Hz	**Top Slab**	6.44lbs	**246mV**	**13 rad/s/s**	**14 rad/s/s**
10.04 Hz	**Bottom Slab**	12.40lbs	**496mV**	**728 mg**	**816 mg**
20.7 Hz	**Bottom Slab**	182.00lbs	**1000mV**	**7723 mg**	**7675 mg**
25.14 Hz	**Bottom Slab**	103.88lbs	**1000mV**	**37 rad/s/s**	**40 rad/s/s**
Safe Limit					
	D/C = 50%				
Safe Force	Predicted Force	Shaker Setting (mV)	Acceleration	Settlement time	
2.2lbs	2.2lbs	**78mV**	**84mg**	2.5min	
15.4lbs	15.4lbs	**579mV**	**932mg**	2.min	
3.2lbs	3.2lbs	**122mV**	**6.5 rad/s/s**	2.min	
6.2lbs	6.2lbs	**246mV**	**364mg**	1.5 min	
91.lbs	19.9lbs	**1000mV**	**3862mg**	30.sec	
51.9lbs	17.9lbs	**1000mV**	**18.5 rad/s/s**	30.sec	

Table 7.8 Safe Amplitudes of Excitation

The predicted force in table 7.8 is an estimate of the shaker's force output at that frequency and voltage based on linear interpolation of the shaker performance data in table 4.1.

The time history analysis in ETABS also allowed for an estimate to be made of the amount of time required for each mode to settle, as indicated by the settlement time in table 7.8.

7.4.2 Predicted Accelerations during Testing

Before testing was completed, a prediction of the expected maximum excitation was done with a time history analysis in ETABS. This was completed by applying a sinusoidal force to the ETABS model in the same orientation as the testing procedure. This was completed for all modes of all configurations that are examined in this thesis. The acceleration value chosen as the metric for comparison is based on the mode, where first modes in each direction are monitored by the acceleration at the top slab. Second modes in each direction are monitored by the acceleration at the bottom slab. This was decided based on the degree of freedom with the maximum excitation for each mode. The orientation of the acceleration is based on the mode, for instance in the 1WA mode the acceleration in the weak axis direction is monitored at the top slab.

These predicted accelerations are based on damping values calculated via the half power band method. The frequency sweeps used for final mode shape collection were used for this calculation, thus the damping values shown here are different than the damping value used for the estimation of maximum safe shaker voltages. In the safe amplitude estimation a conservative damping value is desired, but in this acceleration prediction a more accurate damping measurement is used based on the actual amplitude of testing. The following tables show the modes of each configuration. These tables display the frequency and strength of the applied load, and the measured damping of each mode on the left side. The predicted acceleration is shown on the right, as is the measured acceleration and the percent error between the two.

7.4.2.1 000 Configuration

000 Mode	Modal Period (sec)	Freq. (Hz)	Damping	Load (lbs)	Predicted Acc. (in/s^2 or rad/s^2)	Predicted Acc. (mg or rad/s^2)	Measured Acc. (mg or rad/s^2)	Error (%)
1WA	0.2778	3.60	0.24%	.89	8.43	21.82	18.35	19
1SA	0.1328	7.53	0.34%	3.31	19.27	49.87	63.4	-21
1T	0.1086	9.21	0.41%	1.09	0.63	0.63	0.418	51
2WA	0.1080	9.26	0.20%	1.59	18.11	46.87	75.15	-38
2SA	0.0451	22.18	0.27%	2.01	18	46.58	55.93	-17
2T	0.0390	25.67	0.56%	2.31	0.96	0.96	0.5538	74

Table 7.9 000 Configuration Forced Vibration Predictions

7.4.2.2 L00 Configuration

L00 Mode	Modal Period (sec)	Freq. (Hz)	Damping	Load (lbs)	Predicted Acc. (in/s^2 or rad/s^2)	Predicted Acc. (mg or rad/s^2)	Measured Acc. (mg or rad/s^2)	Error (%)
1WA	0.2244	4.46	0.24%	.88	8.132	21.05	23.58	-11
1SA	0.1328	7.53	0.34%	3.31	23.24	60.14	64.7	-7
1T	0.1084	9.22	0.31%	1.09	0.44	0.44	0.496	-12
2WA	0.0741	13.49	0.22%	1.48	13.87	35.90	50.73	-29
2SA	0.0451	22.17	0.24%	2.01	20.08	51.97	58.56	-11
2T	0.0348	28.74	0.86%	2.13	0.60	0.60	0.3169	91

Table 7.10 L00 Configuration Forced Vibration Predictions

7.4.2.3 L0R Configuration

L0R Mode	Modal Period (sec)	Freq. (Hz)	Damping	Load (lbs)	Predicted Acc. (in/s^2 or rad/s^2)	Predicted Acc. (mg or rad/s^2)	Measured Acc. (mg or rad/s^2)	Error (%)
1WA	0.2029	4.93	0.24%	.88	10.41	26.94	26.58	1
1SA	0.1328	7.53	0.42%	3.31	18.95	49.04	62.65	-22
1T	0.0879	11.38	0.28%	1.05	0.9996	1.00	0.64433	55
2WA	0.0606	16.49	0.19%	1.39	21.12	54.66	68.59	-20
2SA	0.0451	22.17	0.23%	2.01	20.9	54.09	58.87	-8
2T	0.0323	30.95	0.55%	2.01	1.014	1.01	0.54847	85

Table 7.11 L0R Configuration Forced Vibration Predictions

7.4.2.4 LFR Configuration

LFR Mode	Modal Period (sec)	Freq. (Hz)	Damping	Load (lbs)	Predicted Acc. (in/s^2 or rad/s^2)	Predicted Acc. (mg or rad/s^2)	Measured Acc. (mg or rad/s^2)	Error (%)
1WA	0.2029	4.93	0.25%	.88	10	25.88	28.24	-8
1SA	0.1211	8.26	0.38%	3.28	24.25	62.76	67.18	-7
1T	0.0853	11.72	0.25%	1.04	1.10	1.10	0.6586	67
2WA	0.0607	16.49	0.19%	1.39	21.03	54.43	67.58	-19
2SA	0.0421	23.78	0.10%	1.94	55.78	144.36	17.64	718
2T	0.0305	32.83	0.34%	1.91	1.45	1.45	0.74707	94

Table 7.12 LFR Configuration Forced Vibration Predictions

7.4.2.5 LF0 Configuration

LF0 Mode	Modal Period (sec)	Freq. (Hz)	Damping	Load (lbs)	Predicted Acc. (in/s^2 or rad/s^2)	Predicted Acc. (mg or rad/s^2)	Measured Acc. (mg or rad/s^2)	Error (%)
1WA	0.2220	4.50	0.23%	.88	8.878	22.98	24.91	-8
1SA	0.1238	8.08	0.33%	3.29	28.18	72.93	65.64	11
1T	0.1000	10.00	0.20%	1.08	0.77	0.77	0.54567	41
2WA	0.0741	13.50	0.23%	1.48	12.99	33.62	52.65	-36
2SA	0.0422	23.70	0.19%	1.94	29.9	77.38	16.23	377
2T	0.0326	30.65	0.55%	2.02	0.88	0.88	0.52343	67

Table 7.13 LF0 Configuration Forced Vibration Predictions

7.4.2.6 0F0 Configuration

0F0 Mode	Modal Period (sec)	Freq. (Hz)	Damping	Load (lbs)	Predicted Acc. (in/s^2 or rad/s^2)	Predicted Acc. (mg or rad/s^2)	Measured Acc. (mg or rad/s^2)	Error (%)
1WA	0.2778	3.60	0.36%	.89	5.65	14.62	18.06	-19
1SA	0.1248	8.01	0.36%	3.29	26.8	69.36	55.39	25
1T	0.1080	9.26	0.32%	1.09	0.39	0.39	0.46087	-16
2WA	0.0977	10.24	0.20%	1.57	17.54	45.39	73.44	-38
2SA	0.0429	23.33	0.27%	1.96	21.43	55.46	27.63	101
2T	0.0356	28.08	0.64%	2.17lbs	0.70	0.70	0.27617	154

Table 7.14 0F0 Configuration Forced Vibration Predictions

7.4.2.7 Summary

The predicted accelerations tend to have significant errors compared to the measured values. This shows that the damping value in the analytical model is not accurately capturing the structure's behavior. The damping value was calculated using the half power band method, which assumes that the damping value is constant with respect to amplitude. The structure was found to have damping that varied with amplitude, as shown in section 14.2. This variance in damping is believed to be the primary source of error in the predicted acceleration calculations. With the inconsistency in the damping, the model is unable to accurately predict the peak acceleration of the structure.

8.0 TESTING RESULTS

8.1 Forced Vibration Testing of Braced Configurations

Forced Vibration Testing (FVT) was completed on the structure to measure raw mode shapes. The raw mode shapes are composed of acceleration measurements read during testing. These acceleration measurements were calculated from averages taken over 90 seconds once the structure had reached steady state shaking as defined in section 5.4.4.

The following tables show the measured mode shapes of the various configurations tested. See section 4.7 for descriptions of each configuration. For descriptions of measurement locations and mode names see the list of nomenclature on pg xiv.

Force is defined as the peak output of the shaker's sinusoidal movement. This is dependent on the voltage and frequency of the signal sent to the shaker. Forces are calculated using linear interpolation of the performance data in table 4.3.

8.1.1 000 Configuration

The 000 configuration does not have any braces engaged. This creates a symmetric and regular structure. The symmetry of the system allowed for precision excitation of each mode without significant contamination from other modes. See the raw measured mode shapes in table 8.1.

			in/s^2	in/s^2	rad/s^2	in/s^2	in/s^2	rad/s^2
Force	Freq	Mode	TWA	TSA	TTOR	BWA	BSA	BTOR
.96 lbs	3.61 Hz	1WA	7.092	0.248	0.004	4.043	0.032	0.002
3.52 lbs	6.02 Hz	1SA	0.475	24.497	0.058	0.070	12.463	0.012
1.22 lbs	7.78 Hz	1T	0.267	1.194	0.418	-0.358	0.401	0.221
1.68 lbs	10.04 Hz	2WA	-16.296	0.555	0.035	29.038	0.493	0.021
2.14 lbs	20.7 Hz	2SA	0.186	-11.037	0.025	0.130	21.610	-0.006
2.44 lbs	25.14 Hz	2T	-0.041	-0.738	-0.284	-0.222	-1.187	0.554

Table 8.1 Experimental Mode Shapes of 000

8.1.2 L00 Configuration

The L00 configuration has a single brace placed on the left side of the structure in the weak axis frame direction. This has a large impact on the center of rigidity pushing it 25.6” away from the center of mass.

			in/s^2	in/s^2	rad/s^2	in/s^2	in/s^2	rad/s^2
Force	Freq	Mode	TWA	TSA	TTOR	BWA	BSA	BTOR
.81 lbs	4.35 Hz	1WA	9.111	0.256	0.058	3.648	0.107	0.041
3.52 lbs	6.02 Hz	1SA	0.356	24.999	-0.027	-0.006	12.683	-0.008
1.18 lbs	8.5 Hz	1T	5.591	0.877	0.496	5.779	0.264	0.236
1.56 lbs	12.66 Hz	2WA	-5.670	-0.482	-0.355	19.603	-0.858	-0.030
2.14 lbs	20.7 Hz	2SA	0.167	-11.597	-0.005	-0.526	22.629	0.032
1.82 lbs	29.1 Hz	2T	-0.185	-0.186	-0.110	2.278	-0.316	0.317

Table 8.2 Experimental Mode Shapes of L00

8.1.3 L0R Configuration

The L0R configuration has braces on the left and right side of the structure in the weak axis frame direction. It is symmetric in both directions and therefore has aligned centers of mass and rigidity which allows for very accurate mode shapes to be measured.

			in/s^2	in/s^2	rad/s^2	in/s^2	in/s^2	rad/s^2
Force	Freq	Mode	TWA	TSA	TTOR	BWA	BSA	BTOR
.84 lbs	5.08 Hz	1WA	10.269	0.539	0.004	2.262	0.315	0.001
3.52 lbs	6.02 Hz	1SA	0.955	24.209	-0.012	0.075	12.284	-0.016
1.18 lbs	8.5 Hz	1T	0.059	0.794	0.644	0.233	0.512	0.214
1.56 lbs	12.66 Hz	2WA	-5.411	0.373	0.020	26.505	0.362	0.005
2.14 lbs	20.78 Hz	2SA	0.166	-11.718	-0.003	0.611	22.747	0.031
1.82 lbs	30.9 Hz	2T	0.201	0.243	-0.162	0.865	0.332	0.549

Table 8.3 Experimental Mode Shapes of L0R

8.1.4 LFR Configuration

The LFR configuration has all 3 braces engaged, stiffening the frame in both directions. The weak axis is still symmetric due to having braces on both sides, however the strong axis is has a center of rigidity shifted 9.5” away from the center of mass. This is a relatively small eccentricity and allowed for accurate mode shape measurement.

			in/s^2	in/s^2	rad/s^2	in/s^2	in/s^2	rad/s^2
Force	Freq	Mode	TWA	TSA	TTOR	BWA	BSA	BTOR
.84 lbs	5.07 Hz	1WA	10.912	-0.384	-0.002	2.387	0.012	-0.001
3.51 lbs	6.56 Hz	1SA	0.427	25.957	-0.111	0.227	11.631	-0.046
1.13 lbs	10.58 Hz	1T	0.088	2.970	0.659	0.256	0.381	0.198
1.42 lbs	14.54 Hz	2WA	-5.331	-0.452	0.019	26.113	0.301	-0.005
2.14 lbs	22.72 Hz	2SA	0.180	-2.646	0.068	4.889	6.816	-0.095
1.82 lbs	32.8 Hz	2T	0.227	-0.846	-0.194	0.771	4.715	0.747

Table 8.4 Experimental Mode Shapes of LFR

8.1.5 LF0 Configuration

The LF0 configuration has a brace on the left and front sides of the structure. This makes both directions asymmetric with eccentricities of 8.4" and 17.0" in the weak and strong directions respectively.

			in/s^2	in/s^2	rad/s^2	in/s^2	in/s^2	rad/s^2
Force	Freq	Mode	TWA	TSA	TTOR	BWA	BSA	BTOR
.84 lbs	4.4 Hz	1WA	9.625	-0.567	0.054	3.742	0.630	0.037
3.51 lbs	6.56 Hz	1SA	-4.467	25.363	-0.192	0.981	11.604	-0.096
1.16 lbs	9.16 Hz	1T	-5.468	4.907	0.546	7.025	0.845	0.236
1.56 lbs	12.74 Hz	2WA	-5.857	1.002	-0.390	20.344	-0.741	-0.032
2.06 lbs	22.04 Hz	2SA	-0.081	-2.554	0.135	1.157	6.273	-0.168
1.82 lbs	31.3 Hz	2T	-0.462	-0.961	-0.160	-3.075	4.578	0.523

Table 8.5 Experimental Mode Shapes of LF0

8.1.6 0F0 Configuration

The 0F0 configuration has a brace on the front side of the structure. This makes the weak axis symmetric and the strong axis asymmetric with a theoretical eccentricity of 9.0".

			in/s^2	in/s^2	rad/s^2	in/s^2	in/s^2	rad/s^2
Force	Freq	Mode	TWA	TSA	TTOR	BWA	BSA	BTOR
.96 lbs	3.61 Hz	1WA	6.977	-0.240	-0.009	3.988	0.033	-0.002
3.52 lbs	6.28 Hz	1SA	-0.481	21.403	-0.288	-0.318	10.241	-0.157
1.18 lbs	8.66 Hz	1T	0.270	5.421	0.461	0.503	1.222	0.212
1.68 lbs	10.04 Hz	2WA	-15.938	-0.390	0.039	28.377	0.467	0.022
2.06 lbs	22.3 Hz	2SA	0.059	-4.293	0.161	0.042	10.675	-0.211
2.13 lbs	28.1 Hz	2T	0.024	-1.039	-0.111	0.194	3.919	0.276

Table 8.6 Experimental Mode Shapes of 0F0

8.2 Frequency Comparison to Analytical Model

8.2.1 000 Configuration

000	1WA	1SA	1T	2WA	2SA	2T
Measured	3.61Hz	6.02Hz	7.78Hz	10.04Hz	20.7Hz	25.14Hz
Analytical	3.6Hz	7.53Hz	9.21Hz	9.25Hz	22.12Hz	25.58Hz
Error	-0.3%	25.1%	18.4%	-7.9%	6.9%	1.8%

Table 8.7 Frequency Errors of 000

The comparison of the experimental to measured frequencies yielded some surprising results. The strong axis orientation had significant error at 25.1% and 6.9% errors for the first and second modes respectively, as can be seen in table 8.7 above. This is a significant error that is believed to be primarily due to the interaction of the slab foundation with the bottom column. This hypothesis is investigated further in section 11.3. The first and second weak axis modes had errors of -.3% and -7.9% respectively. This is a significantly more accurate result than in the strong axis direction and agrees with the hypothesis that the slab interaction has a considerable effect in the strong direction behavior.

8.2.2 L00 Configuration

L00	1WA	1SA	1T	2WA	2SA	2T
Measured	4.35Hz	6.02Hz	8.5Hz	12.66Hz	20.7Hz	29.1Hz
Analytical	4.46Hz	7.53Hz	9.22Hz	13.46Hz	22.08Hz	28.65Hz
Error	2.5%	25.1%	8.5%	6.3%	6.7%	-1.5%

Table 8.8 Frequency Errors of L00

All modal frequencies for this configuration, except for the 1st strong axis mode, had errors below 9%. This shows a moderate level of agreement between the structure and the analytical model. The 1st strong axis mode had an error of 25.1%, the same as in the 000 configuration and is due to the same issues discussed previously. In general, the frequencies were higher in the analytical model than the actual structure. This is believed to be due to an over-estimation of the stiffness of the braces.

8.2.3 L0R Configuration

L0R	1WA	1SA	1T	2WA	2SA	2T
Measured	5.08Hz	6.02Hz	8.5Hz	12.66Hz	20.78Hz	30.9Hz
Analytical	4.93Hz	7.53Hz	11.36Hz	16.45Hz	22.08Hz	30.86Hz
Error	-3.0%	25.1%	33.6%	29.9%	6.3%	-0.1%

Table 8.9 Frequency Errors of L0R

The analytical model for the L0R configuration had significant errors in the first strong axis and torsional modes as well as the second weak axis mode of 25.1%, 33.6% and 29.9% respectively as shown by the highlighted values in table 8.9 above.

8.2.4 LFR Configuration

LFR	1WA	1SA	1T	2WA	2SA	2T
Measured	5.07Hz	6.56Hz	10.58Hz	14.54Hz	22.72Hz	32.8Hz
Analytical	4.93Hz	8.25Hz	11.71Hz	16.45Hz	23.7Hz	32.68Hz
Error	-2.8%	25.8%	10.7%	13.1%	4.3%	-0.4%

Table 8.10 Frequency Errors of LFR

This configuration had significant errors in the first strong and torsional modes as well as the second weak axis mode of 25.8%, 10.7% and 13.1% respectively. The 000

configuration had errors of 25.1%, 18.4% and -7.9% for the same modes. The increase in error in the weak axis from -7.9% to 13.1% suggests that the braces are not increasing the stiffness as much as the analytical model is predicting.

8.2.5 LF0 Configuration

LF0	1WA	1SA	1T	2WA	2SA	2T
Measured	4.4Hz	6.56Hz	9.16Hz	12.74Hz	22.04Hz	31.3Hz
Analytical	4.5Hz	8.08Hz	9.99Hz	13.46Hz	23.58Hz	30.49Hz
Error	2.3%	23.2%	9.1%	5.7%	7.0%	-2.6%

Table 8.11 Frequency Errors of LF0

Five of the six modes for the LF0 configuration had frequency errors below 10%, this suggests a moderate level of agreement between the experimental and analytical models. The main error comes in the first strong axis mode, with an error of 23.2% as shown by the highlighted value in table 8.11.

8.2.6 0F0 Configuration

0F0	1WA	1SA	1T	2WA	2SA	2T
Measured	3.61Hz	6.28Hz	8.66Hz	10.04Hz	22.3Hz	28.1Hz
Analytical	3.6Hz	8.01Hz	9.25Hz	10.22Hz	23.26Hz	27.93Hz
Error	-0.3%	27.5%	6.8%	1.8%	4.3%	-0.6%

Table 8.12 Frequency Errors of 0F0

The 0F0 configuration has frequency errors below 7% for all modes except the first strong axis mode at 27.5%. This is increased from 25.1% in the 000 configuration, which indicates the brace is increasing the stiffness of the structure slightly more than the analytical model is estimating. The difference is believed to be due to the error in the stiffness of the strong axis direction discussed in further detail in 7.2.2.

8.2.7 Summary

Overall the frequencies tend to have significant levels of error with an average of 9.9%. This result is reflective of the absolute method of comparison that the frequency metric utilizes. The weak axis directions tend to have better accuracy than the strong axis directions. This is believed to be due to the interaction with the slab having a more significant impact on the strong axis directions because of the greater stiffness relative to the weak axis direction. The slab and column are working in series, and because the stiffness of the strong axis is closer to the stiffness of the slab, the slab plays a more significant role in the behavior of the strong axis than in the weak axis. In the weak direction the slab is relatively stiff and therefore does not considerably impact the stiffness of the overall system.

The widespread error in the frequency comparisons indicates that modal frequencies are not a reliable or robust way to predict damage in a structure. The lack of correlation that was found motivated the decision to stop further analysis of modal frequencies.

9.0 ANALYSIS

The mode shape and frequency analyses are completed independently. In this chapter, the prediction of the change to the structure is decided through use of the mode shape derived prediction metrics detailed in section 5.1. Before any further analysis is completed, the raw measured mode shapes shown in section 8.1 are normalized using the procedure discussed in section 5.1.6.

9.1 Modal Contamination

Modal contamination is where two modes have similar shapes and tend to be excited together. A quantitative metric of the degree of contamination is created through the modal contamination matrix, as detailed in section 5.1.3. Contamination can occur if a translational mode gains significant torsional behavior due to a brace configuration that is asymmetric. Torsional modes also may gain significant translational behavior in these configurations.

Other factors that can influence modal contamination are the relationship between the frequencies of the two modes, and their damping values. If the modes have similar frequencies then excitation of one mode will tend to excite the other. Large amounts of damping exacerbate this because they spread out the dynamic amplification response. See section 5.3 for a detailed discussion of this change to the dynamic amplification characteristics.

Contamination is partially driven by the relationship between the frequencies and damping of each mode. If the two modes have frequencies that are close to each other, excitation of one will tend to excite the other. Higher damping values can exacerbate this contamination because they spread out the dynamic amplification response, but the low damping in this particular structure minimizes the amount of contamination. For more details on the relationship between damping and the dynamic amplification factor see section 5.3.

9.1.1 000 Configuration

000	1WA	1SA	1T	2WA	2SA	2T
1WA	1.0000	0.0020	0.0004	0.0011	0.0000	0.0001
1SA	0.0020	1.0000	0.0239	0.0003	0.0006	0.0085
1T	0.0004	0.0239	1.0000	0.0000	0.0001	0.0003
2WA	0.0011	0.0003	0.0000	1.0000	0.0001	0.0001
2SA	0.0000	0.0006	0.0001	0.0001	1.0000	0.0044
2T	0.0001	0.0085	0.0003	0.0001	0.0044	1.0000

Table 9.1 000 Modal Contamination

Table 9.1 shows the modal contamination of the 000 configuration. This is calculated using Mass Weighted Modal Assurance Criterion (MWMAC) as detailed in section 5.1.1.1. This table represents the degree to which the modes are contaminated with each other.

The 000 configuration has no eccentricity between the centers of mass and rigidity. This makes contamination insignificant for this configuration as indicated by the low off-diagonal terms in table 9.1. The largest value is .0239 for the interaction between

the 1SA and 1T modes as seen by the highlighted values in table 9.1. This value shows a slight degree of contamination between these modes. The other off-diagonal terms are all below .01 indicating very little contamination for this configuration.

9.1.2 L00 Configuration

L00	1WA	1SA	1T	2WA	2SA	2T
1WA	1.0000	0.0012	0.3651	0.0017	0.0000	0.0159
1SA	0.0012	1.0000	0.0014	0.0009	0.0004	0.0012
1T	0.3651	0.0014	1.0000	0.0082	0.0000	0.0277
2WA	0.0017	0.0009	0.0082	1.0000	0.0019	0.1160
2SA	0.0000	0.0004	0.0000	0.0019	1.0000	0.0000
2T	0.0159	0.0012	0.0277	0.1160	0.0000	1.0000

Table 9.2 L00 Modal Contamination

L00 has significant contamination between the 1WA and 1T modes. This is indicated by the large value of .3651 as highlighted in table 9.2. This shows that the measured 1WA and 1T modes are significantly contaminated by each other.

Figure 9.1 displays these two mode shapes that were found to have significant contamination. The displayed mode shapes are normalized and therefore do not have specific units, but are proportionately correct.

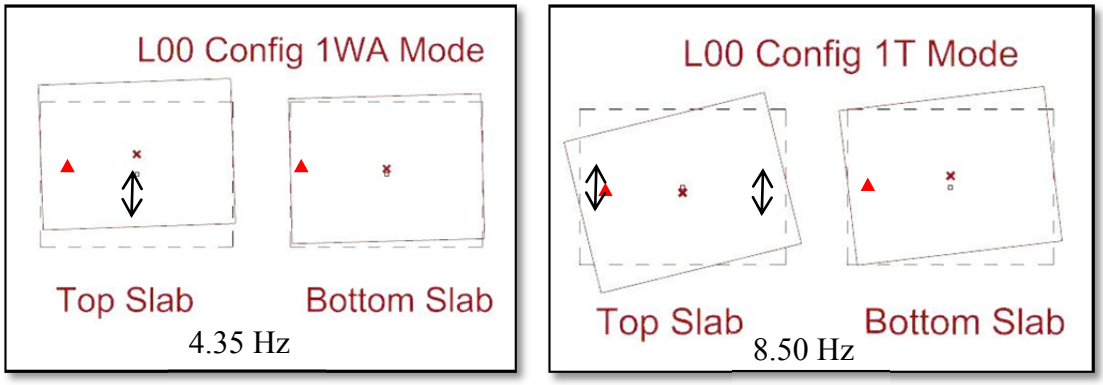

Figure 9.1 L00 Modal Contamination Relationship

Legend

= Location and orientation of shaker
= Undeformed center of mass location
= Deformed center of mass location
= Undeformed center of rigidity
= Undeformed slab outline

These two modes were found to have the most significant contamination of any tested configuration. This is due to the translation at the top slab in the first torsional (1T) mode.

The translation of the center of mass in the 1T mode contributes to incidental excitation when the 1WA mode is excited. This is because the shaker location for the 1WA configuration is in a similar orientation to the translation of the center of mass in the 1T mode. The shaker placement could be refined in future testing to minimize this contamination as discussed in section 11.1.

9.1.3 L0R Configuration

L0R	1WA	1SA	1T	2WA	2SA	2T
1WA	1.0000	0.0088	0.0004	0.0008	0.0003	0.0008
1SA	0.0088	1.0000	0.0015	0.0002	0.0003	0.0002
1T	0.0004	0.0015	1.0000	0.0011	0.0002	0.0004
2WA	0.0008	0.0002	0.0011	1.0000	0.0008	0.0033
2SA	0.0003	0.0003	0.0002	0.0008	1.0000	0.0020
2T	0.0008	0.0002	0.0004	0.0033	0.0020	1.0000

Table 9.3 L0R Modal Contamination

The L0R configuration has off-diagonal terms of the modal contamination matrix that are all lower than .009, indicating the second smallest amount of contamination of any tested configuration. This is theorized to be lower than the 000 configuration because the braces in the weak direction reduce incidental torsion when exciting the 1SA mode. The very low amount of contamination in this configuration means that sweeping will have a negligible impact on the mode shapes because they are already very close to orthogonal.

9.1.4 LFR Configuration

LFR	1WA	1SA	1T	2WA	2SA	2T
1WA	1.0000	0.0002	0.0000	0.0007	0.0210	0.0004
1SA	0.0002	1.0000	0.0028	0.0000	0.0028	0.0025
1T	0.0000	0.0028	1.0000	0.0007	0.0068	0.0005
2WA	0.0007	0.0000	0.0007	1.0000	0.2841	0.0010
2SA	0.0210	0.0028	0.0068	0.2841	1.0000	0.0047
2T	0.0004	0.0025	0.0005	0.0010	0.0047	1.0000

Table 9.4 LFR Modal Contamination

The LFR configuration was found to have significant contamination between the 2WA and 2SA modes as indicated by the highlighted off diagonal terms of .2841 in table 9.4. The primary factor theorized to be responsible for this contamination is the position of the shaker. In testing the 2SA mode, the shaker is located on the bottom slab at the center of mass, which is 9.5" eccentric from the center of rigidity and contributes to contamination of the 2WA and 2SA modes. While using the bottom slab for excitation of the higher modes worked well for the 000 configuration, the addition of braces reduces the effectiveness of this approach. The braces reduce the displacement experienced at the bottom slab, making the shaker placement here at the bottom slab less effective. This could be improved upon in future testing as discussed in further detail in section 11.1.

9.1.5 LF0 Configuration

LF0	1WA	1SA	1T	2WA	2SA	2T
1WA	1.0000	0.0324	0.0001	0.0011	0.0121	0.0017
1SA	0.0324	1.0000	0.0239	0.0276	0.0007	0.0020
1T	0.0001	0.0239	1.0000	0.0086	0.0251	0.0000
2WA	0.0011	0.0276	0.0086	1.0000	0.0041	0.0106
2SA	0.0121	0.0007	0.0251	0.0041	1.0000	0.0933
2T	0.0017	0.0020	0.0000	0.0106	0.0933	1.0000

Table 9.5 LF0 Modal Contamination

The modal contamination matrix of the LF0 configuration did not have large amounts of contamination between any two modes, however it was found to have a moderate degree of contamination in many different modes indicated by the 12 off-diagonal values that are between .01 and .04. The most significant contamination was between the 2SA and 2T modes with off diagonal terms of .0933, but this value is not considered significant enough to warrant re-ordering of the sweeping procedure. This shows that modes are not being discretely coupled such as in the L00 configuration, but are more widely contaminated by a variety of other modes.

9.1.6 0F0 Configuration

0F0	1WA	1SA	1T	2WA	2SA	2T
1WA	1.0000	0.0014	0.0000	0.0010	0.0001	0.0006
1SA	0.0014	1.0000	0.0030	0.0003	0.0017	0.0042
1T	0.0000	0.0030	1.0000	0.0026	0.0036	0.0004
2WA	0.0010	0.0003	0.0026	1.0000	0.0003	0.0009
2SA	0.0001	0.0017	0.0036	0.0003	1.0000	0.0000
2T	0.0006	0.0042	0.0004	0.0009	0.0000	1.0000

Table 9.6 0F0 Modal Contamination

No significant contamination was observed with the 0F0 configuration as seen by the off diagonal terms in table 9.6 all being lower than .005. This shows the least amount of contamination of any tested configuration. This is theorized to be due to the shaker placement as detailed in section 11.1, and shows that the measured modes are very close to orthogonal.

9.2 Sweeping Order

Sweeping the modes ensures the measured mode shapes are orthogonal. The sweeping calculation is described in further detail in section 5.1.2. This is only required for the experimental results, as the results from ETABS are already orthogonal. Sweeping reduces the impact of modal contamination on the accuracy of the analysis by removing traces of modes from each other. The order in which sweeping occurs requires much examination and consideration of the modal contamination matrices.

The default approach is to sweep starting with the lowest frequency mode and moving up to the highest frequency mode. In configuration without significant

contamination this process works well. It was discovered that in configurations with significant contamination this sweeping method was found to have contaminated some modes by sweeping them with impure modes. A solution to this issue was found by ordering the sweeping based on observed modal contamination.

In the tested configurations, two pairs of modes were considered to be have degrees of contamination that required changing the sweeping order as seen in the following tables. These two pairs of modes were the 1WA and 1T modes of the L00 configuration, and the 2WA and 2SA modes of the LFR configuration as discussed previously in section 9.1. The other configurations were swept in the default order as seen in figure 9.7.

As a way of defining a specific sweeping order, a matrix is used. This sweeping order matrix shows which modes are being used for sweeping and which are being swept, along with the order in which this process occurs. Each row of the matrix represents a step in the sweeping process. Each column represents a mode. The value in each cell is the mode that is being used for sweeping in that step. The resulting matrix clearly displays the exact order in which the sweeping process occurs.

9.2.1 000, L0R, LF0, 0F0 Configurations

Step	1WA (1)	1SA (2)	1T (3)	2WA (4)	2SA (5)	2T (6)
1st	-	1	1	1	1	1
2nd	-	-	2	2	2	2
3rd	-	-	-	3	3	3
4th	-	-	-	-	4	4
5th	-	-	-	-	-	5
6th	-	-	-	-	-	-

Table 9.7 Default Sweeping Order

The 000, L0R, LF0 and 0F0 configurations did not display signs of significant contamination, and therefore were swept in the default order moving from the lowest frequency mode to the highest, as indicated in table 9.7 above.

9.2.2 L00 Configuration

Step	1WA (1)	1SA (2)	1T (3)	2WA (4)	2SA (5)	2T (6)
1st	2	-	2	2	2	2
2nd	4	-	4	-	4	4
3rd	5	-	5	-	-	5
4th	6	-	6	-	-	-
5th	-	-	1	-	-	-
6th	-	-	-	-	-	-

Table 9.8 L00 Sweeping Order

For the L00 configuration, the 1WA and 1T modes were found to be significantly coupled. To prevent these impure modes from contaminating other modes, they are moved to the end of the sweeping process as shown in table 9.8. The other four modes are swept as normal, but the 1WA and 1T are delayed until the end of the process preventing them from being used for sweeping of other modes. The decision to sweep

with the 1WA mode and leave the 1T mode for last is based on the theory that the lower frequency modes should be more pure than higher frequency modes. This is based on observations from research completed by Dr. Graham and Dr. McDaniel that showed greater difficulty in measuring higher frequency mode shapes.

9.2.3 LFR Configuration

Step	1WA (1)	1SA (2)	1T (3)	2WA (4)	2SA (5)	2T (6)
1st	-	1	1	1	1	1
2nd	-	-	2	2	2	2
3rd	-	-	-	3	3	3
4th	-	-	-	6	6	-
5th	-	-	-	-	4	-
6th	-	-	-	-	-	-

Table 9.9 LFR Sweeping Order

The LFR configuration had contamination between the 4th (2WA) and 5th (2SA) modes, which caused the decision to re-order the sweeping process of these modes. They are moved to the end of the sweeping process and this prevents them from contaminating more pure modes.

9.3 Sweeping of Experimental Mode Shapes

The following tables display the normalized experimental mode shapes before and after sweeping has been completed. Normalization is detailed in section 5.1.6 and is required for proper comparison with the computational mode shapes. After sweeping, many of the modes that were not originally coupled have remained essentially the same; however impure modes show noticeable changes. This swept set of mode shapes is used

for further analysis because it does not contain the impurities of the raw data, which ensures a proper comparison between the analytical and measured mode shapes.

9.3.1 000 Configuration

Raw	1WA	1SA	1T	2WA	2SA	2T	Units
TWA	7.251	0.144	0.184	-4.023	0.063	-0.022	in/s/s
TSA	0.254	7.440	0.823	0.137	-3.736	-0.393	in/s/s
TTOR	0.004	0.018	0.288	0.009	0.009	-0.151	rad/s/s
BWA	4.134	0.021	-0.247	7.168	0.044	-0.118	in/s/s
BSA	0.032	3.785	0.276	0.122	7.316	-0.631	in/s/s
BTOR	0.002	0.004	0.152	0.005	-0.002	0.295	rad/s/s

Swept	1WA	1SA	1T	2WA	2SA	2T	Units
TWA	7.251	-0.184	0.071	-4.257	0.102	0.009	in/s/s
TSA	0.254	7.428	-0.325	0.011	-3.911	0.042	in/s/s
TTOR	0.004	0.017	0.285	0.010	0.007	-0.149	rad/s/s
BWA	4.134	-0.166	-0.302	7.033	-0.002	-0.015	in/s/s
BSA	0.032	3.783	-0.307	0.060	7.227	0.181	in/s/s
BTOR	0.002	0.004	0.151	0.006	-0.003	0.295	rad/s/s

Table 9.10 000 Swept Experimental Mode Shapes

The 000 configuration did not experience large impurities which led to sweeping having a minor effect on the mode shapes. The most significant impact was to the torsional modes which had noticeable changes to the translational modes, but the torsional measurements were essentially unchanged.

9.3.2 L00 Configuration

Raw	1WA	1SA	1T	2WA	2SA	2T	Units
TWA	7.644	0.106	2.880	-2.081	0.054	-0.177	in/s/s
TSA	0.215	7.453	0.452	-0.177	-3.745	-0.178	in/s/s
TTOR	0.049	-0.008	0.256	-0.130	-0.002	-0.105	rad/s/s
BWA	3.061	-0.002	2.977	7.197	-0.170	2.180	in/s/s
BSA	0.089	3.781	0.136	-0.315	7.308	-0.302	in/s/s
BTOR	0.035	-0.002	0.122	-0.011	0.010	0.303	rad/s/s
Swept	1WA	1SA	1T	2WA	2SA	2T	Units
TWA	7.668	0.106	-1.877	-2.078	-0.039	0.534	in/s/s
TSA	-0.059	7.453	0.141	0.044	-3.890	0.125	in/s/s
TTOR	0.061	-0.008	0.220	-0.131	-0.007	-0.061	rad/s/s
BWA	2.788	-0.002	2.055	7.197	0.143	-0.266	in/s/s
BSA	-0.009	3.781	0.108	-0.203	7.225	-0.219	in/s/s
BTOR	0.001	-0.002	0.060	-0.011	0.010	0.307	rad/s/s

Table 9.11 L00 Swept Experimental Mode Shapes

The L00 configuration had significant contamination between the 1WA and 1T modes. Sweeping reduces the weak axis translational component of the 1T mode as shown by the highlighted values in figure 9.11. This shows how sweeping is making the modes orthogonal and has the impact of reducing translational movement in torsional modes.

9.3.3 L0R Configuration

Raw	1WA	1SA	1T	2WA	2SA	2T	Units
TWA	8.189	0.294	0.029	-1.635	0.053	0.117	in/s/s
TSA	0.430	7.450	0.382	0.113	-3.761	0.142	in/s/s
TTOR	0.003	-0.004	0.310	0.006	-0.001	-0.095	rad/s/s
BWA	1.804	0.023	0.112	8.010	0.196	0.503	in/s/s
BSA	0.252	3.780	0.246	0.109	7.301	0.193	in/s/s
BTOR	0.001	-0.005	0.103	0.002	0.010	0.319	rad/s/s
Swept	1WA	1SA	1T	2WA	2SA	2T	Units
TWA	8.189	-0.476	-0.113	-1.860	-0.020	-0.009	in/s/s
TSA	0.430	7.410	0.101	0.015	-3.888	0.195	in/s/s
TTOR	0.003	-0.004	0.310	-0.004	-0.005	-0.100	rad/s/s
BWA	1.804	-0.147	0.083	7.958	-0.049	0.011	in/s/s
BSA	0.252	3.757	0.103	0.057	7.234	-0.169	in/s/s
BTOR	0.001	-0.005	0.103	-0.002	0.009	0.317	rad/s/s

Table 9.12 L0R Swept Experimental Mode Shapes

The L0R configuration did not have significant modal impurities, as discussed in section 9.1.3, which led to sweeping having minimal effects on its mode shapes as shown in table 9.12.

9.3.4 LFR Configuration

Raw	1WA	1SA	1T	2WA	2SA	2T	Units
TWA	8.202	0.125	0.041	-1.635	0.160	0.095	in/s/s
TSA	-0.288	7.593	1.391	-0.139	-2.342	-0.354	in/s/s
TTOR	-0.001	-0.033	0.308	0.006	0.060	-0.081	rad/s/s
BWA	1.794	0.067	0.120	8.010	4.327	0.323	in/s/s
BSA	0.009	3.402	0.178	0.092	6.032	1.975	in/s/s
BTOR	-0.001	-0.014	0.093	-0.002	-0.084	0.313	rad/s/s
Swept	1WA	1SA	1T	2WA	2SA	2T	Units
TWA	8.202	0.238	0.043	-1.848	-0.073	-0.091	in/s/s
TSA	-0.288	7.589	0.989	-0.087	-2.805	-0.750	in/s/s
TTOR	-0.001	-0.033	0.310	0.000	0.031	-0.086	rad/s/s
BWA	1.794	0.091	0.118	7.952	-0.139	0.278	in/s/s
BSA	0.009	3.402	-0.001	0.059	5.951	1.804	in/s/s
BTOR	-0.001	-0.014	0.093	-0.014	-0.059	0.312	rad/s/s

Table 9.13 LFR Swept Experimental Mode Shapes

The LFR configuration had significant contamination between the 2WA and 2SA modes as discussed in section 9.1.4. This led to sweeping significantly impacting these mode shapes as shown by the highlighted values in table 9.13. The 2WA mode had reductions in the strong axis direction measurements, and the 2SA mode had reductions in the weak axis direction measurements. This shows that in the swept mode shapes, the primary direction of movement is closer to the orientation of shaking than it was originally as shown in figures 9.2 through 9.5.

LFR 2WA Mode Shape before Sweeping

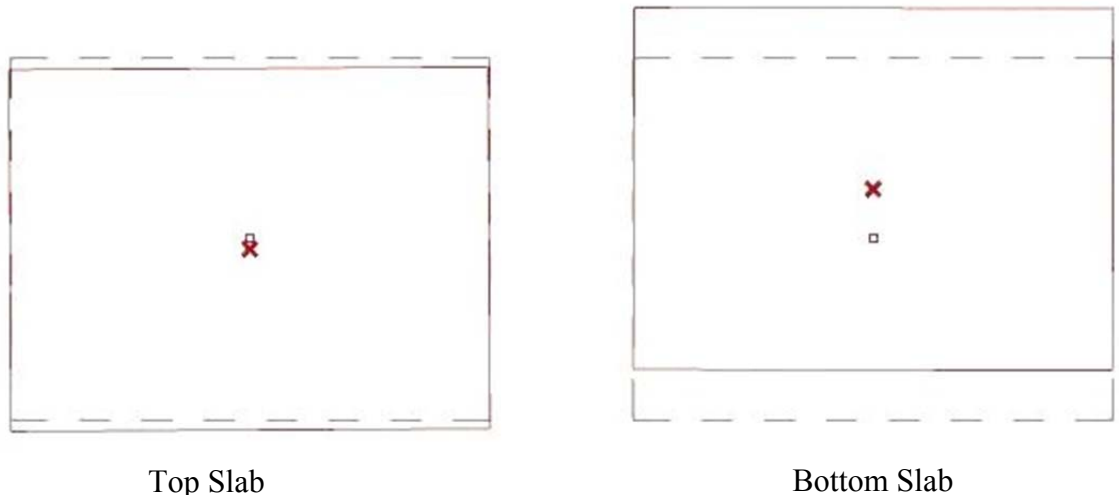

Figure 9.2 LFR 2WA Mode Shape before Sweeping

LFR 2SA Mode Shape before Sweeping

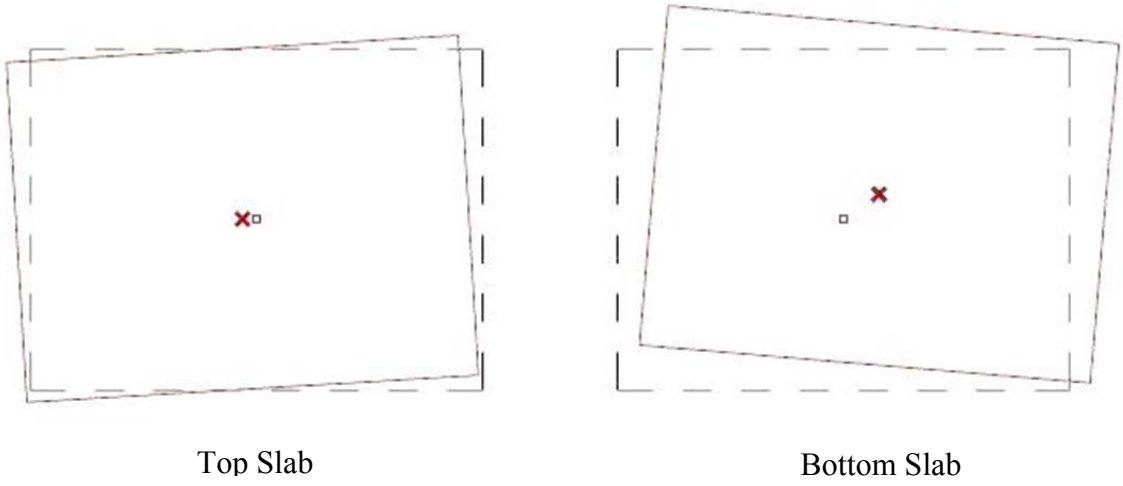

Figure 9.3 LFR 2SA Mode Shape before Sweeping

LFR 2WA Mode Shape after Sweeping

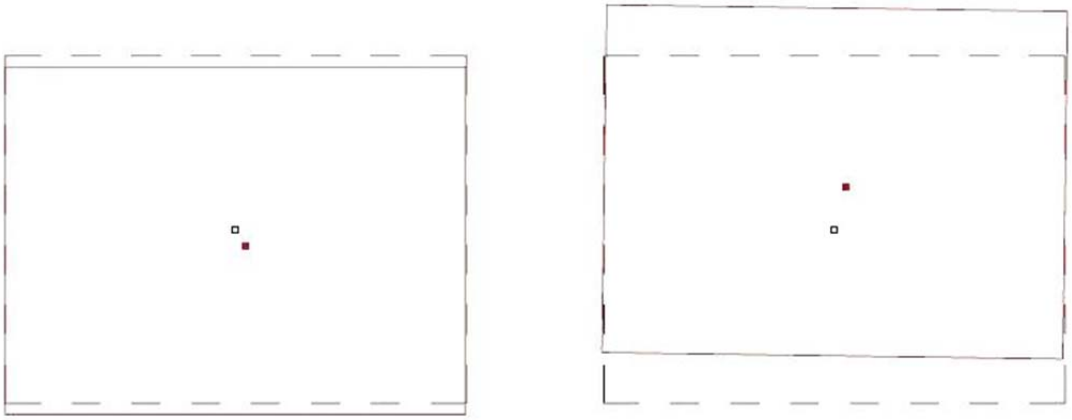

Figure 9.4 LFR 2WA Mode Shape after Sweeping

LFR 2SA Mode Shape after Sweeping

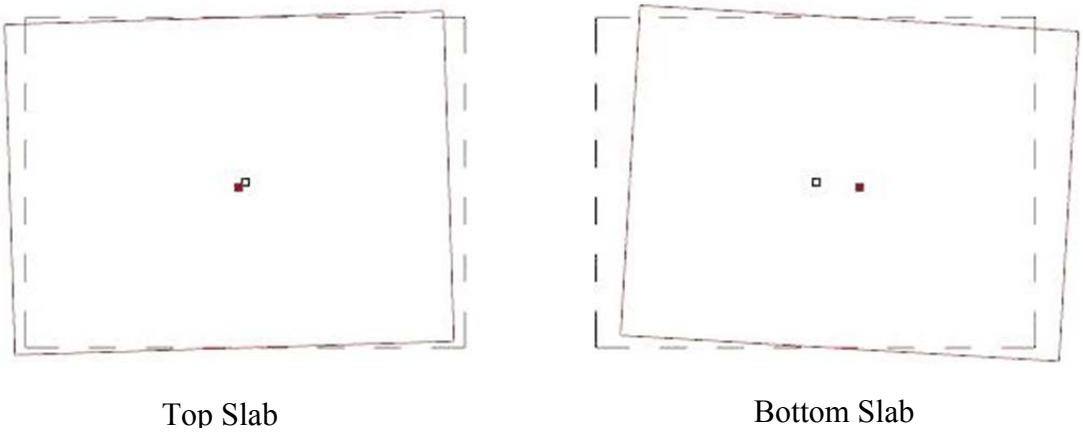

Figure 9.5 LFR 2SA Mode Shape after Sweeping

The 2WA mode is not as significantly altered by sweeping as the 2SA mode as shown in figures 9.2 through 9.5. This is due to the eccentricity in the strong axis direction that added impurities to the measured mode shapes. The displaced center of mass in the unswept 2SA mode shape, shown in figure 9.3, is not close to parallel with

the strong axis direction. This indicates that the 2WA is contaminating the measured 2SA mode because it is also excited during excitation of the 2SA mode.

9.3.5 LF0 Configuration

Raw	1WA	1SA	1T	2WA	2SA	2T	Units
TWA	7.684	-1.299	-2.493	-2.051	-0.076	-0.260	in/s/s
TSA	-0.453	7.373	2.237	0.351	-2.409	-0.540	in/s/s
TTOR	0.043	-0.056	0.249	-0.137	0.127	-0.090	rad/s/s
BWA	2.987	0.285	3.203	7.125	1.091	-1.728	in/s/s
BSA	0.503	3.373	0.385	-0.259	5.917	2.573	in/s/s
BTOR	0.030	-0.028	0.107	-0.011	-0.158	0.294	rad/s/s

Swept	1WA	1SA	1T	2WA	2SA	2T	Units
TWA	7.684	0.085	-2.433	-2.164	-0.741	-0.437	in/s/s
TSA	-0.453	7.292	1.118	-0.963	-2.953	-1.843	in/s/s
TTOR	0.043	-0.048	0.257	-0.147	0.073	-0.077	rad/s/s
BWA	2.987	0.823	3.105	6.678	0.827	-0.627	in/s/s
BSA	0.503	3.464	-0.140	-0.864	5.647	4.123	in/s/s
BTOR	0.030	-0.023	0.111	-0.016	-0.179	0.240	rad/s/s

Table 9.14 LF0 Swept Experimental Mode Shapes

The LF0 configuration was found to have impurities in many of the modes, but with fairly low levels of contamination, as shown in section 0. None of the impurities were significant enough to warrant changing the sweeping order and thus the default sweeping order was used.

9.3.6 0F0 Configuration

Raw	1WA	1SA	1T	2WA	2SA	2T	Units
TWA	7.244	-0.160	0.160	-4.025	0.037	0.023	in/s/s
TSA	-0.250	7.114	3.216	-0.099	-2.657	-1.016	in/s/s
TTOR	-0.009	-0.096	0.273	0.010	0.099	-0.109	rad/s/s
BWA	4.140	-0.106	0.298	7.167	0.026	0.189	in/s/s
BSA	0.035	3.404	0.725	0.118	6.608	3.835	in/s/s
BTOR	-0.002	-0.052	0.125	0.006	-0.131	0.270	rad/s/s

Swept	1WA	1SA	1T	2WA	2SA	2T	Units
TWA	7.244	0.108	0.170	-4.264	0.006	-0.037	in/s/s
TSA	-0.250	7.105	2.830	-0.122	-3.112	-1.535	in/s/s
TTOR	-0.009	-0.096	0.279	-0.006	0.087	-0.106	rad/s/s
BWA	4.140	0.047	0.305	7.019	-0.154	-0.133	in/s/s
BSA	0.035	3.405	0.540	0.144	6.432	3.623	in/s/s
BTOR	-0.002	-0.052	0.128	-0.002	-0.136	0.271	rad/s/s

Table 9.15 0F0 Swept Experimental Mode Shapes

The measured mode shapes of the 0F0 configuration were found to have very little contamination, thus the default sweeping order was used. The low level of modal contamination led to sweeping have an insignificant effect on the mode shapes as shown in table 9.15.

9.4 Mode Shape Comparison to Analytical Model

The following tables display the comparative MAC matrices of the ETABS mode shapes versus the swept experimental mode shapes for the correct configurations. The calculation of MAC matrices is detailed in section 5.1.1.1. The full set of comparative MAC matrices is included in section 0. These matrices represent the correlation between

the analytical model and the physical structure. The diagonal terms show the correlation value for the correct mode shapes, and should ideally be 1 indicating identical mode shapes. The off diagonal terms represent the correlation between different configurations, and should ideally be 0 indicating that the modes are perfectly orthogonal. These matrices are used for the prediction analysis in section 9.5. A perfect match between all modes would yield a comparative MAC matrix equal to the identity matrix, thus the identity matrix is the ideal output.

9.4.1 000 Comparative MAC Matrix

000	1WA	1SA	1T	2WA	2SA	2T
1WA	0.9972	0.0008	0.0001	0.0051	0.0001	0.0000
1SA	0.0008	0.9950	0.0028	0.0001	0.0040	0.0002
1T	0.0001	0.0027	0.9952	0.0007	0.0004	0.0001
2WA	0.0017	0.0000	0.0006	0.9941	0.0000	0.0000
2SA	0.0001	0.0012	0.0003	0.0000	0.9952	0.0003
2T	0.0000	0.0002	0.0010	0.0000	0.0003	0.9995

Table 9.16 000 Comparative MAC Matrix

The comparative MAC matrix for the 000 configuration shows very strong correlation with diagonal values all greater than .994 and off diagonal values all lower than .003. This indicates that the analytical mode shapes are nearly identical to the experimentally measured mode shapes. This degree of correlation creates a high level of confidence as discussed in section 9.5.1.

9.4.2 L00 Comparative MAC Matrix

L00	1WA	1SA	1T	2WA	2SA	2T
1WA	0.9807	0.0001	0.0068	0.0017	0.0000	0.0156
1SA	0.0002	0.9981	0.0006	0.0000	0.0038	0.0000
1T	0.0058	0.0007	0.9330	0.0244	0.0000	0.0239
2WA	0.0014	0.0000	0.0418	0.9721	0.0004	0.0054
2SA	0.0000	0.0011	0.0000	0.0005	0.9951	0.0006
2T	0.0122	0.0000	0.0262	0.0011	0.0007	0.9446

Table 9.17 L00 Comparative MAC Matrix

The L00 comparative MAC indicates that the 1T and 2T modes are not close to perfectly correlating with the analytical model as shown by the highlighted MAC values of .9330 and .9446 in table 9.17. These values are between .9 and .95, which is considered a fair correlation. The remaining diagonal values are all above .97 and considered excellent correlations.

The 1T mode shapes of the analytical model are compared with the measured experimental 1T mode shape in figure 9.6.

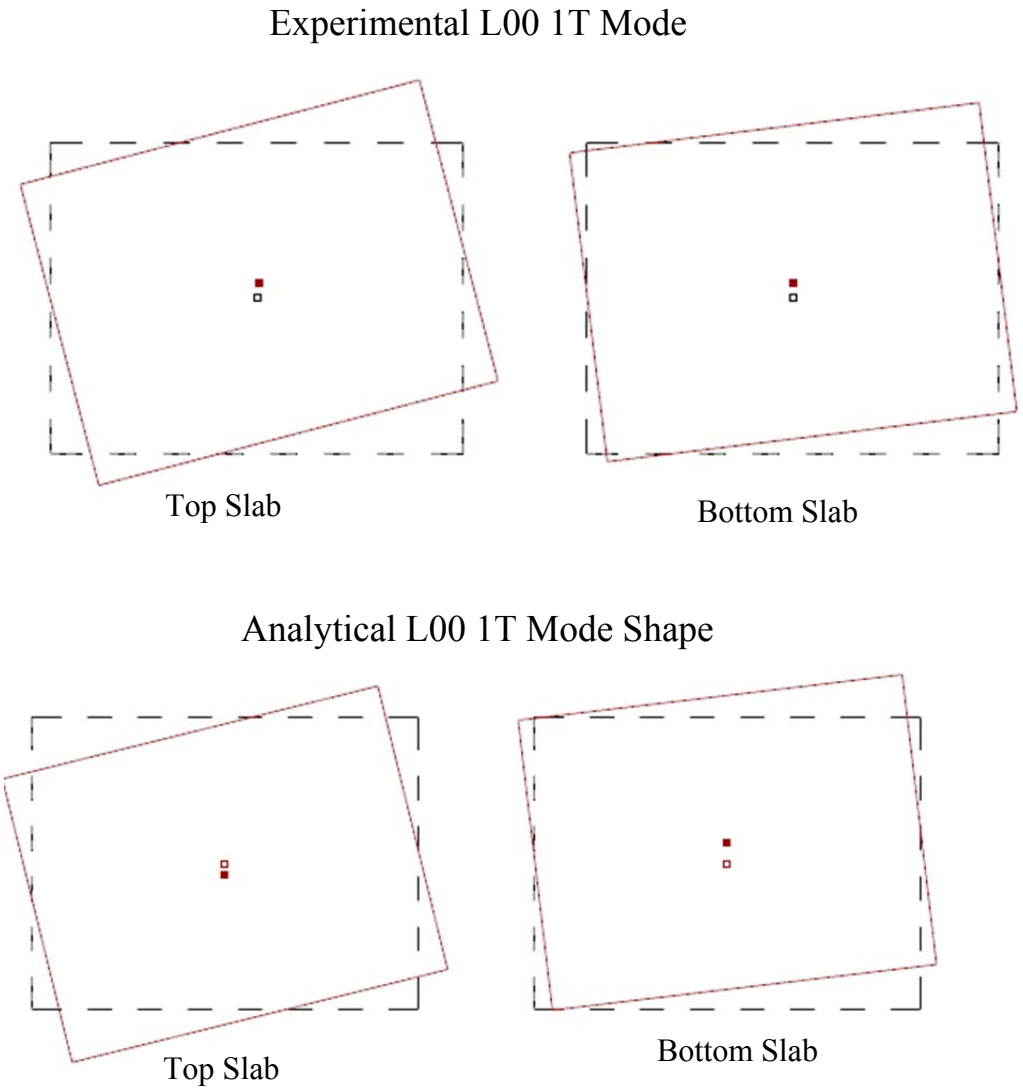

Figure 9.6 Example of Fair Mode Shape Correlation

The correlation metric between the modes shown in figure 9.6 is .933. This degree of correlation is shown in the figure above and is considered a fair level of correlation because it is between .9 and .95.

9.4.3 L0R Comparative MAC Matrix

L0R	1WA	1SA	1T	2WA	2SA	2T
1WA	0.9878	0.0035	0.0001	0.0104	0.0001	0.0000
1SA	0.0034	0.9953	0.0000	0.0001	0.0037	0.0001
1T	0.0001	0.0000	0.9986	0.0001	0.0000	0.0002
2WA	0.0087	0.0000	0.0002	0.9893	0.0000	0.0000
2SA	0.0000	0.0010	0.0000	0.0000	0.9959	0.0003
2T	0.0000	0.0001	0.0011	0.0000	0.0004	0.9994

Table 9.18 L0R Comparative MAC Matrix

The measured modes of the L0R configuration have very little modal contamination, which allows for a very close correlation with the analytical model. All diagonal values of the comparative MAC matrix are above .98 indicating mode shapes that are very well correlated. The largest off diagonal is .0104 as indicated by the highlighted value in table 9.18. This shows a very small level of inaccuracy in the analytical mode shapes.

9.4.4 LFR Comparative MAC Matrix

LFR	1WA	1SA	1T	2WA	2SA	2T
1WA	0.9907	0.0007	0.0001	0.0101	0.0002	0.0000
1SA	0.0006	0.9953	0.0018	0.0001	0.0047	0.0020
1T	0.0000	0.0012	0.9961	0.0003	0.0001	0.0004
2WA	0.0084	0.0001	0.0003	0.9878	0.0005	0.0012
2SA	0.0002	0.0017	0.0001	0.0006	0.9892	0.0017
2T	0.0000	0.0010	0.0016	0.0010	0.0053	0.9947

Table 9.19 LFR Comparative MAC Matrix

This configuration has very close correlations between all analytical and experimental mode shapes as indicated by all diagonal values of the comparative MAC

matrix being above .98. All off-diagonal values are below .011, indicating little confusion between the mode shapes.

9.4.5 LF0 Comparative MAC Matrix

LF0	1WA	1SA	1T	2WA	2SA	2T
1WA	0.9763	0.0003	0.0109	0.0072	0.0094	0.0000
1SA	0.0007	0.9016	0.0772	0.0214	0.0084	0.0011
1T	0.0089	0.0582	0.9043	0.0076	0.0000	0.0000
2WA	0.0045	0.0302	0.0096	0.9611	0.0017	0.0060
2SA	0.0067	0.0032	0.0000	0.0000	0.8174	0.1400
2T	0.0029	0.0019	0.0011	0.0031	0.1526	0.8640

Table 9.20 LF0 Comparative MAC Matrix

The analytical mode shapes of this LF0 configuration were found to have significant degrees of confusion between the 2SA and 2T modes as indicated by the highlighted values in the bottom right of table 9.20. The correct mode shapes have MAC values of .8174 and .8640 which shows a low level of correlation. The associated off diagonal terms of .1526 and .1400 indicate that contamination of these modes is likely the cause of issue as discussed in section 9.1.5. The 1SA and 1T modes were also found to contaminate each other as indicated by the highlighted values in the top left of table 9.4.5. This contamination is less severe than the 2SA and 2T modes as indicated by the diagonal values of .9016 and .9043, and off-diagonal values of .0582 and .0772. This weak level of correlation in 4 of the 6 modes indicates that the utilized sweeping order detailed in section 0 did not fully resolve the impurities of the measured mode shapes.

An alternative approach to sweeping based on a metric of contamination is discussed in section 11.3.

Figure 9.7 shows the experimental 2SA mode in relation to the 2SA analytical mode. This comparison yields a MAC value of .8174 as shown in table 9.20. This is an example of a mode shape that has a weak correlation with the analytical model.

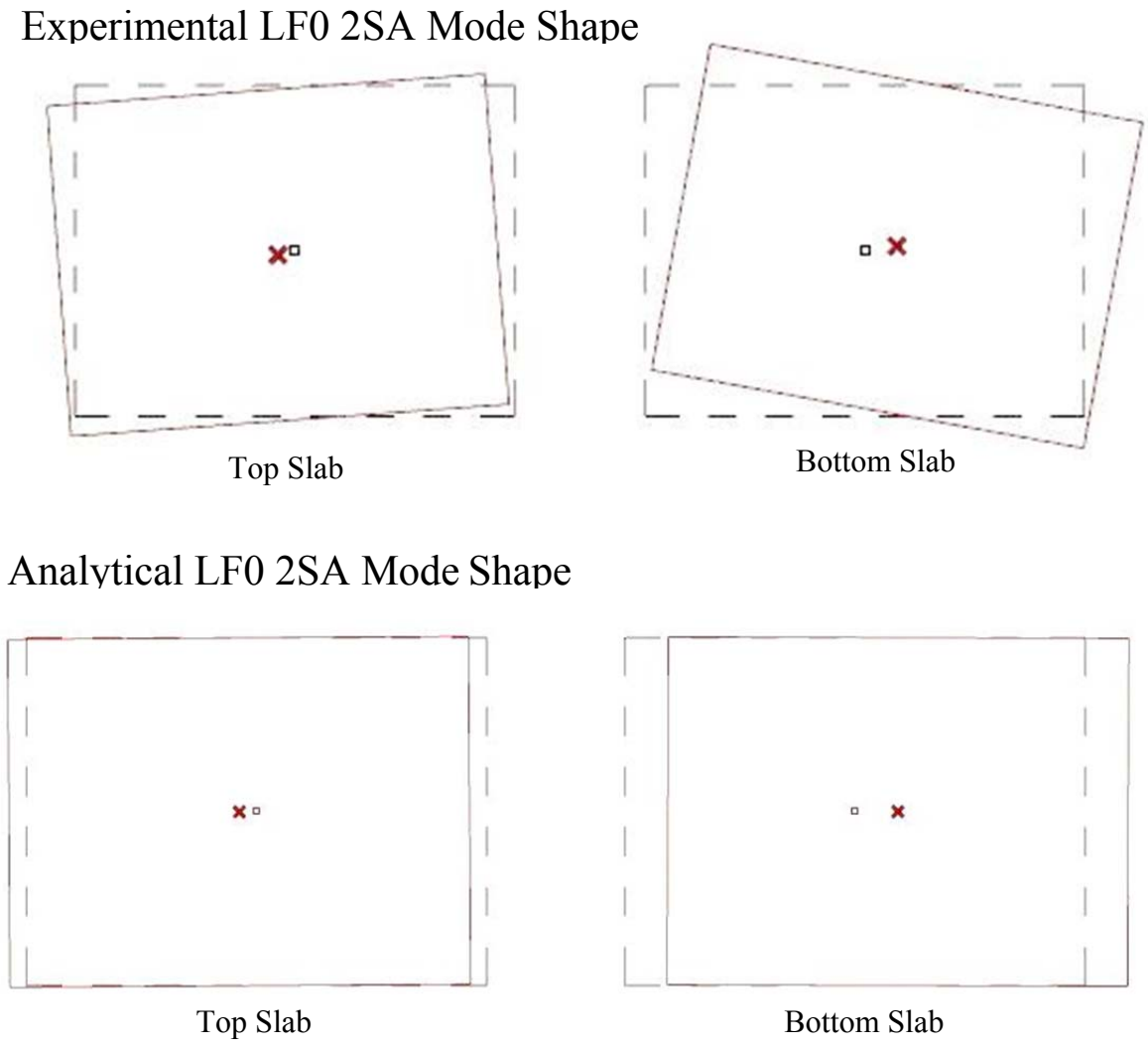

Figure 9.7 Example of Weak Mode Shape Correlation

It can be seen in figure 9.7 that the experimentally measured mode shape has significant rotation at each level. This is not similar to the analytical mode shapes which have very little rotation at each level. The translation in the strong axis direction is similar to the analytical mode, as is the lack of translation in the weak axis. This rotation is the issue that causes the MAC metric to have a weak correlation of .8174.

9.4.6 0F0 Comparative MAC Matrix

0F0	1WA	1SA	1T	2WA	2SA	2T
1WA	0.9966	0.0002	0.0014	0.0052	0.0001	0.0001
1SA	0.0002	0.9972	0.0015	0.0000	0.0036	0.0032
1T	0.0012	0.0002	0.9938	0.0011	0.0000	0.0008
2WA	0.0019	0.0000	0.0010	0.9933	0.0003	0.0001
2SA	0.0001	0.0014	0.0000	0.0003	0.9823	0.0028
2T	0.0001	0.0010	0.0023	0.0001	0.0136	0.9930

Table 9.21 0F0 Comparative MAC Matrix

The 0F0 configuration was found to have strong correlations between the analytical and measured mode shapes as indicated by the diagonal values in table 9.21 all greater than .98. All off-diagonal terms are below .01 which indicates little confusion between the modes. This very close correlation is better than was initially expected given the asymmetry of the structure, but it is theorized that this is caused by the shaker location for the torsional modes aligning well with the centers of rigidity and mass, as discussed in further detail in section 11.1.

9.5 Mode Shape Derived Metrics

The following tables show the metrics of the MAC matrices for each configuration comparison. The optimal value is 0, representing a perfect correlation between all mode shapes. The predicted configuration is determined by the lowest metric value of the attempted structures.

Legend

Yellow highlighted values indicate the correct configuration. The ideal value of this cell is 0.

Underlined values denote the values being used for the confidence calculation. This includes the predicted configuration and the next closest prediction.

Confidence (C) is the percent change from the correct value to the next closest value as shown in Equation 9.1 below. It is used to provide a metric for the degree of certainty of the prediction. The confidence has a range of 0% to 100%, where 100% indicates the predicted mode matches exactly with the analytical model, and 0% means that the two best prediction metrics are exactly the same.

Equation 9.1 Confidence Metric

$$C = \frac{(M_1 - M_2)}{M_2}$$

M_1 = Prediction metric for the predicted configuration
M_2 = Prediction metric for next closest prediction

9.5.1 000 Configuration

000	L00	L0R	LFR	LF0	0F0	Confidence
0.00010	0.49020	0.09770	0.09780	0.60650	0.11750	99.9%

Table 9.22 000 Mode Shape Derived Prediction

Prediction – 000 – Correct with the highest level of confidence (99.9%)

This 000 configuration was correctly predicted with the greatest confidence level of any tested structure in this study. The correct configuration had an extremely good metric value of .0001, this is very close to the ideal value of 0. The next best metric was for the L0R configuration at .0977, significantly higher than the correct configuration which shows a large degree of confidence in the prediction with a confidence value of 99.9%.

9.5.2 L00 Configuration

000	L00	L0R	LFR	LF0	0F0	Confidence
0.14620	0.00940	0.10750	0.11570	0.07220	0.19270	87.0%

Table 9.23 L00 Mode Shape Derived Prediction

Prediction - L00 – Correct with the 5th highest level of confidence (87.0%)

The L00 configuration was correctly predicted by the metric with a confidence level of 87%. Being above 80% makes this a strong enough confidence level to predict the configuration; however it is the second least prediction of the tested configurations. This configuration experienced issues due to modal contamination stemming from the shaker placement that lowered the confidence of this prediction. The shaker placement

for the torsional modes does not relate well to the centers of mass and rigidity as discussed further in section 11.1.2.

9.5.3 L0R Configuration

000	L00	L0R	LFR	LF0	0F0	Confidence
0.01620	0.33300	0.00050	0.01000	0.42680	0.14510	95.0%

Table 9.24 L0R Mode Shape Derived Prediction

Prediction – L0R – Correct with the 4th highest level of confidence (95.0%)

This symmetric configuration had a strong correct prediction of L0R. The next closest configuration was LFR, with a prediction metric of .005, quite close to 0. This is related to the fact that the brace in the strong axis direction does not have as significant an impact on the mode shapes than the weak axis direction. This is because the relative stiffness of the strong direction is 7x that of the weak direction. The alteration of the brace in the strong axis direction is a much smaller change than in the weak axis direction and therefore does not impact the mode as significantly. The confidence of 95% shows a high confidence level due to the close correlation of the correct configuration.

9.5.4 LFR Configuration

000	L00	L0R	LFR	LF0	0F0	Confidence
0.02020	0.34710	0.01580	0.00040	0.38500	0.01900	97.5%

Table 9.25 LFR Mode Shape Derived Prediction

Prediction – LFR – Correct with the 3rd highest level of confidence (97.5%)

This configuration is slightly asymmetric and had a strong correct prediction of LFR, with a prediction metric of .0004 for the proper configuration. The L0R configuration had the next lowest metric at .01580, producing a confidence value of 97.5%. This shows that with the given shaker placement locations, eccentricity in the strong axis direction does not significantly impact the modal contamination. This is theorized to be due to the shaker placement for the torsional modes as discussed in section 11.1.

9.5.5 LF0 Configuration

000	L00	L0R	LFR	LF0	0F0	Confidence
0.51060	0.53220	0.52780	0.21550	0.09480	0.25480	56.0%

Table 9.26 LF0 Mode Shape Derived Prediction

Prediction – LF0 - Correct with the lowest confidence level (56.0%)

This configuration had the least confident prediction, with a metric value of .0948 for the correct configuration. The next lowest metric belongs to the LFR configuration at .2155. While the prediction metric of the correct configuration is relatively high compared to the other tests at .0948, the correct configuration still has the best prediction metric. Asymmetry in the strong axis direction is theorized to be the primary factor skewing the mode shape measurement and lowering the confidence level. This can be compensated for in future studies through revision of the shaker placement as detailed in section 11.1. The modal contamination matrix for this configuration in section 0 shows

that the contamination of each mode is distributed and is not discretely coupled such as in the L00 and LFR configurations, which makes the given sweeping order less effective.

9.5.6 0F0 Configuration

000	L00	L0R	LFR	LF0	0F0	Confidence
0.22150	0.40370	0.23120	0.09890	0.33870	0.00060	99.4%

Table 9.27 0F0 Mode Shape Derived Prediction

Prediction – 0F0 - Correct

This 0F0 configuration had a very confident prediction, with a metric value of .0006 for the correct configuration. The next closest metric belonged to the LFR configuration with a metric of .0989. This creates a confidence of 99.4%, representing a strong confidence level and showing positive results for the mode shape derived metric.

9.5.7 Summary

	000	L00	L0R	LFR	LF0	0F0	Confidence
000	0.00010	0.49020	0.09770	0.09780	0.60650	0.11750	99.9%
L00	0.14620	0.00940	0.10750	0.11570	0.07220	0.19270	87.0%
L0R	0.01620	0.33300	0.00050	0.01000	0.42680	0.14510	95.0%
LFR	0.02020	0.34710	0.01580	0.00040	0.38500	0.01900	97.5%
LF0	0.51060	0.53220	0.52780	0.21550	0.09480	0.25480	56.0%
0F0	0.22150	0.40370	0.23120	0.09890	0.33870	0.00060	99.4%

Table 9.28 Summary of Mode Shape Derived Metrics

Table 9.28 above displays the metrics of each comparison that was completed. The yellow highlighted values along the diagonal indicate the values for the correct configurations that should be close to 0.

Overall this approach has a relatively good success rate of 5/6 (83%). This shows the degree of robustness in the approach when dealing with the impure mode shapes that were collected. The confidence of each decision appears to correlate with the contamination of the measured modes. The analysis of the LF0 configuration that was inconclusive had the lowest confidence level of 56%. This shows a very high level of uncertainty in the decision. With the next lowest confidence is the L00 configuration at 87%. This configuration is also highly asymmetric with eccentricities in the weak and strong axis directions of 8.4" and 17.0" respectively. This lack of symmetry tends to negatively impact the contamination of affected modes with the given testing procedure, but could be improved on in the future as discussed in section 11.1. The shaker placement based on the center of mass resulted in the force vector imparting modal excitation to multiple modes. This issue Section 5.3.2 discusses how the force needs to be applied for accurate mode shape collection.

The symmetric configurations, 000 and L0R, had confidences of 99.9% and 95.0% respectively. Both of these represent a strong confidence level. The 0F0 configuration surprisingly has a confidence of 99.4% which shows a high degree of certainty. The relatively small amount of eccentricity (9") did not have a large negative impact on the technique's ability to predict the proper configuration, which shows the robustness of the approach.

The braces used in this study create a substantial change in the stiffness of the structure. In the strong axis, a single brace adds 30% to the stiffness of that direction, and in the weak axis a single brace adds 210% to the stiffness of that direction. The relationship between the prediction metrics of the 000 configuration versus the other arrangements helps estimate the minimum degree of stiffness change that this analysis approach can detect.

9.5.8 Minimum Detectable Stiffness Change

To estimate the minimum degree of stiffness change that can be detected the prediction metrics of the L00 and 0F0 configurations are examined. This allows for the effect of a single brace in the weak axis direction to be examined in the L00 configuration, and the effect of a single brace in the strong axis direction to be examined in the 0F0 configurations. In the L00 configuration the prediction metric for the 000 analytical model is .14620, and the prediction metric for the correct L00 configuration is .00940, as can be seen in table 9.28. The ratio of these two metrics is 15.6. The estimated minimum stiffness change that this method can detect is equal to the actual percent change over this ratio, which is equal to 210%/15.5 = 14% change in stiffness.

In the 0F0 configuration, the prediction metric for the 000 analytical model is .22150, and for the correct 0F0 analytical model the prediction metric is .0006. The ratio between these two metrics is .22150/.0006 = 369, therefore the estimated minimum stiffness change that could be predicted according to this estimate is 30%/369 = .1%.

This indicates a much higher level of accuracy when examining the strong axis direction versus the weak axis direction.

This difference is primarily due to the effects of the shaker location on the accuracy of the collected mode shapes. In the configurations that are asymmetric in the weak axis direction, the shaker placement for the torsional modes had a significant negative impact on the accuracy of the measured mode shapes. This resulted in lower levels of accuracy in configurations that had asymmetry in the weak axis direction, as shown in table 9.28 by the low confidence values of 87% and 56% for the L00 and LF0 configurations respectively. These are the only configurations that are asymmetric in the weak axis, and they have significantly lower confidence levels than all the other tested configurations. See section 11.1 for a discussion of better shaker locations for future testing, these would improve the accuracy of the collected mode shapes leading to a smaller estimated minimum detectable stiffness change.

10.0 CONCLUSIONS

This thesis evaluates the question "What is the accuracy of damage detection techniques that utilize experimental mode shapes?" To answer this question, a method of mode shape analysis is explored. The approach was tested on a structural steel model as a laboratory demonstration of the efficacy of this technique. The results show that the proposed analysis process utilizing mode shapes can be used as a reliable method of detecting and locating a change in stiffness to a structure. Modal frequencies were also investigated as a means of damage detection and were not found to provide reliable results for this structure.

To provide multiple tests of the proposed analysis technique, the test structure had braces installed that can be easily engaged or disengaged. This allowed for six configurations of braces to be examined and provided multiple data sets to help confirm the accuracy of the technique. Forced vibration testing was completed on each configuration to obtain the mode shapes of the structure. The mode shapes were then compared with analytical models with various brace configurations. The predicted configuration of braces was then decided based on which analytical model had mode shapes that correlated best with the experimental results.

10.1 Mode Shape Analysis

It was found that the proposed analysis procedure provided a successful method of detecting changes in stiffness to a structure. In this test sample the technique correctly

predicted all tested cases. Five of the six cases had very high confidence levels. These configurations had mode shapes that were extremely close to the analytical model as discussed in section 9.5. This shows the accuracy of the testing procedure and the analytical model. These cases all had prediction metrics below .01, which is very close to the ideal value of 0. For all of these cases the next closest prediction metric is at least eight times higher, showing that the predicted configuration is a clear choice and leading to the high confidence levels.

The LF0 configuration has a lower degree of confidence which is believed to be caused by method of modal excitation causing significant impurities in the measured mode shapes. Its prediction metric of .095 indicates that the analytical model is not correlating perfectly with experimental results, however it is still the best prediction metric of the examined configurations. LF0 is asymmetric in both directions, which led to contamination occurring in more mode shapes than the other configurations. This could be improved upon in future research by refining the shaker locations, as detailed in section 11.1. The fact that the method worked a majority of the time even with impure mode shapes is representative of this technique's robustness.

Testing of a full size building would experience similar complications in obtaining accurate mode shapes. Interactions of the structure with the foundation, façade, or architectural components all have the ability to cause impurities in measured modes. Larger amounts of damping in a building would contribute to possible modal contamination and require careful consideration of the testing procedure as discussed in

sections 5.3 and 6.1.4 respectively. Based on the results of this study, the robustness of this approach reflects positively on the future application of this technique in more complex systems subject to such complicating issues.

It is theorized that the proposed mode shape analysis would be able to locate damage in a building with a maximum precision of identifying a damaged line of walls or frames. The intricacy of the data collection system plays a large role in the potential accuracy of this technique. To a degree, more measurement locations allow for a more precise location of damage because they allow for more degrees of freedom to be utilized in the analytical model. The additional degrees of freedom are more locations that can be used for comparison between the analytical and physical model.

10.2 Frequency Analysis

The frequencies of the computation model did not show reliable correlation with the measured frequencies of the physical structure. This is due to the requirement of this analysis to have a model with a higher level of absolute accuracy than the mode shape analysis which utilized relative comparisons as discussed in section 5.1. Degrees of accuracy this high require more time than deemed feasible for a large scale effort to aid building inspection after a natural disaster, which is the intended application of this technique, and therefore, not explored further. The results of this study indicate that analyzing frequencies alone will not provide useful information to inform the location of

damage in a building and that mode shapes must be utilized for structural damage detection.

10.3 Summary

This thesis confirmed the hypothesis that analysis of mode shapes can be used to reliably detect changes in stiffness to a building. The purpose of this thesis is to take structural damage detection research a step further towards commercial implementation by demonstrating reliable and robust performance on a physical structure in a laboratory demonstration. This validation of damage detection techniques provides evidence that this damage detection technique should be utilized as a tool to aid engineers in evaluation of structural damage. Widespread implementation of this technique can save millions of dollars in damage repair and hopefully thousands of lives through its application in structural health monitoring.

11.0 RECOMMENDATIONS

11.1 Relocation of Shaker for Reduced Modal Contamination

During analysis of the data obtained from testing it was noticed that some of the modes were coupled. That is to say, they had significant amounts of other modes participating in the behavior that contaminated the mode shape measurements. This stems from the method of testing where the shaker is placed in relation to the center of mass. The following sections contain figures showing the centers of mass and rigidity for each configuration with the recommended shaker locations identified.

11.1.1 000 Configuration

The chosen location based on center of mass was a good location for shaking the 000 configuration. This is because the center of mass and rigidity align due to the symmetry in both directions. This symmetry causes each mode to be excited independently when the shaker is oriented in the given locations.

11.1.2 L00 Configuration

This configuration has a center of rigidity at the top slab that is 10.1" eccentric from the center of mass. This means if the shaker is placed at the center of mass, when the torsional modes are being measured, the weak axis modes will also be excited. This results in contamination between these two sets of modes. To reduce this modal

contamination a better shaking location can be used for that is based on the center of rigidity as seen in figure 11.1, rather than the center of mass.

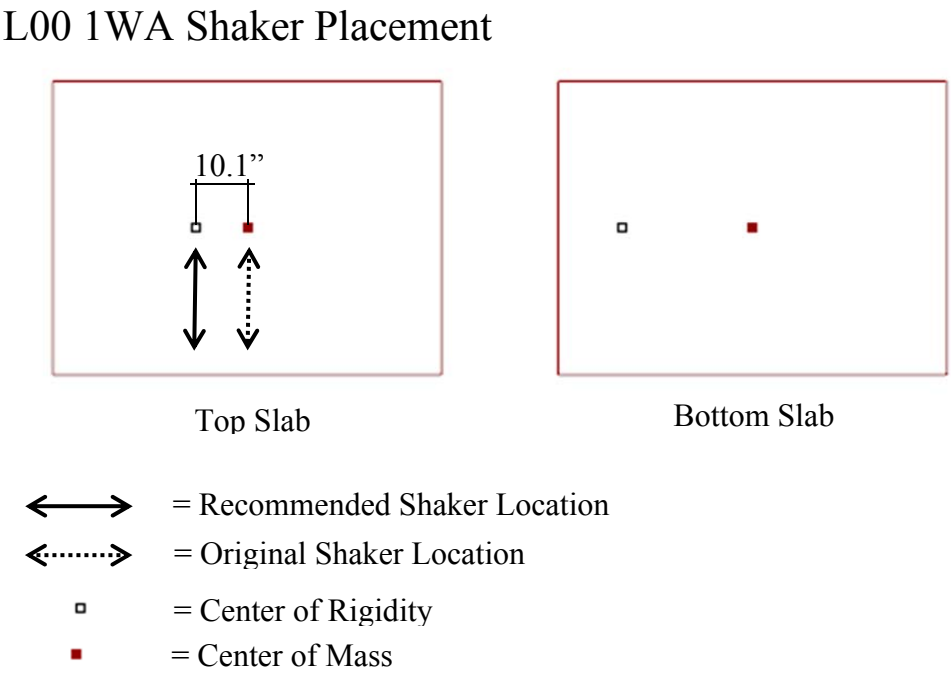

Figure 11.1 L00 1WA Shaker Placement

The shaker for the 1WA mode of the L00 configuration should be placed at the center of rigidity, which is theoretically 10.1” eccentric from the indicated in figure 11.1.

L00 1T Shaker Placement

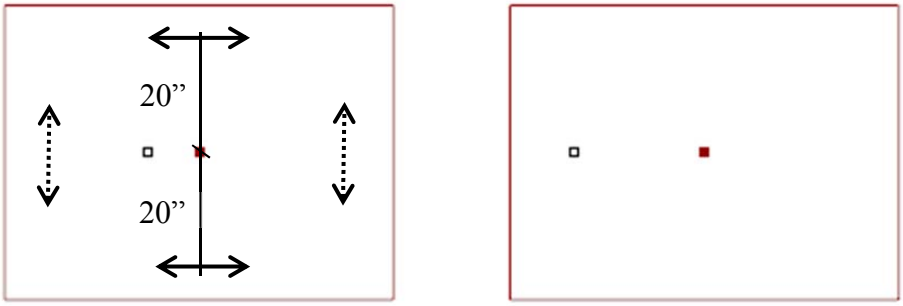

= Recommended Shaker Locations

= Original Shaker Locations

= Center of Rigidity

= Center of Mass

Figure 11.2 L00 1T Shaker Placement

To excite the first torsional (1T) mode, the shakers should be equally spaced from the center of mass, but in the strong axis direction. This makes the force couple created from the shakers center around the center of rigidity, preventing the translational modes from being excited.

L00 2WA Shaker Placement

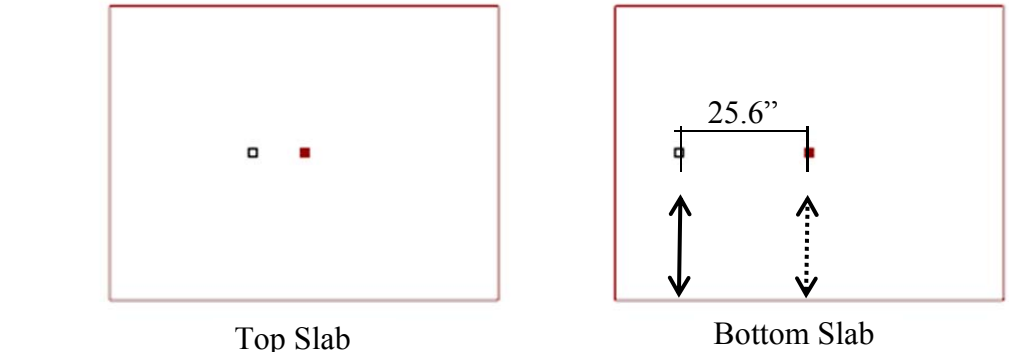

Figure 11.3 L00 2WA Shaker Placement

For the L00 2WA testing the shaker should be located at the center of rigidity, which is 25.6” eccentric from the center of mass, as shown in figure 11.3

L00 2T Shaker Placement

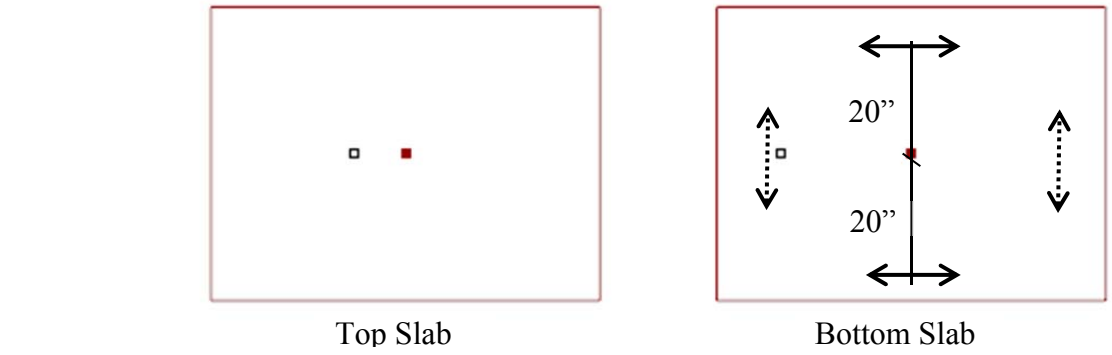

Figure 11.4 L00 2T Shaker Placement

11.1.3 L0R Configuration

This configuration is symmetric and therefore has aligned centers of mass and rigidity. For this reason the shaking location based on center of mass is deemed appropriate for future testing.

11.1.4 LFR Configuration

This configuration was found to have significant contamination between the 2WA and 2SA modes as discussed in section 9.1.4. This is due to the eccentricity between the center of rigidity and the shaker placement when exciting the 2SA mode.

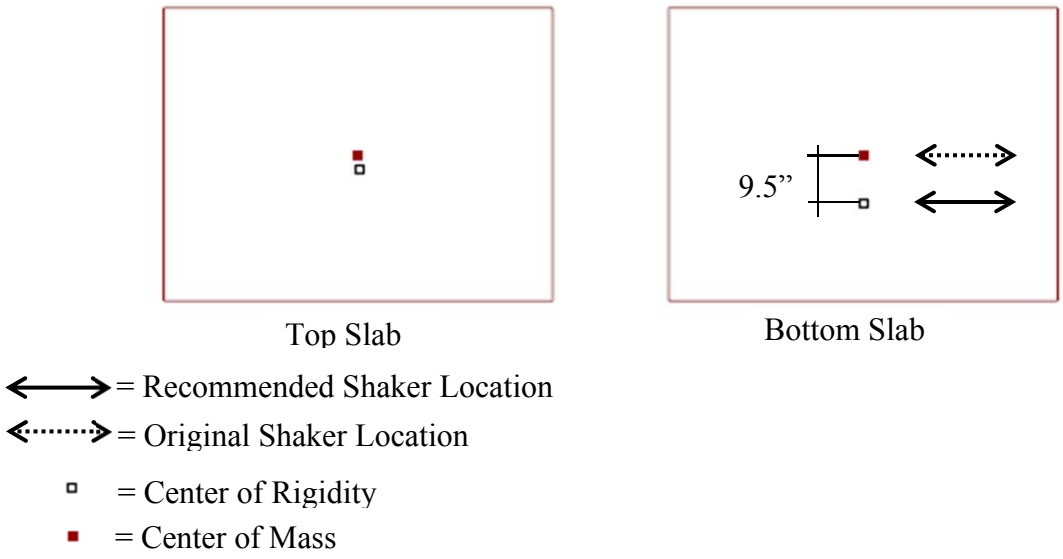

Figure 11.5 LFR 2SA Shaker Placement

11.1.5 LF0 Configuration

The LFO configuration is the least symmetric of all tested arrangements with a single brace in each direction. This results in asymmetry of both translational directions. The shaking positions based on the center of mass were shown to result in considerable modal contamination, described in further detail in section 0. There is a contamination between the 2WA, 2SA and 2T modes which could be minimized by revising the shaker location as detailed in the figures 11.6 through 11.8.

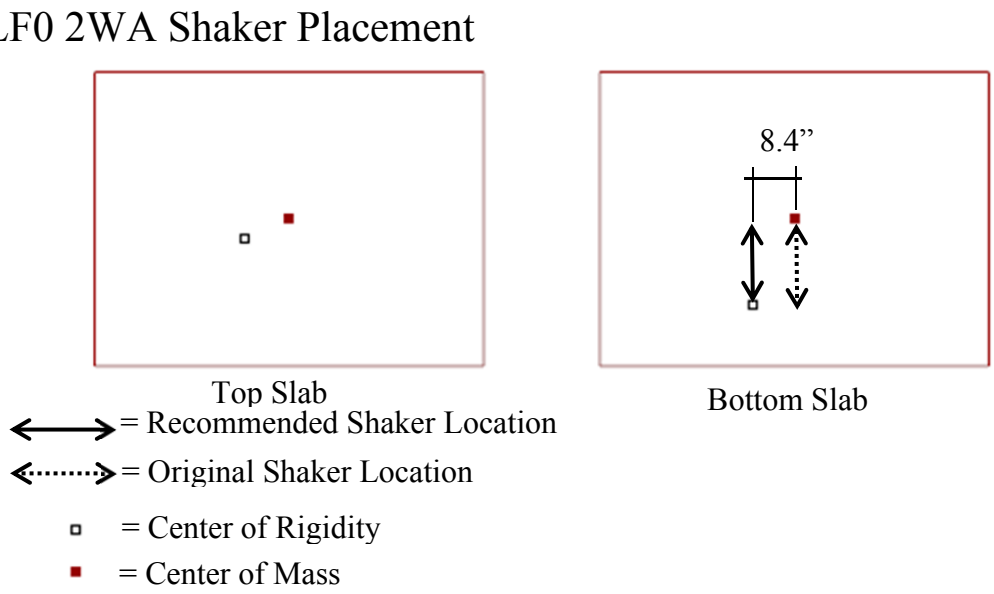

Figure 11.6 LF0 2WA Shaker Placement

LF0 2SA Shaker Placement

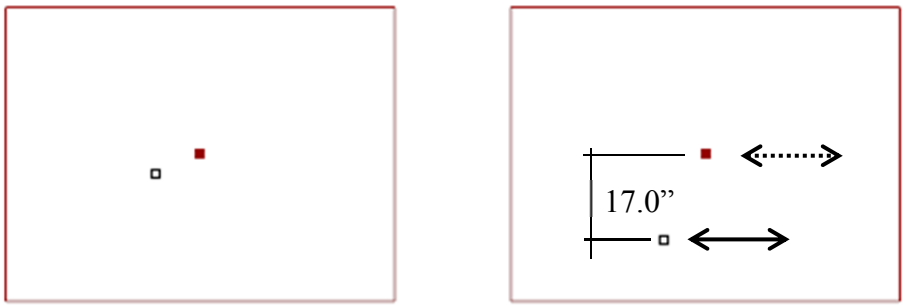

= Recommended Shaker Location

= Original Shaker Location

= Center of Rigidity

= Center of Mass

Figure 11.7 LF0 2SA Shaker Placement

LF0 2T Shaker Placement

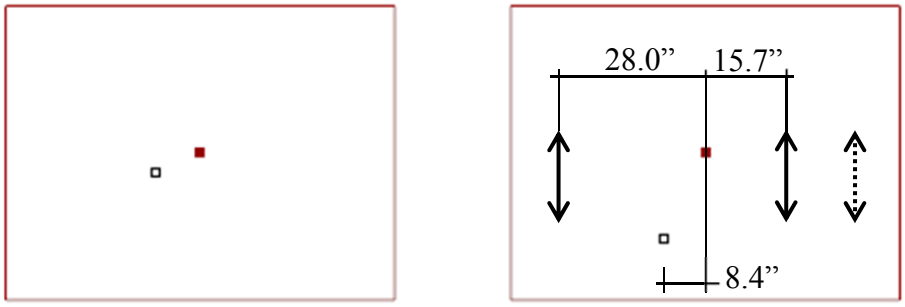

= Recommended Shaker Locations

= Original Shaker Locations

= Center of Rigidity

= Center of Mass

Figure 11.8 LF0 2T Shaker Placement

The shakers for the LF0 2T testing should be centered on the center of rigidity, as shown in figure 11.8.

11.1.6 0F0 Configuration

While there is a small amount of eccentricity in the strong axis direction, it did not appear to impact the accuracy of the measured mode shapes as discussed in section 0. For this reason the original shaking location is deemed appropriate for this configuration.

11.2 Rotational Springs at Base Connection

Much consideration was required to determine the restraints at the base plate connection to the slab. While the design increased the base plate thickness to increase the stiffness of the base, there was little that could be done to increase the stiffness of the slab. This is theorized to have played a significant role in the error of the strong axis frequencies.

One consideration to improve the correlation of modal frequencies between the analytical and physical model is to utilize rotational springs at the base of the columns. This captures the behavior of the slab interaction, but is difficult to accurately model. The soil interaction is highly unknown and would require many assumptions to be made, as would the interaction of the slab with the nearby retaining wall and isolated slab in the seismic laboratory. Due to the many assumptions required for this to be implemented in the model, the results could have been unique to this structure, and thus this avenue was not explored further.

11.3 Sweeping Order Based on Contamination

A method of ordering sweeping based on the contamination of each mode was investigated. This is calculated using a one-norm of the off-diagonal terms of the modal contamination matrix. These terms are ideally 0, and larger values represent contamination from another mode. This approach sweeps with the most pure modes first, thus avoiding contaminating the more pure modes. The results of this sweeping method are shown in the following sections.

11.3.1 Contamination Metric

To consolidate the several values representing modal contamination, a one norm is used to create a single metric. A completely pure mode will have a metric of 0, and a high value represents a contaminated mode.

11.3.1.1 000 Configuration

000 Modal Contamination

	1WA (1)	1SA (2)	1T (3)	2WA (4)	2SA (5)	2T (6)	Contam. (1-norm)	Order (Contam based)	Order (Orig.)
1WA (1)	1	0.002	0.0004	0.0011	0	0.0001	0.0036	2	1
1SA (2)	0.002	1	0.0239	0.0003	0.0006	0.0085	0.0353	6	2
1T (3)	0.0004	0.0239	1	0.0000	0.0001	0.0003	0.0247	5	3
2WA (4)	0.0011	0.0003	0.0000	1	0.0001	0.0001	0.0016	1	4
2SA (5)	0.0000	0.0006	0.0001	0.0001	1	0.0044	0.0052	3	5
2T (6)	0.0001	0.0085	0.0003	0.0001	0.0044	1	0.0134	4	6

Table 11.1 000 Modal Contamination Sorting

000 Sweeping Order

Step	1WA (1)	1SA (2)	1T (3)	2WA (4)	2SA (5)	2T (6)
1	4	4	4	-	4	4
2	-	1	1	-	1	1
3	-	5	5	-	-	5
4	-	6	6	-	-	-
5	-	3	-	-	-	-
6	-	-	-	-	-	-

Table 11.2 000 Sweeping Order

11.3.1.2 L00 Configuration

L00 Modal Contamination

	1WA (1)	1SA (2)	1T (3)	2WA (4)	2SA (5)	2T (6)	Contam. (1-norm)	Order (Contam based)	Order (Orig.)
1WA (1)	1	0.0012	0.3651	0.0017	0.0000	0.0159	0.3839	5	5
1SA (2)	0.0012	1	0.0014	0.0009	0.0004	0.0012	0.0051	2	1
1T (3)	0.3651	0.0014	1	0.0082	0.0000	0.0277	0.4024	6	6
2WA (4)	0.0017	0.0009	0.0082	1	0.0019	0.116	0.1287	3	2
2SA (5)	0.0000	0.0004	0.0000	0.0019	1	0.0000	0.0023	1	3
2T (6)	0.0159	0.0012	0.0277	0.116	0.0000	1	0.1608	4	4

Table 11.3 L00 Modal Contamination Sorting

L00 Sweeping Order Matrix

Step	1WA (1)	1SA (2)	1T (3)	2WA (4)	2SA (5)	2T (6)
1	5	5	5	5	-	5
2	2	-	2	2	-	2
3	4	-	4	-	-	4
4	6	-	6	-	-	-
5	-	-	1	-	-	-
6	-	-	-	-	-	-

Table 11.4 L00 Sweeping Order

11.3.1.3 L0R Configuration

L0R Modal Contamination

	1WA (1)	1SA (2)	1T (3)	2WA (4)	2SA (5)	2T (6)	Contam. (1-norm)	Order (Contam based)	Order (Orig.)
1WA (1)	1	0.0088	0.0004	0.0008	0.0003	0.0008	0.0111	6	1
1SA (2)	0.0088	1	0.0015	0.0002	0.0003	0.0002	0.011	5	2
1T (3)	0.0004	0.0015	1	0.0011	0.0002	0.0004	0.0036	1	3
2WA (4)	0.0008	0.0002	0.0011	1	0.0008	0.0033	0.0062	3	4
2SA (5)	0.0003	0.0003	0.0002	0.0008	1	0.002	0.0036	2	5
2T (6)	0.0008	0.0002	0.0004	0.0033	0.002	1	0.0067	4	6

Table 11.5 L0R Modal Contamination Sorting

L0R Sweeping Order Matrix

Step	1WA (1)	1SA (2)	1T (3)	2WA (4)	2SA (5)	2T (6)
1	3	3	-	3	3	3
2	5	5	-	5	-	5
3	4	4	-	-	-	4
4	6	6	-	-	-	-
5	2	-	-	-	-	-
6	-	-	-	-	-	-

Table 11.6 L0R Sweeping Order

11.3.1.4 LFR Configuration

LFR Modal Contamination

	1WA (1)	1SA (2)	1T (3)	2WA (4)	2SA (5)	2T (6)	Contam. (1-norm)	Order (Contam based)	Order (Orig.)
1WA (1)	1	0.0002	0.0000	0.0007	0.021	0.0004	0.0223	4	1
1SA (2)	0.0002	1	0.0028	0.0000	0.0028	0.0025	0.0083	1	2
1T (3)	0.0000	0.0028	1	0.0007	0.0068	0.0005	0.0108	3	3
2WA (4)	0.0007	0.0000	0.0007	1	0.2841	0.001	0.2865	5	5
2SA (5)	0.0210	0.0028	0.0068	0.2841	1	0.0047	0.3194	6	6
2T (6)	0.0004	0.0025	0.0005	0.001	0.0047	1	0.0091	2	4

Table 11.7 LFR Modal Contamination Sorting

LFR Sweeping Order Matrix

Step	1WA (1)	1SA (2)	1T (3)	2WA (4)	2SA (5)	2T (6)
1	2	-	2	2	2	2
2	6	-	6	6	6	-
3	3	-	-	3	3	-
4	-	-	-	1	1	-
5	-	-	-	-	4	-
6	-	-	-	-	-	-

Table 11.8 LFR Sweeping Order

11.3.1.5 LF0 Configuration

LF0 Modal Contamination

	1WA (1)	1SA (2)	1T (3)	2WA (4)	2SA (5)	2T (6)	Contam. (1-norm)	Order (Contam based)	Order (Orig.)
1WA (1)	1	0.0324	0.0001	0.0011	0.0121	0.0017	0.0474	1	1
1SA (2)	0.0324	1	0.0239	0.0276	0.0007	0.0020	0.0866	4	2
1T (3)	0.0001	0.0239	1	0.0086	0.0251	0.0000	0.0577	3	3
2WA (4)	0.0011	0.0276	0.0086	1	0.0041	0.0106	0.052	2	4
2SA (5)	0.0121	0.0007	0.0251	0.0041	1	0.0933	0.1353	6	5
2T (6)	0.0017	0.0020	0.0000	0.0106	0.0933	1	0.1076	5	6

Table 11.9 LF0 Modal Contamination Sorting

LF0 Sweeping Order Matrix

Step	1WA (1)	1SA (2)	1T (3)	2WA (4)	2SA (5)	2T (6)
1	-	1	1	1	1	1
2	-	4	4	-	4	4
3	-	3	-	-	3	3
4	-	-	-	-	2	2
5	-	-	-	-	6	-
6	-	-	-	-	-	-

Table 11.10 LF0 Sweeping Order

11.3.1.6 0F0 Configuration

0F0 Modal Contamination

	1WA (1)	1SA (2)	1T (3)	2WA (4)	2SA (5)	2T (6)	Contam. (1-norm)	Order (Contam based)	Order (Orig.)
1WA (1)	1	0.0014	0.0000	0.001	0.0001	0.0006	0.0031	1	1
1SA (2)	0.0014	1	0.003	0.0003	0.0017	0.0042	0.0106	6	2
1T (3)	0.0000	0.003	1	0.0026	0.0036	0.0004	0.0096	5	3
2WA (4)	0.001	0.0003	0.0026	1	0.0003	0.0009	0.0051	2	4
2SA (5)	0.0001	0.0017	0.0036	0.0003	1	0.0000	0.0057	3	5
2T (6)	0.0006	0.0042	0.0004	0.0009	0.0000	1	0.0061	4	6

Table 11.11 0F0 Modal Contamination Sorting

0F0 Sweeping Order Matrix

Step	1WA (1)	1SA (2)	1T (3)	2WA (4)	2SA (5)	2T (6)
1	-	1	1	1	1	1
2	-	4	4	-	4	4
3	-	5	5	-	-	5
4	-	6	6	-	-	-
5	-	3	-	-	-	-
6	-	-	-	-	-	-

Table 11.12 0F0 Sweeping Order

11.3.1.7 Mode Shape Derived Metric Summary

The following tables display the result of the same analytical process detailed in sections 9.4 and 9.5. This approach to sweeping yielded better confidence values than the sweeping order derived from modal contamination. This is potentially unique to this structure due to the low damping of the system. In a structure with higher damping this metric of contamination may not perform in the same manner as with this particular structure.

	000	L00	L0R	LFR	LF0	0F0	Confidence (Contam. based)	Confidence (Original)
000	0.00073	0.46866	0.07114	0.07124	0.51286	0.11021	99.0%	99.9%
L00	0.14655	0.00946	0.10778	0.11710	0.07222	0.19445	86.9%	87.0%
L0R	0.02357	0.33298	0.00014	0.00959	0.41031	0.14419	98.6%	95.0%
LFR	0.02250	0.35161	0.01589	0.00040	0.38861	0.01940	97.5%	97.5%
LF0	0.16472	0.04717	0.14650	0.12786	0.00809	0.12331	82.9%	56.0%
0F0	0.22685	0.53996	0.23695	0.09820	0.43175	0.00052	99.5%	99.4%

Table 11.13 Modal Contamination Derived Sweeping

Using this method of sweeping based on the contamination of each mode yielded excellent results. All configurations were correctly predicted with high confidence levels above 80%. This shows that for this structure the contamination based sweeping approach improved the observed results for this particular study.

This phenomenon is possibly unique to this structure because of very low damping levels and relationship between the modal frequencies. Low damping levels minimize the level of modal mixing due to frequencies that are close together. In larger more complex structures the damping is expected to be significantly higher, which could potentially reduce the effectiveness of this sweeping technique.

12.0 BIBLIOGRAPHY

(Celebi, Phan and Marshall 1993) Celebi, M., Phan, L., Marshall, R. "Dynamic Characteristics of Five Tall Buildings During Strong and Low-Amplitude Motions." *The Structural Design of Tall Buildings.* 2.1 (1993) 1-15. Wiley-Blackwell Journals. California Polytechnic State University, San Luis Obispo, Kennedy Library. 23 April 2013. <http://0-onlinelibrary.wiley.com.library.colby.edu>.

(Clinton et al 2006) Clinton, John, Bradford, S., Heaton, Thomas, Favela, Javier "The Observed Wander of the Natural Frequencies in a Structure."*Bulletin of the Seismological Society of America.* 96.1 (2006) 237–257. Geo Science World.California Polytechnic State University, San Luis Obispo, Kennedy Library.27April2013. <bssa.geoscienceworld.org>.

(Hou, Noori and Amand 2000) Hou, Z., Noori, M., and Amand, R. "Wavelet-based Approach for Structural Damage Detection."*Journal of Engineering Mechanics.*126.7 (2000) 677–683. ASCE Library. California Polytechnic State University, San Luis Obispo, Kennedy Library. 27 April 2013. <ascelibrary.org>

(Lin, Yang and Zhou 2005) Lin, Silian, Yang, Jann, and Zhou, Li. "Damage Identification of a Benchmark Building for Structural Health Monitoring."*Smart Materials and Structures* 14.3 (2005): S162–S169. IOPScience.California Polytechnic State University, San Luis Obispo, Kennedy Library.2 May 2013.<iopscience.iop.org>

(Pastor, Binda, Harčarik 2012) Pastor, Binda, Harčarik . "Modal Assurance Criterion." *Procedia Engineering* Volume 48 (2012) 543-548.Science Direct. California Polytechnic State University, San Luis Obispo, Kennedy Library. 15 December 2013. < sciencedirect.com>

(Chopra 2007) Chopra. "Dynamics of Structures: Theory and Applications to Earthquake Engineering." Third Edition. *Pearson Education* 406-408. California Polytechnic State University, San Luis Obispo, Kennedy Library. 4 February 2014.

(Todorovska, Trifunac 2006) Todorovska, Maria I., and Mihailo D. Trifunac. "Earthquake Damage Detection in the Imperial County Services Building I: The Data and Time–frequency Analysis." *Soil Dynamics and Earthquake Engineering* 27.6 (2006) 564–576.SciVerse.California Polytechnic State University, San Luis Obispo, Kennedy Library. 29 April 2013. <sciencedirect.com>

(Wu, Xu and Yokohama 2002) Wu, Zhishen, Bin Xu, and Koichi Yokoyama.“Decentralized Parametric Damage Detection Based on Neural Networks.”*Computer-Aided Civil and Infrastructure Engineering* 17.3 (2002) 175–184.Wiley Online Library.California Polytechnic State University, San Luis Obispo, Kennedy Library. 30 April 2013. <onlinelibrary.wiley.com>

(Xu et al 2005) Xu, Bin et al. “A Soft Post-earthquake Damage Identification Methodology Using Vibration Time Series.”*Smart Materials and Structures* 14.3 (2005): S116–S124.IOPScience.California Polytechnic State University, San Luis Obispo, Kennedy Library. 22 Apr. 2013.

13.0 WORKS CONSULTED

(Todorovska, Trifunac 2006) Todorovska, Maria I., and Mihailo D. Trifunac. "Earthquake Damage Detection in the Imperial County Services Building II: Analysis of Novelties via Wavelets." *Structural Control and Health Monitoring* 17.8 (2006) 895–917.Wiley Online Library. California Polytechnic State University, San Luis Obispo, Kennedy Library. 29 April 2013.<onlinelibrary.wiley.com>

(Todorovska, Trifunac 2007) Todorovska, Maria I., and Mihailo D. Trifunac. "Earthquake Damage Detection in the Imperial County Services Building III: Analysis of Wave Travel Times via Impulse Response Functions." *Soil Dynamics and Earthquake Engineering* 28.5 (2007) 387–404.SciVerse. California Polytechnic State University, San Luis Obispo, Kennedy Library. 29 April 2013. <sciencedirect.com>

14.0 APPENDIX

14.1 Free Vibration

Initially free vibration testing was completed to investigate the possibility of using time history acceleration data of the structure settling from steady state shaking. The results showed unexpected trends in damping that are theorized to be due to the interaction of the shaker as it turned off. This is potentially adding damping to the structure from the internal mechanism of the shaker absorbing kinetic energy from the vibrating frame.

The following tables display the raw time history recordings, the frequency of the structure versus amplitude of excitation, and the damping of the structure vs amplitude of excitation for each mode of the 000 configuration.

14.1.1 1WA Modal Behavior

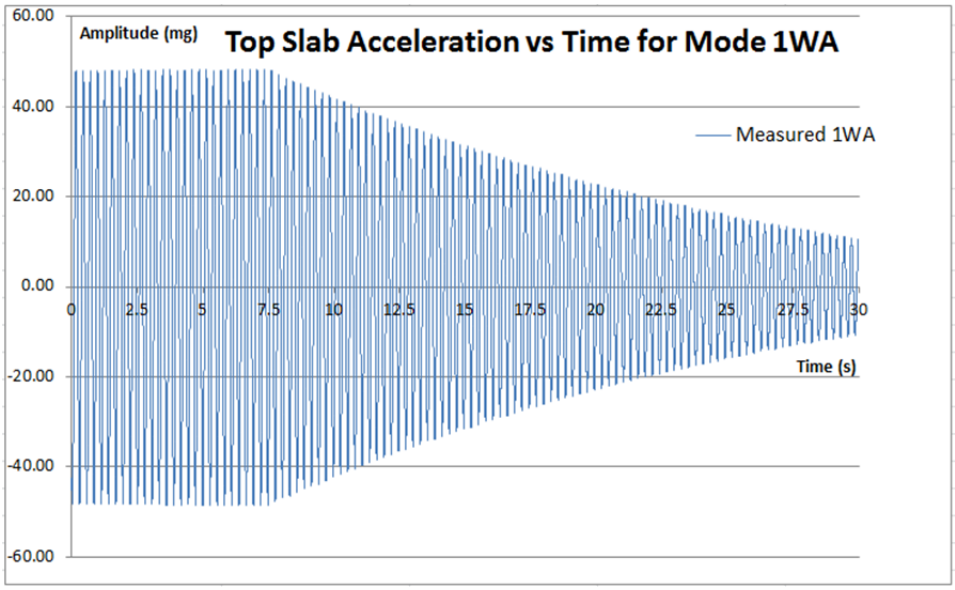

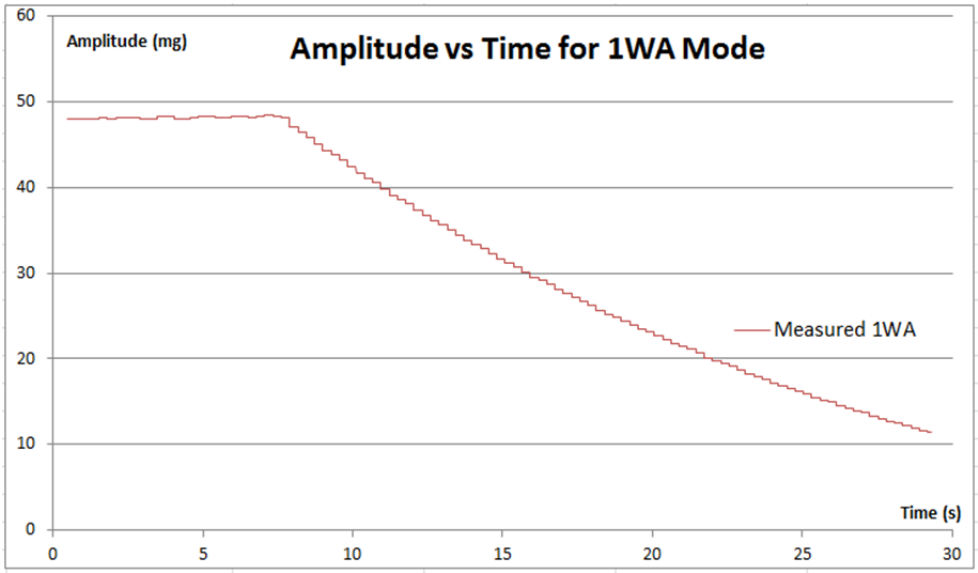

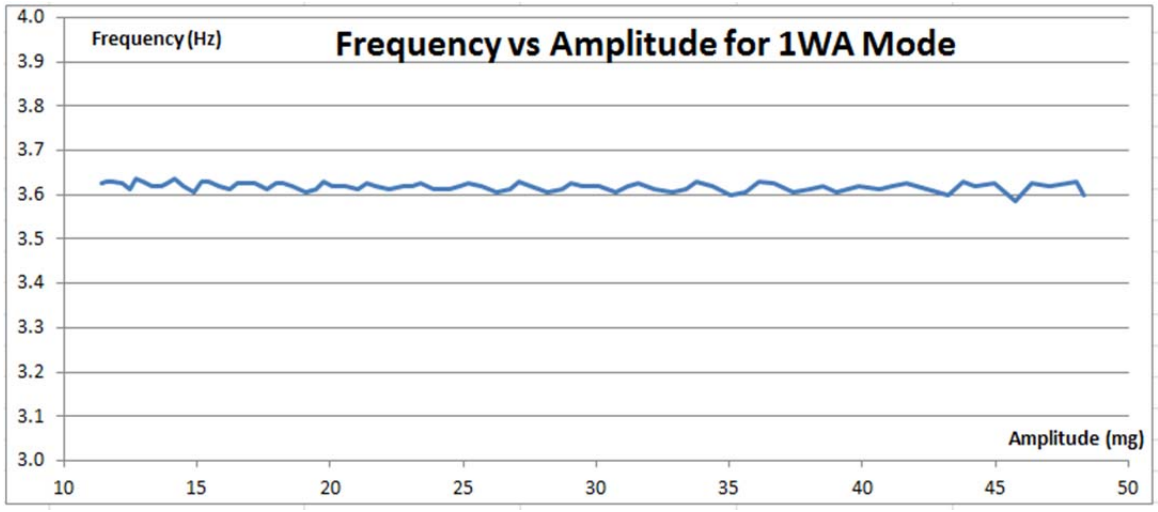
Frequency (Hz)
Frequency vs Amplitude for 1WA Mode
4.0
3.9
3.8
3.7
3.6
3.5
3.4
3.3
3.2
3.1
3.0
Amplitude (mg)
10
15
20
25
30
35
40
45
50

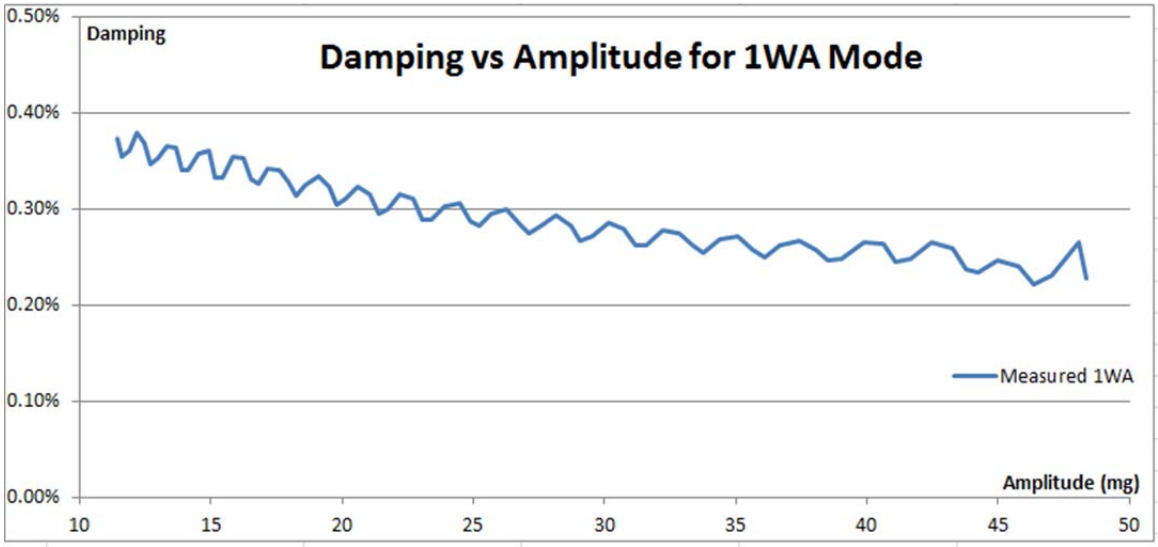
Damping
Damping vs Amplitude for 1WA Mode
0.50%
0.40%
0.30%
0.20%
0.10%
0.00%
Measured 1WA
Amplitude (mg)
10
15
20
25
30
35
40
45
50

14.1.2 1SA Modal Behavior

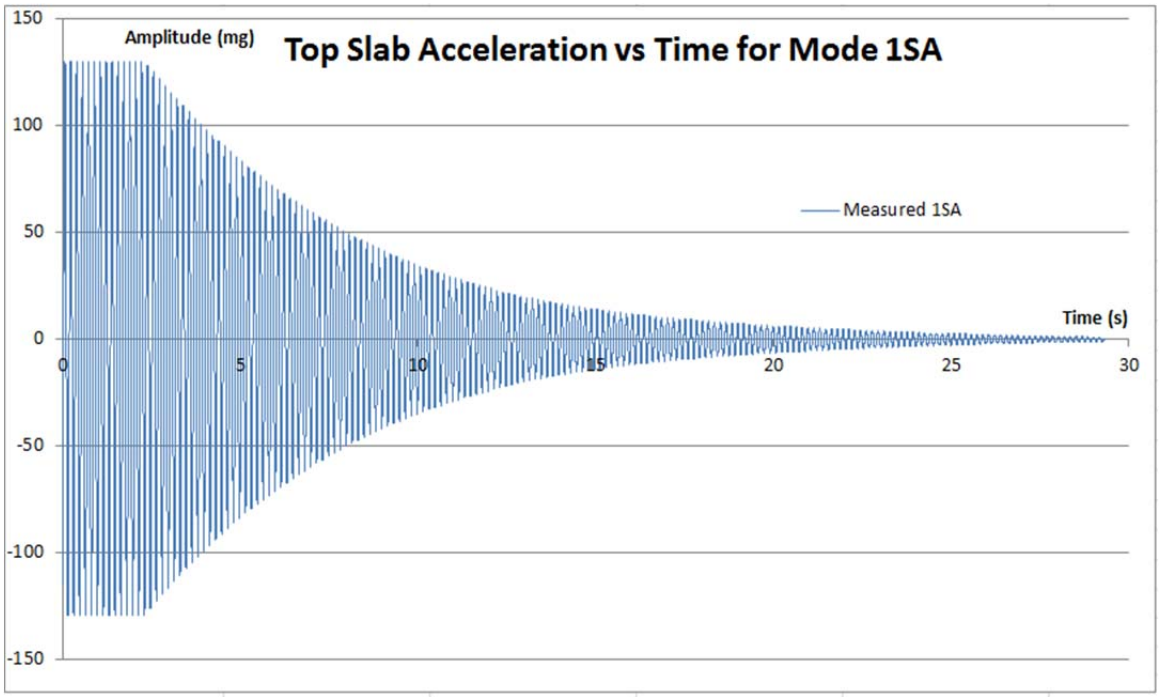

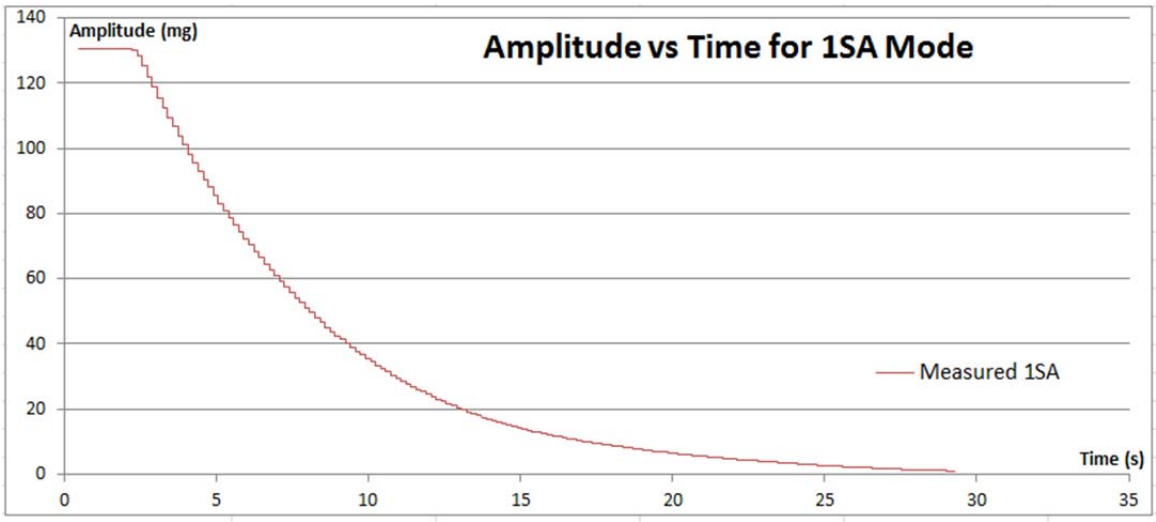

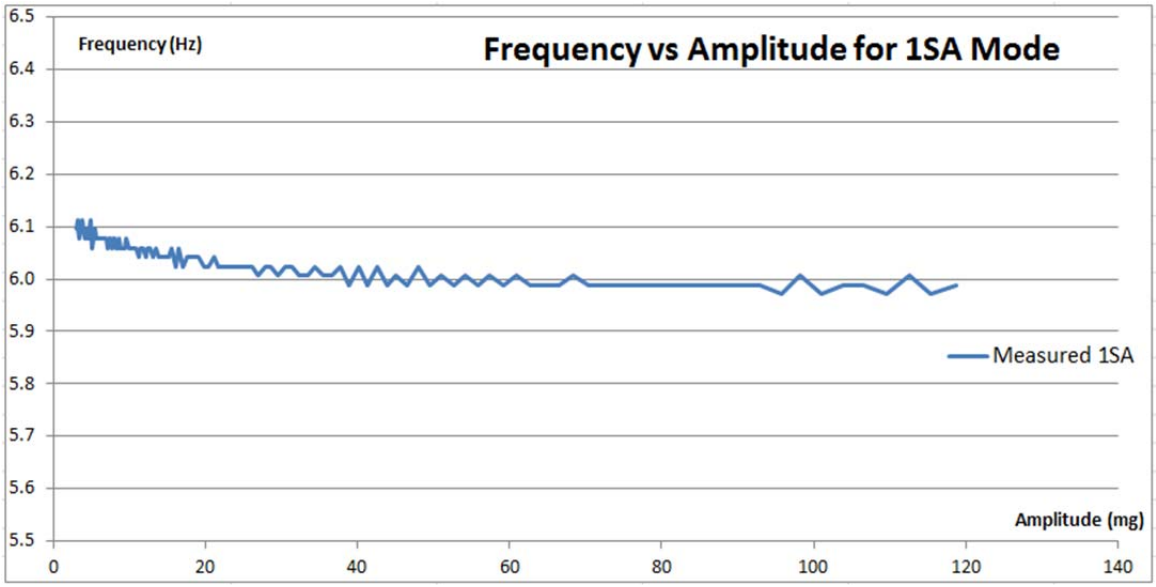
Frequency (Hz)
Frequency vs Amplitude for 1SA Mode
6.5
6.4
6.3
6.2
6.1
6.0
5.9
5.8
5.7
5.6
5.5
Measured 1SA
Amplitude (mg)
0
20
40
60
80
100
120
140

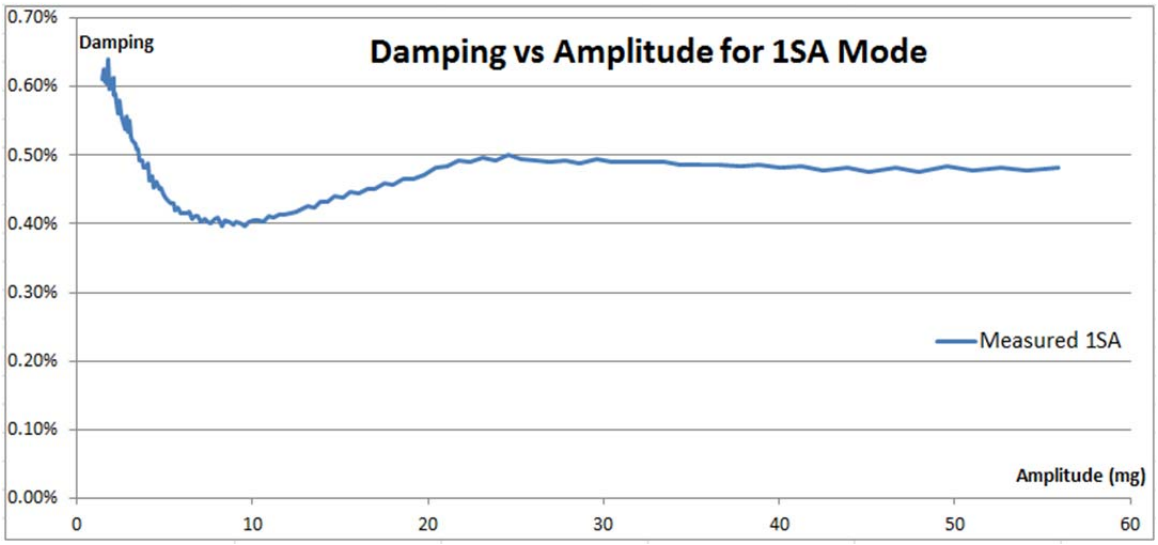
Damping
Damping vs Amplitude for 1SA Mode
0.70%
0.60%
0.50%
0.40%
0.30%
0.20%
0.10%
0.00%
Measured 1SA
Amplitude (mg)
0
10
20
30
40
50
60

14.1.3 1T Modal Behavior

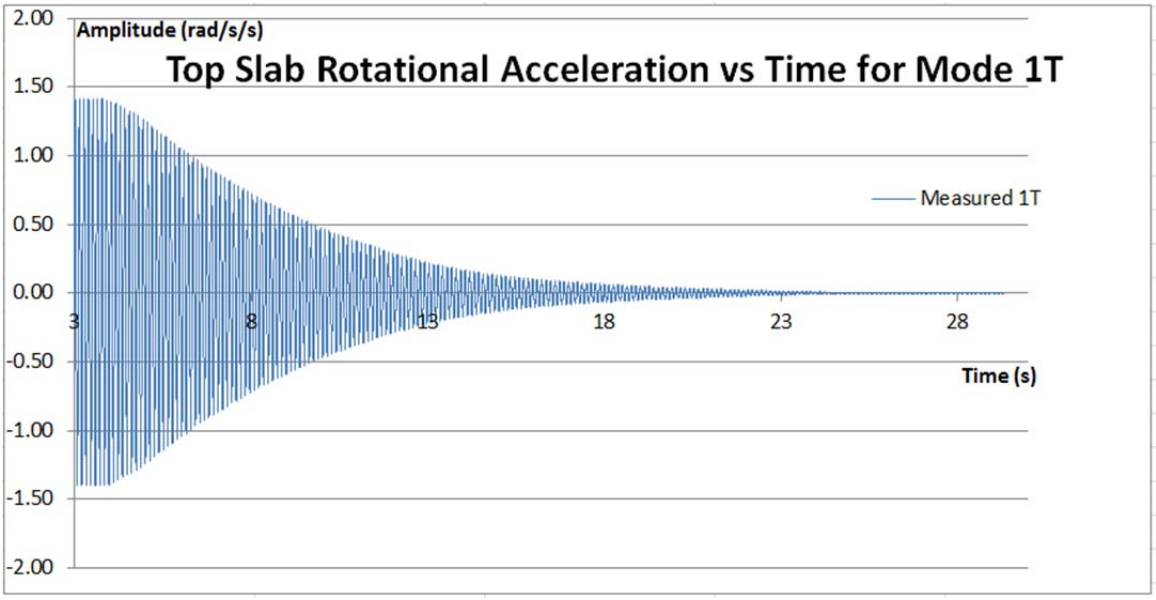

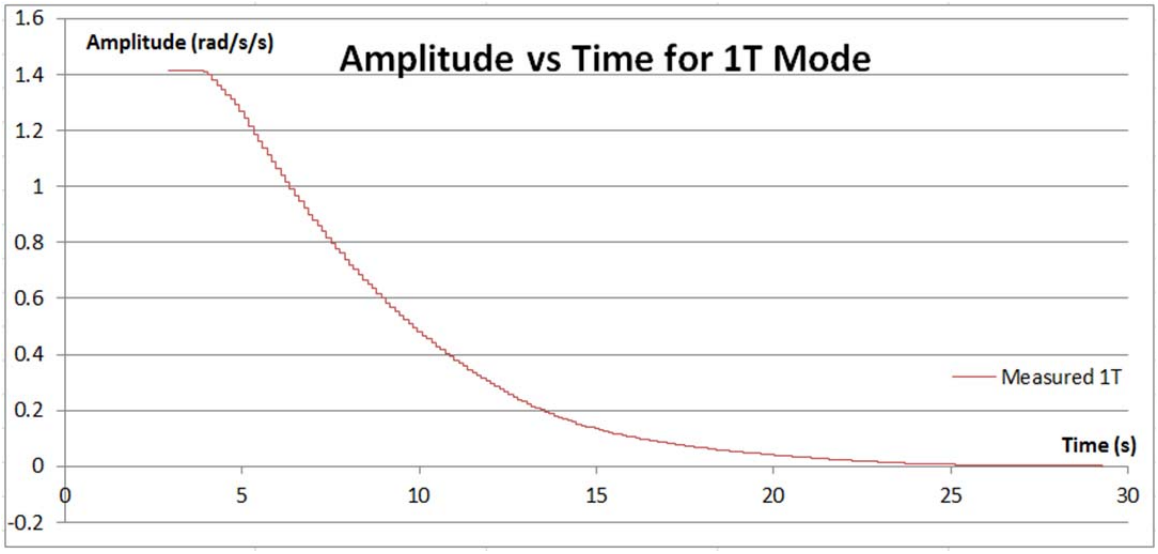

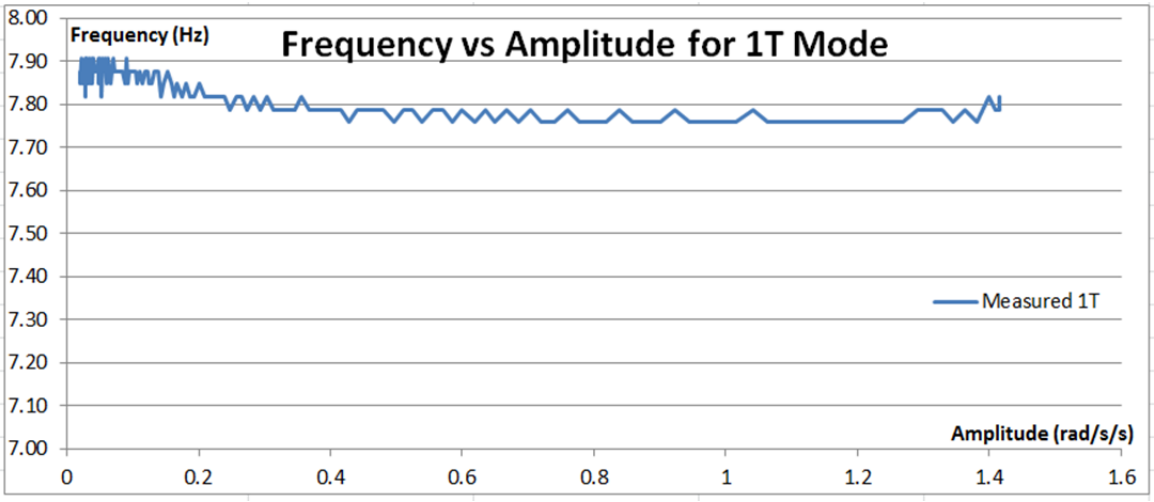
Frequency vs Amplitude for 1T Mode
Frequency (Hz)
8.00
7.90
7.80
7.70
7.60
7.50
7.40
7.30
7.20
7.10
7.00
Measured 1T
Amplitude (rad/s/s)
0
0.2
0.4
0.6
0.8
1
1.2
1.4
1.6

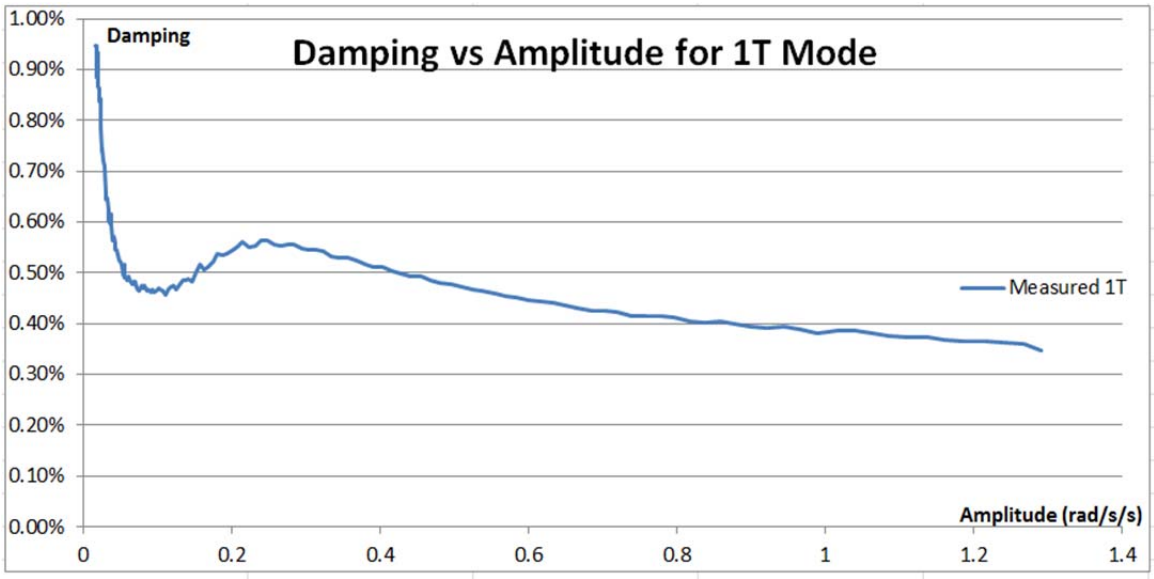
Damping vs Amplitude for 1T Mode
Damping
1.00%
0.90%
0.80%
0.70%
0.60%
0.50%
0.40%
0.30%
0.20%
0.10%
0.00%
Measured 1T
Amplitude (rad/s/s)
0
0.2
0.4
0.6
0.8
1
1.2
1.4

14.1.4 2WA Modal Behavior

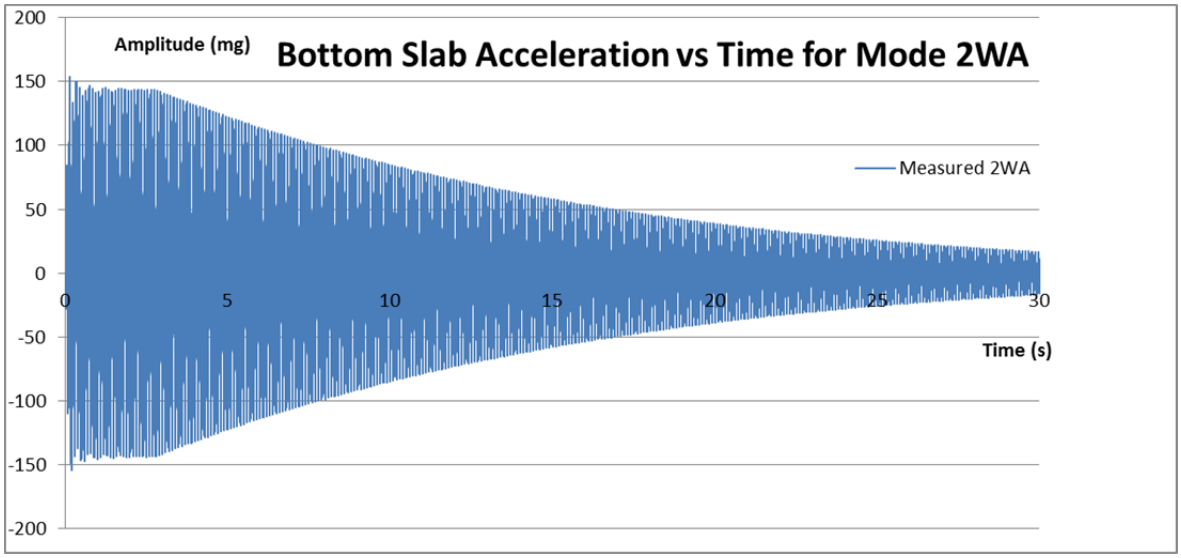

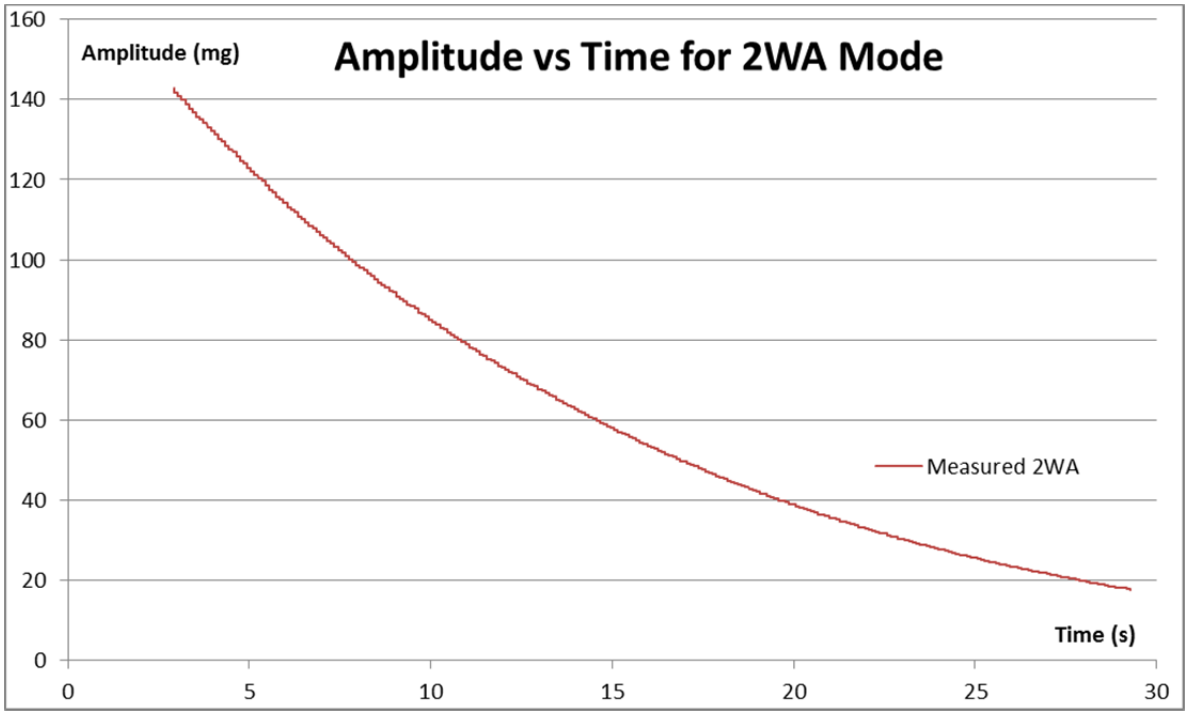

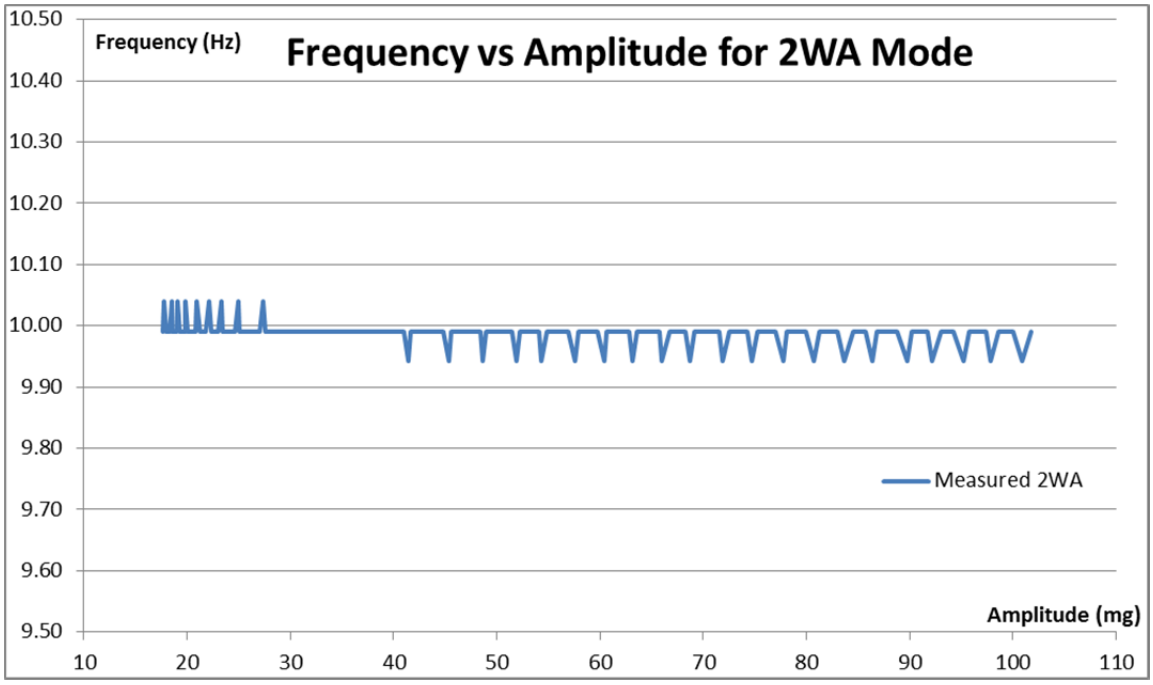
Frequency (Hz)
Frequency vs Amplitude for 2WA Mode
10.50
10.40
10.30
10.20
10.10
10.00
9.90
9.80
9.70
9.60
9.50
Measured 2WA
Amplitude (mg)
10
20
30
40
50
60
70
80
90
100
110

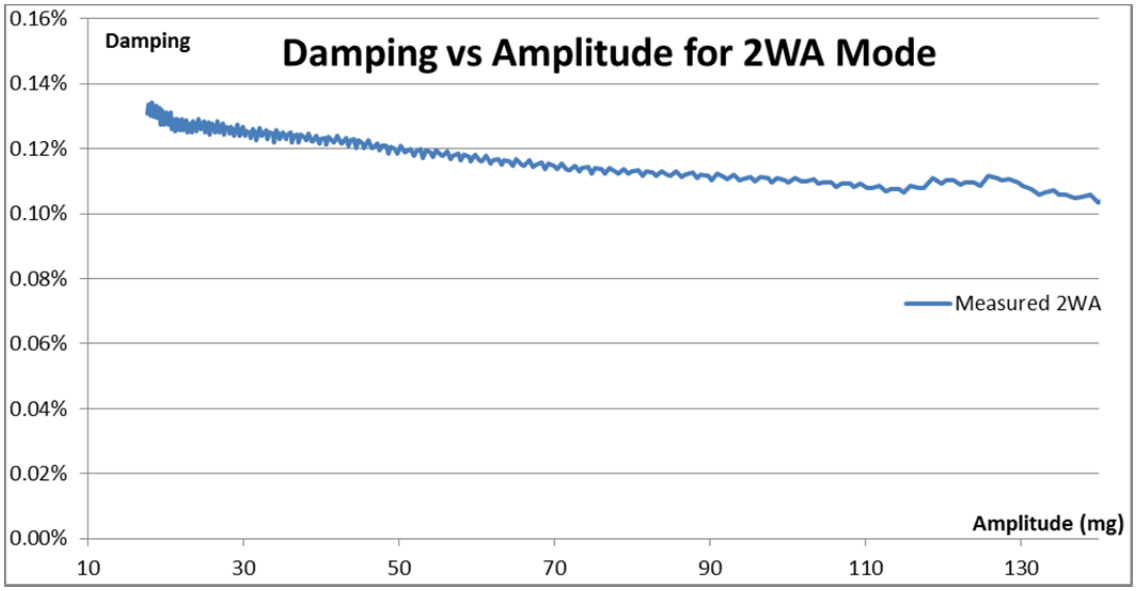
Damping
Damping vs Amplitude for 2WA Mode
0.16%
0.14%
0.12%
0.10%
0.08%
0.06%
0.04%
0.02%
0.00%
Measured 2WA
Amplitude (mg)
10
30
50
70
90
110
130

14.1.5 2SA Modal Behavior

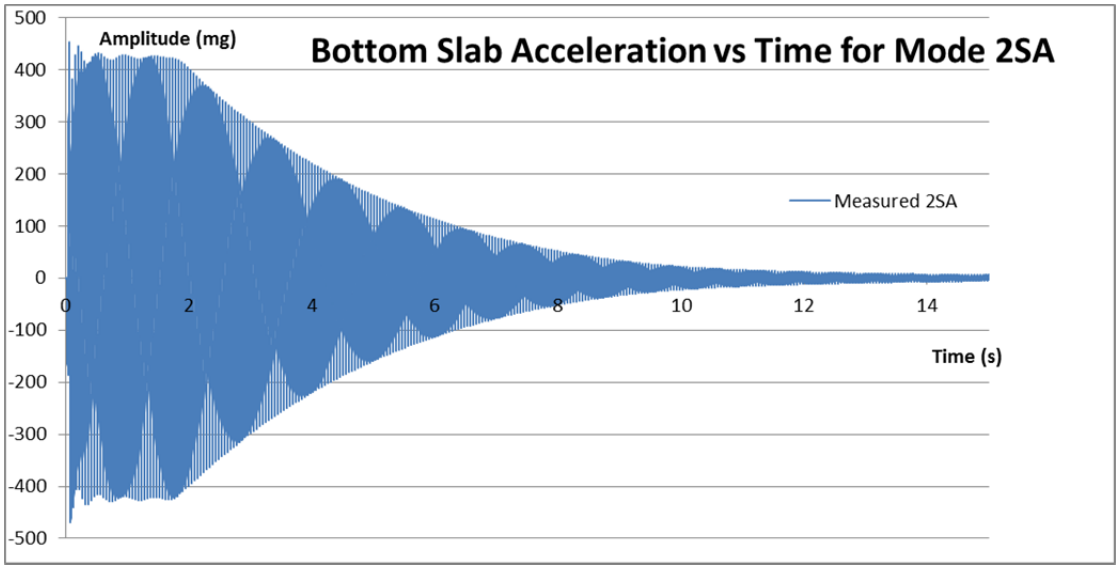

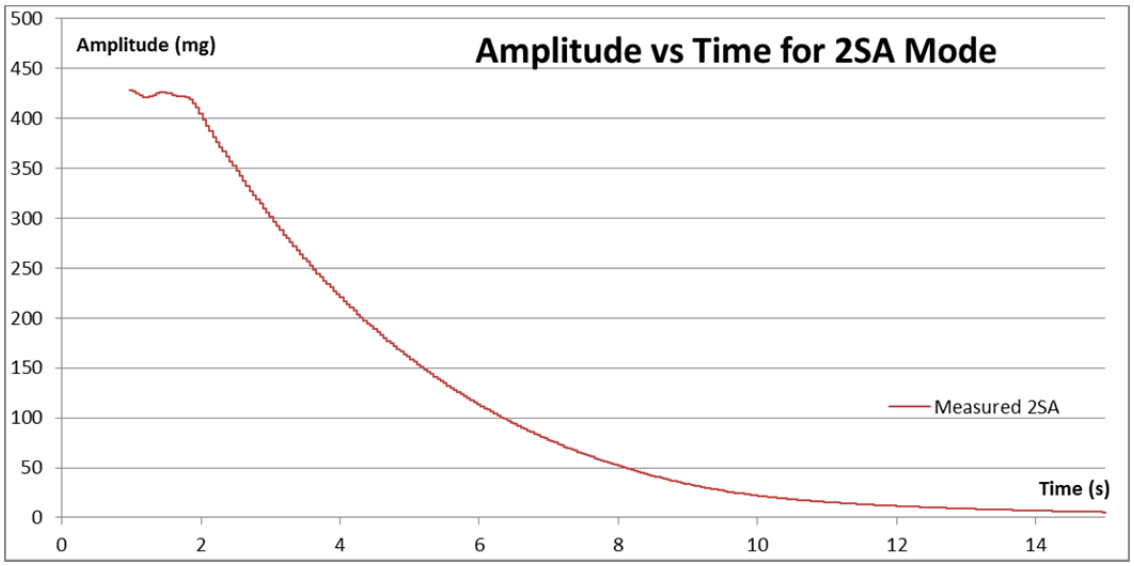

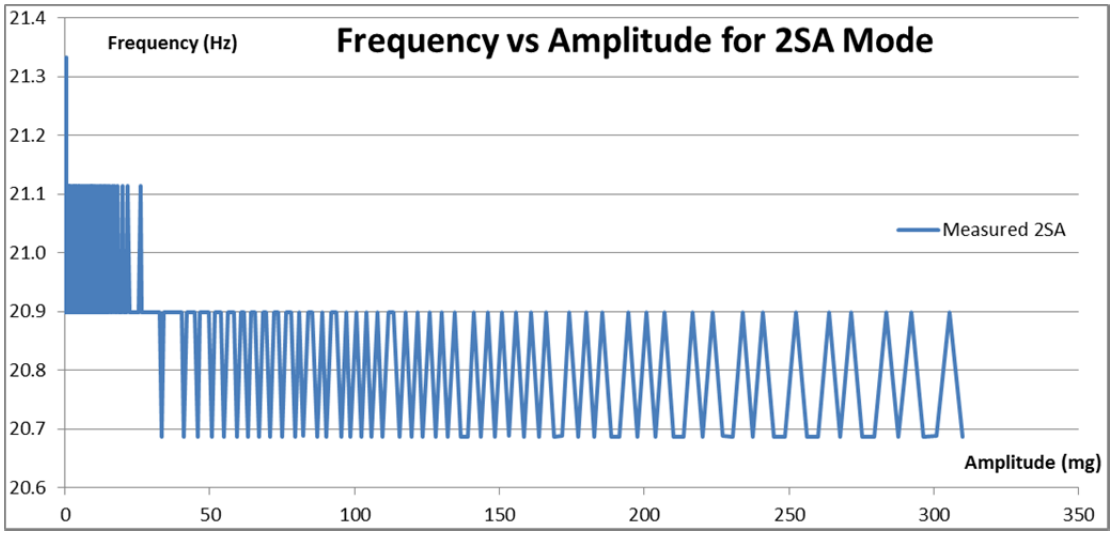
Frequency (Hz)
Frequency vs Amplitude for 2SA Mode
21.4
21.3
21.2
21.1
21.0
20.9
20.8
20.7
20.6
Measured 2SA
Amplitude (mg)
0
50
100
150
200
250
300
350

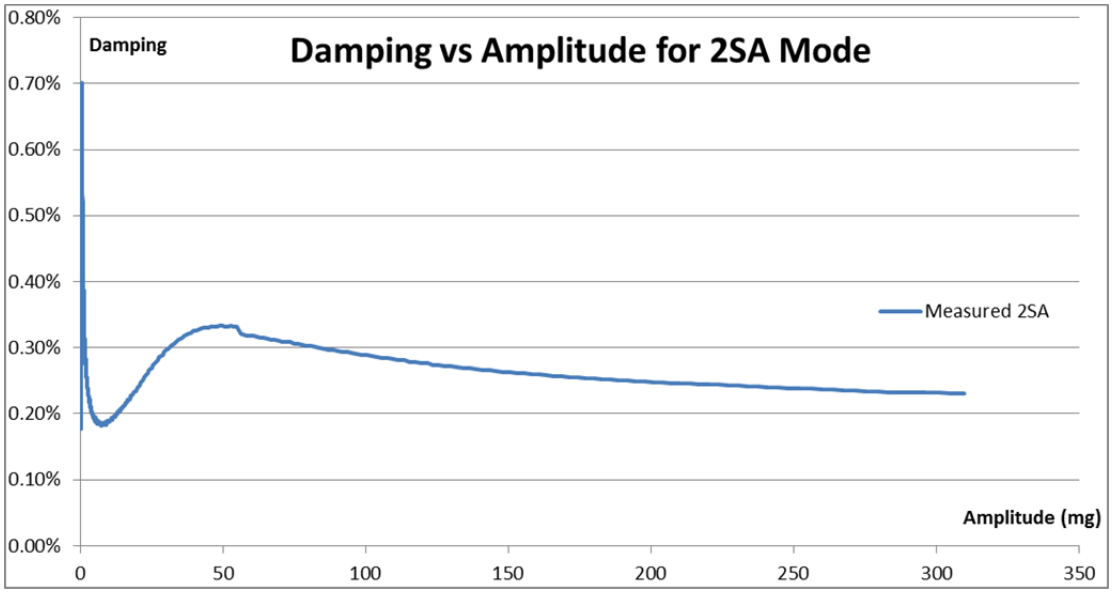
Damping
Damping vs Amplitude for 2SA Mode
0.80%
0.70%
0.60%
0.50%
0.40%
0.30%
0.20%
0.10%
0.00%
Measured 2SA
Amplitude (mg)
0
50
100
150
200
250
300
350

14.1.6 2T Modal Behavior

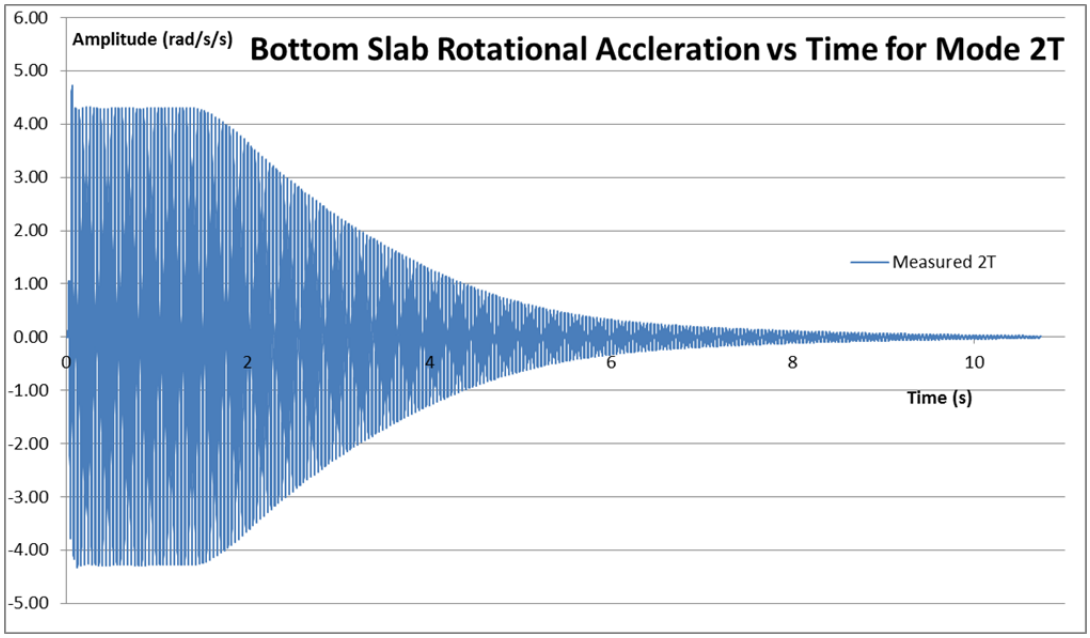

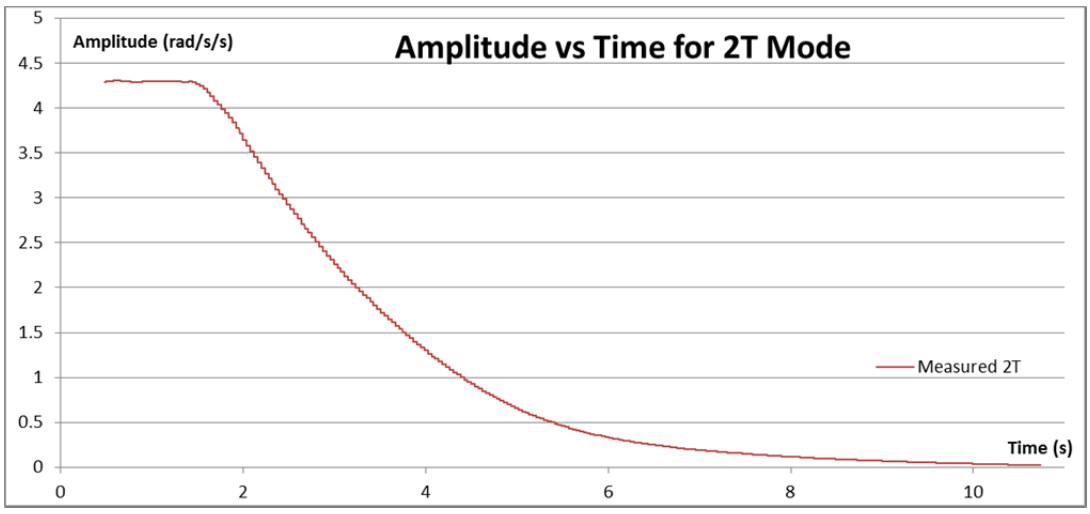

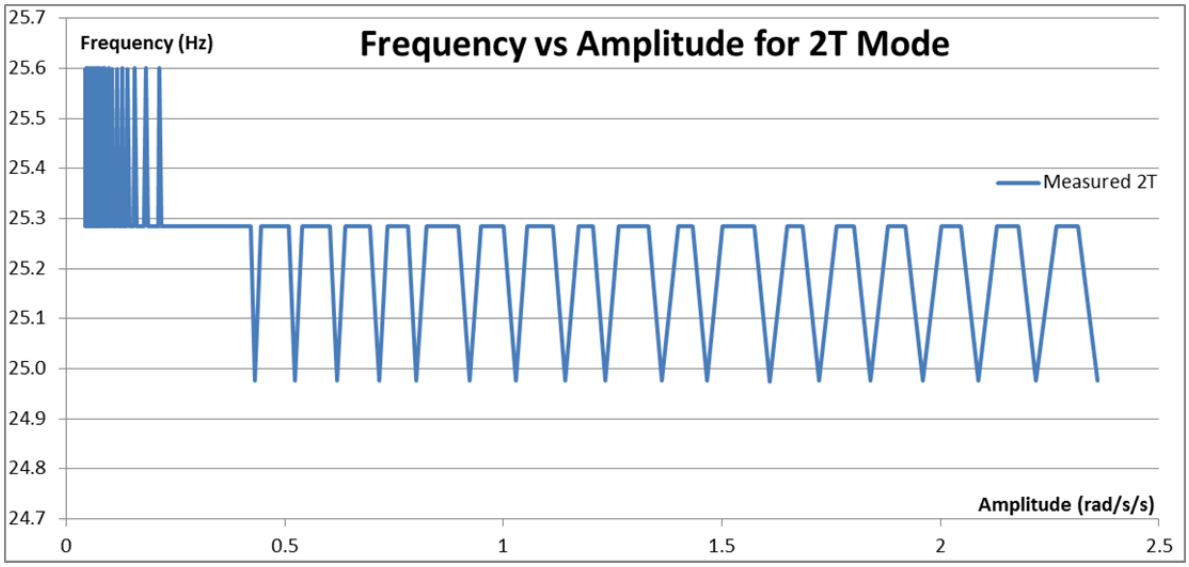
Frequency (Hz)
Frequency vs Amplitude for 2T Mode
25.7
25.6
25.5
25.4
25.3
25.2
25.1
25.0
24.9
24.8
24.7
Measured 2T
Amplitude (rad/s/s)
0
0.5
1
1.5
2
2.5

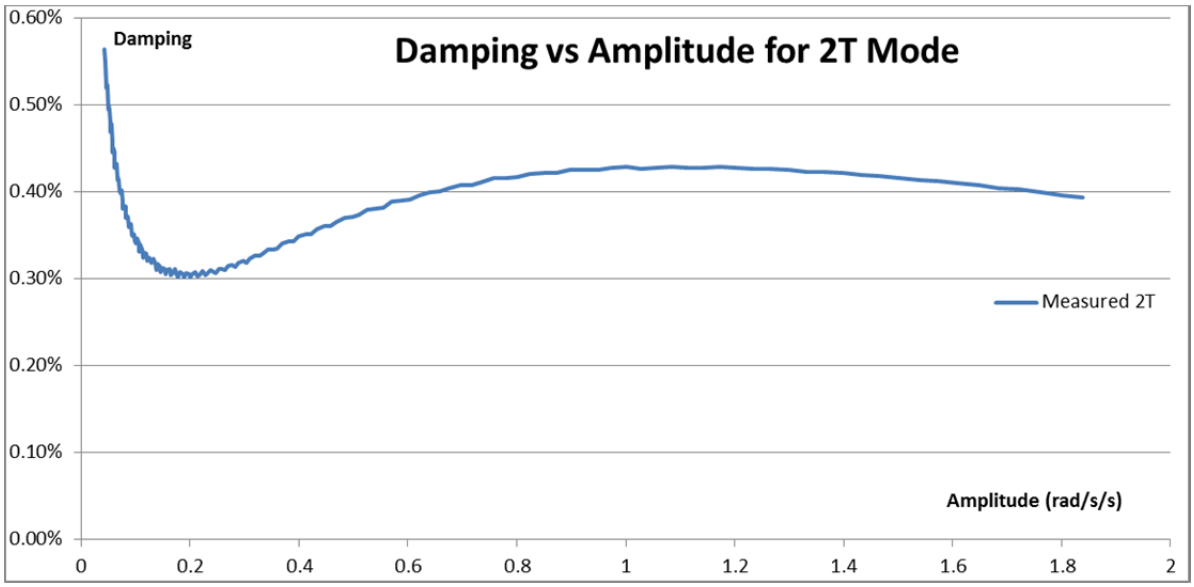
Damping
Damping vs Amplitude for 2T Mode
0.60%
0.50%
0.40%
0.30%
0.20%
0.10%
0.00%
Measured 2T
Amplitude (rad/s/s)
0
0.2
0.4
0.6
0.8
1
1.2
1.4
1.6
1.8
2

14.2 Initial Forced Vibration Testing of Base Configuration (000)

The base configuration was tested extensively in the beginning of the study to determine both the accuracy of the analytical model and the damping of each mode. This testing informed the final decision on amplitudes of excitation to test each mode.

It was discovered that the structure's exact modal frequencies were not perfectly constant with respect to amplitude of excitation in the initial time history testing. The following graphs display the measured modal frequencies over several tests at various amplitudes and dates. It is believed that the structure needed to be tested to moderately high amplitude to settle anything that would change with vibration.

In the following figures the test data from 2/13 and 2/18 are derived from free vibration tests. The results from 2/23 are derived from forced vibration frequency sweeps. Both of these test methods were investigated to estimate the damping of the structure's modes. Damping values derived from frequency sweeps are calculated using the half power bandwidth method.

14.2.1 1WA Modal Consistency

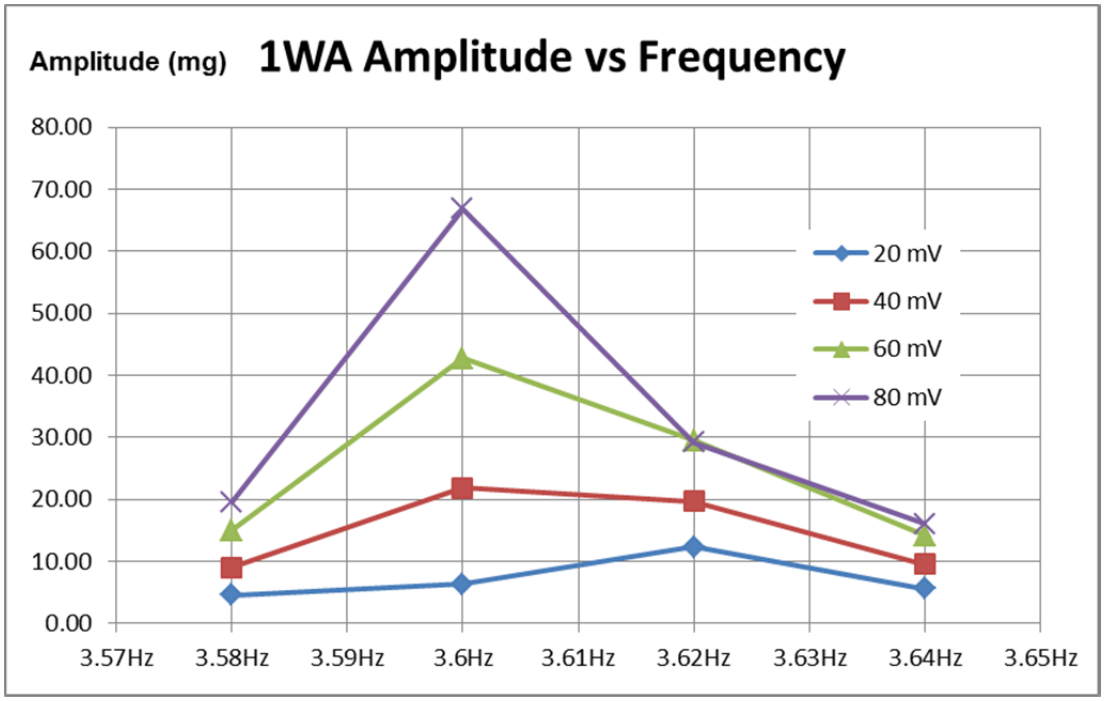

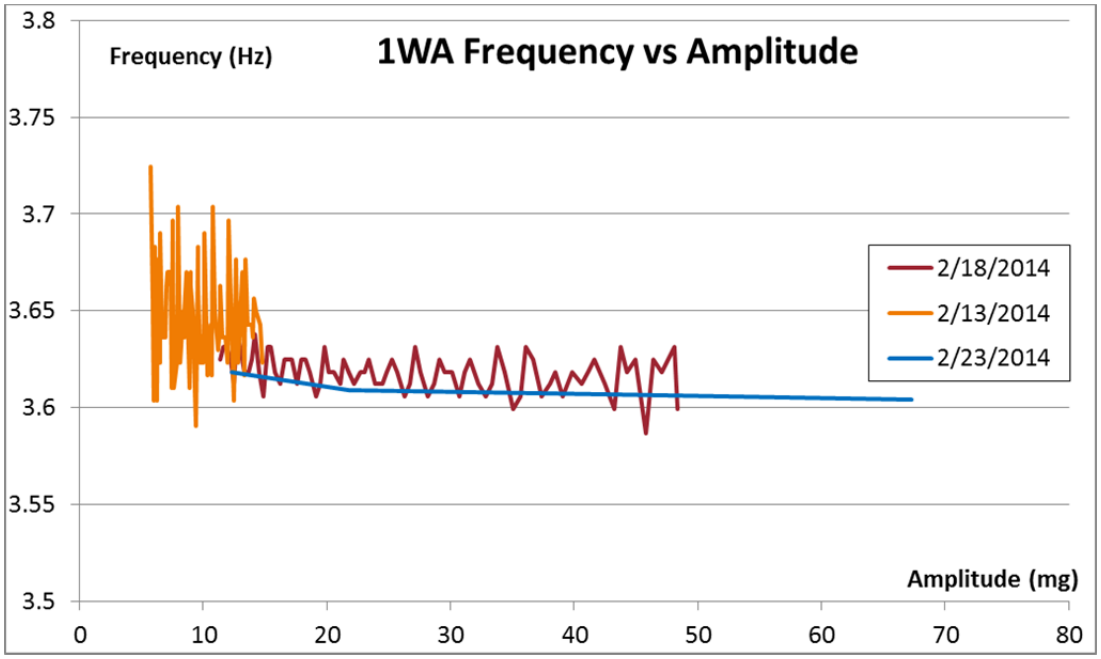

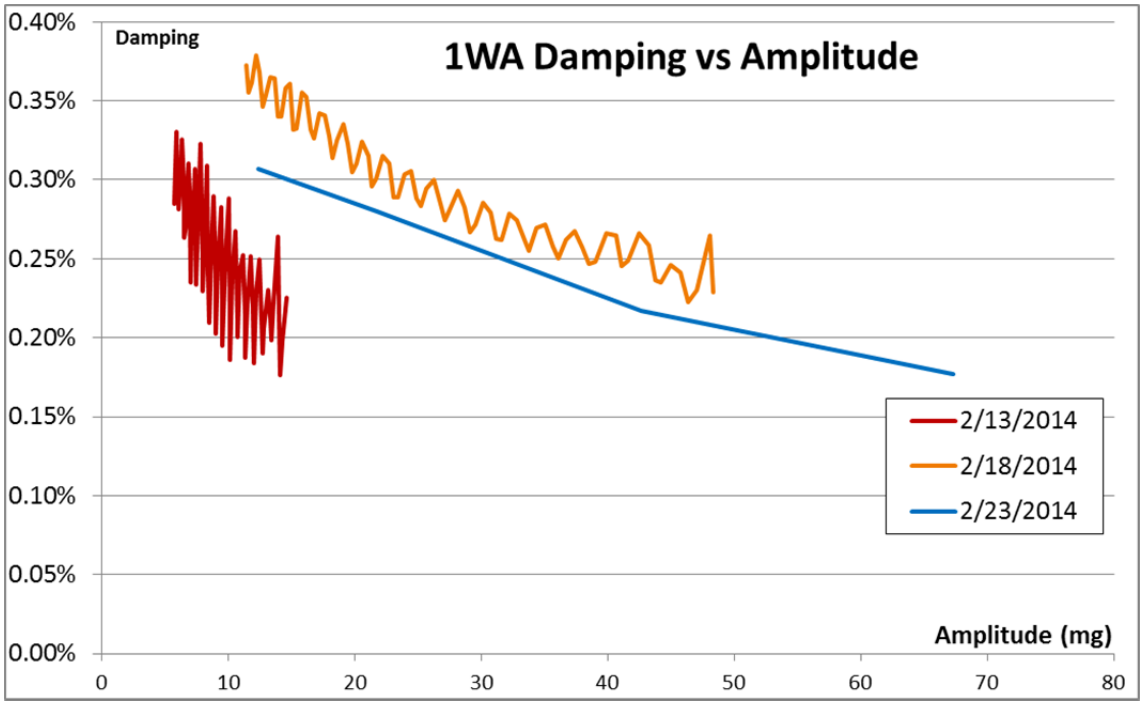

14.2.2 1SA Modal Consistency

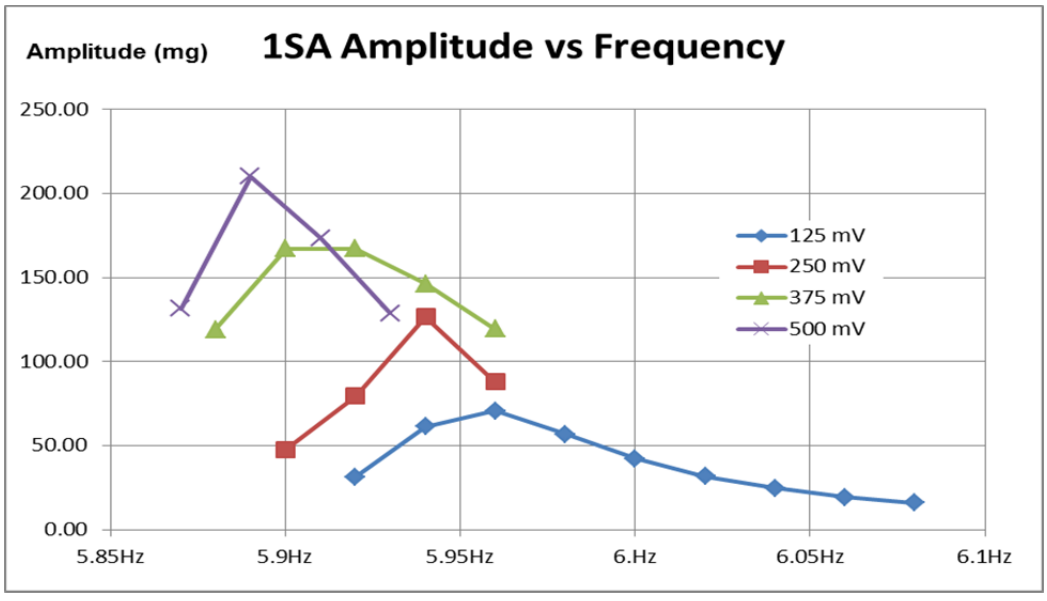

The graph above shows the results of several forced vibration frequency sweeps at several amplitudes.

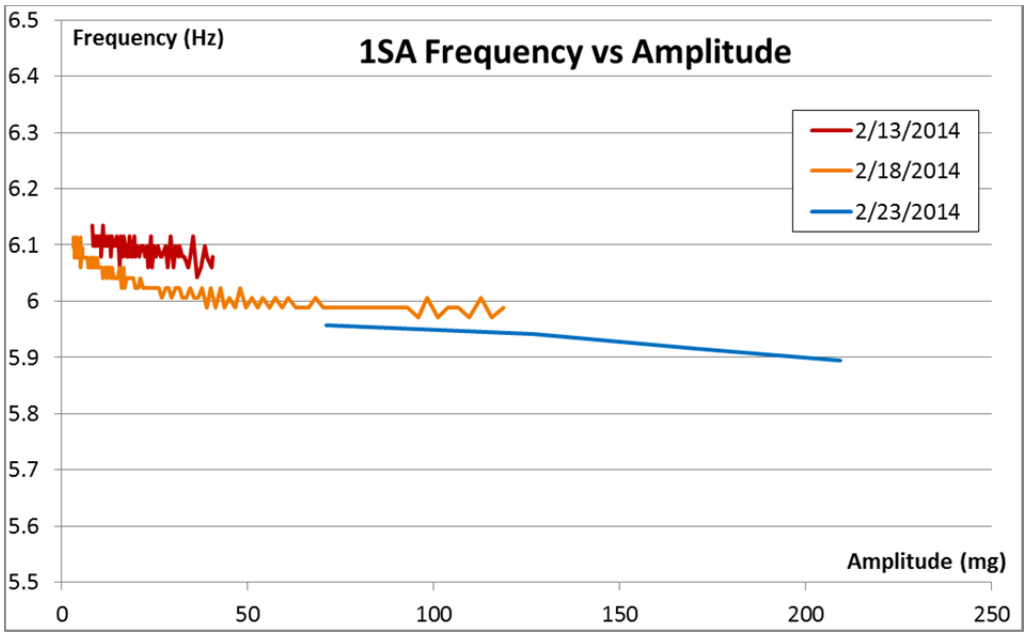

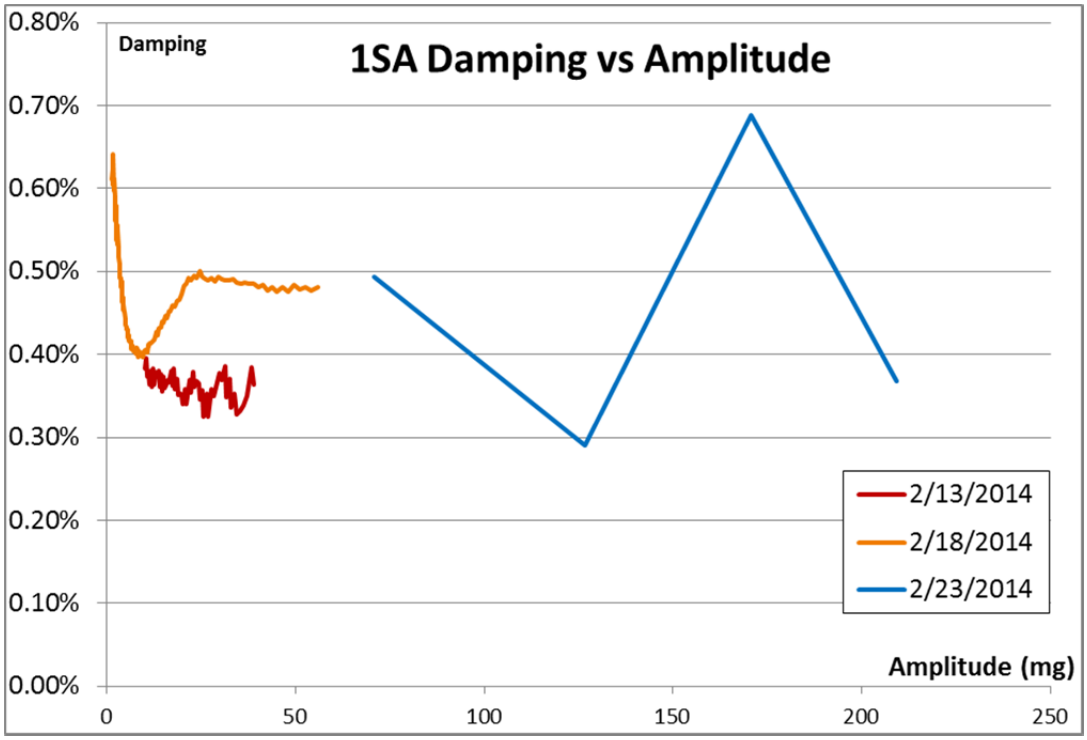

14.2.3 1T Modal Consistency

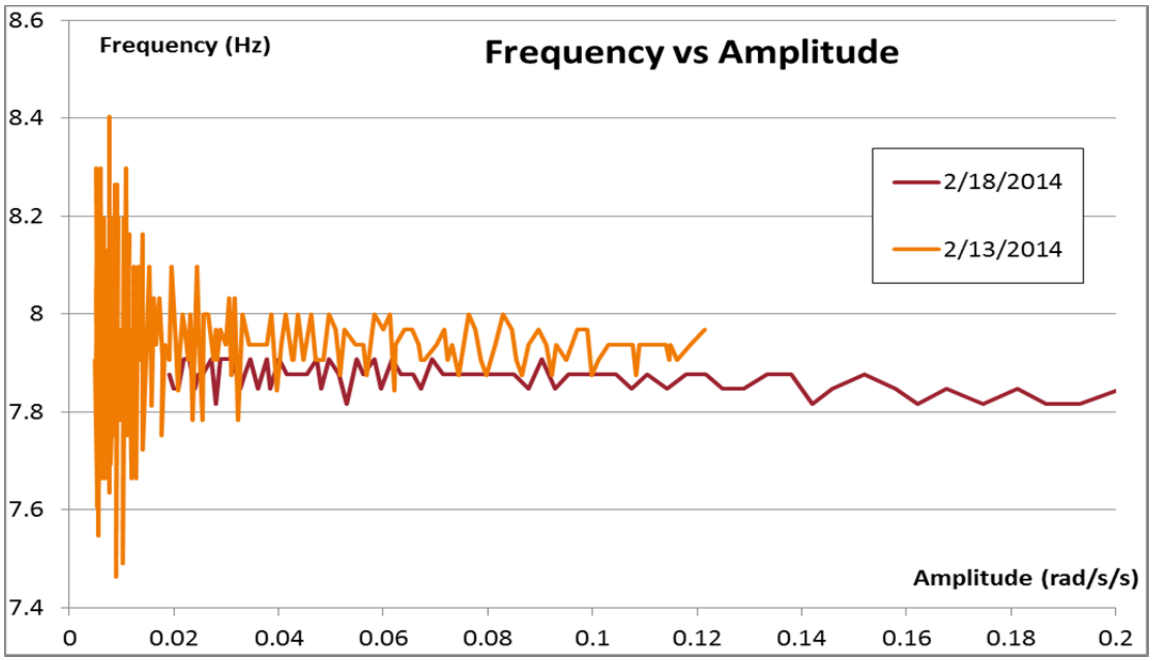

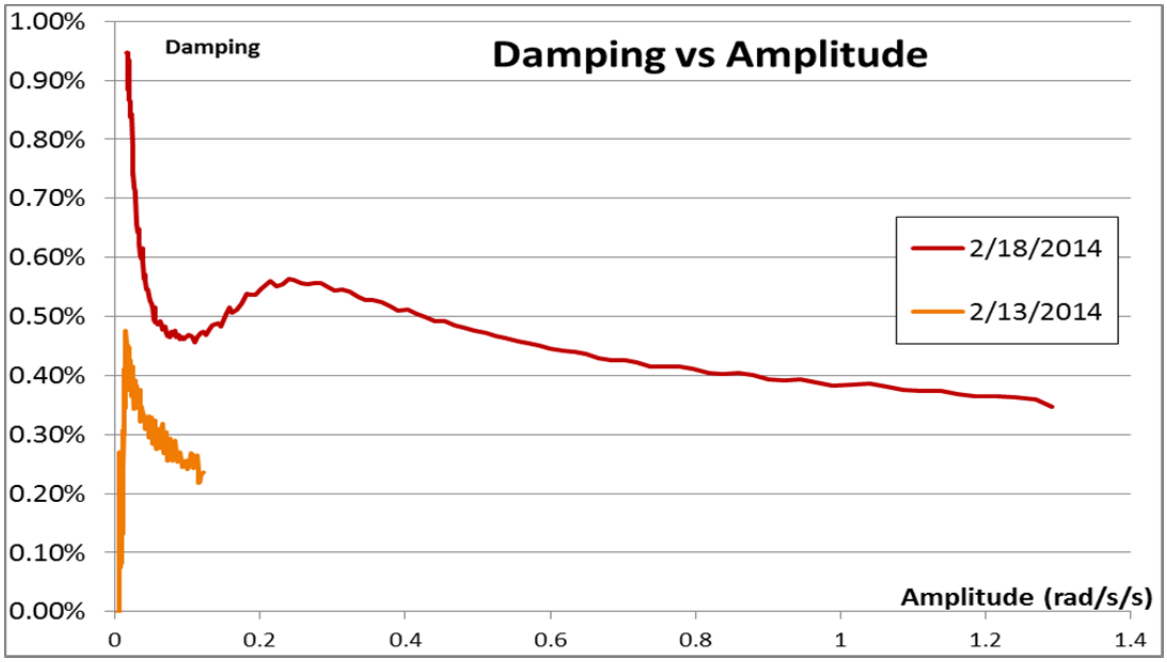

14.2.4 2WA Modal Consistency

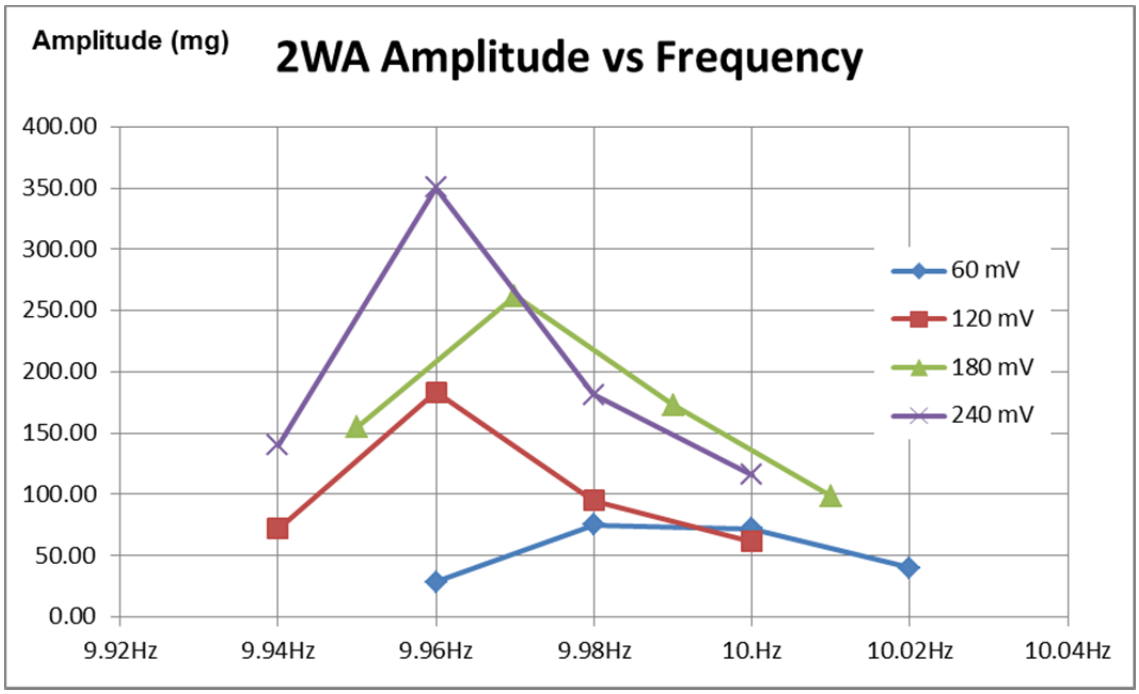

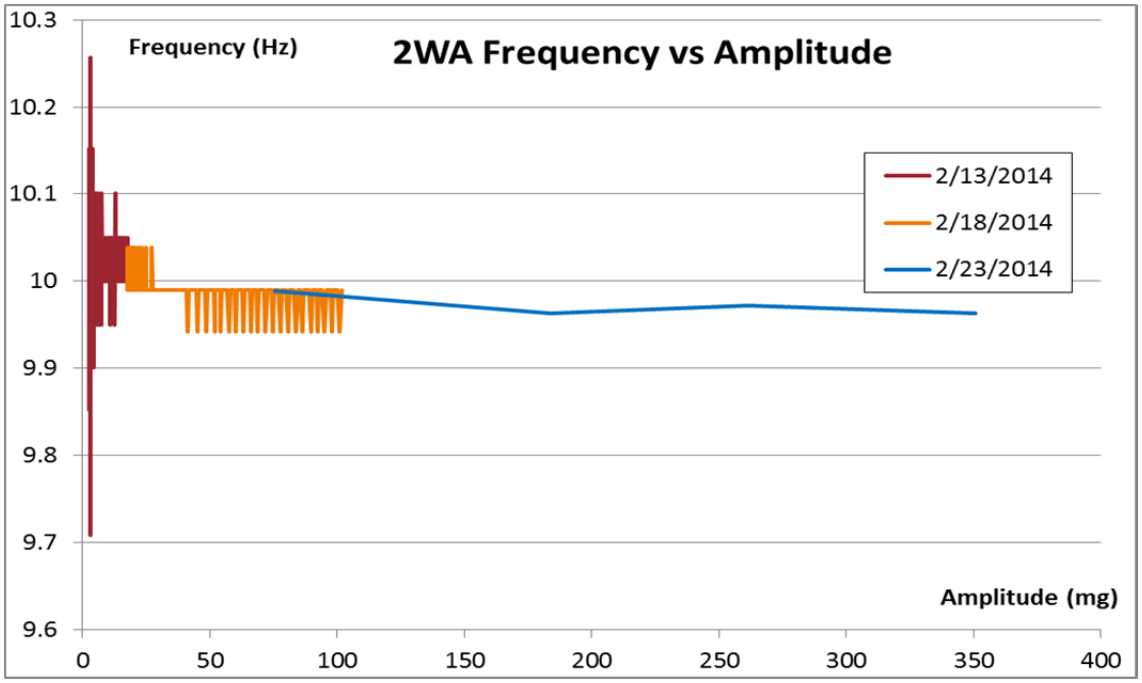
Frequency (Hz)
2WA Frequency vs Amplitude
10.3
10.2
10.1
10
9.9
9.8
9.7
9.6
2/13/2014
2/18/2014
2/23/2014
Amplitude (mg)
0
50
100
150
200
250
300
350
400

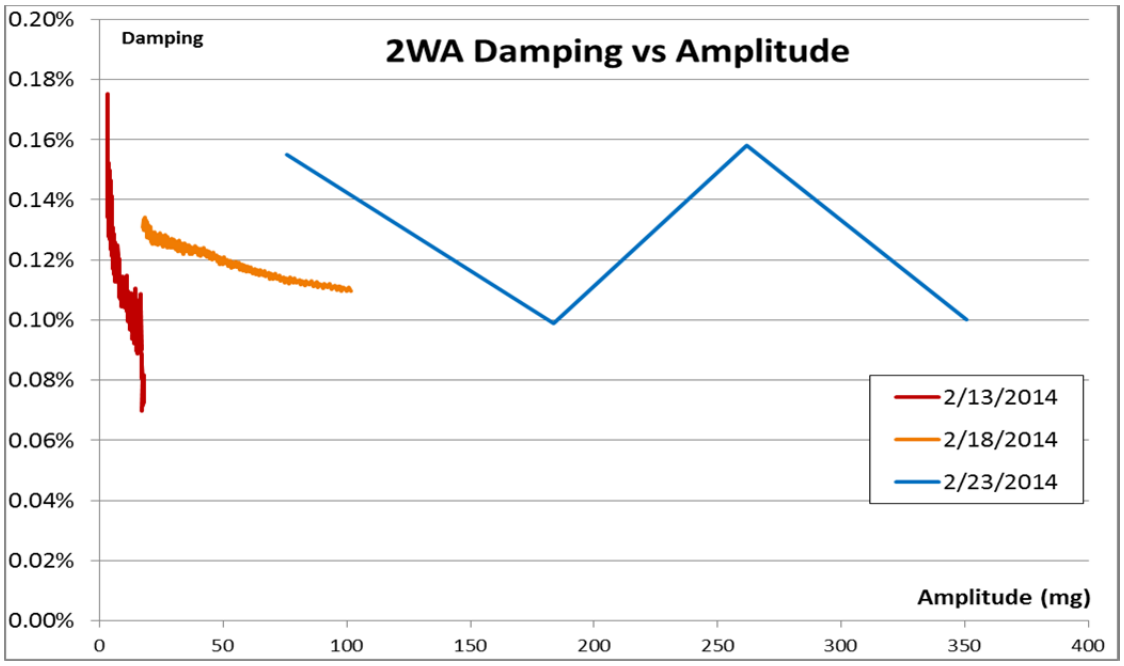
Damping
2WA Damping vs Amplitude
0.20%
0.18%
0.16%
0.14%
0.12%
0.10%
0.08%
0.06%
0.04%
0.02%
0.00%
2/13/2014
2/18/2014
2/23/2014
Amplitude (mg)
0
50
100
150
200
250
300
350
400

14.2.5 2SA Modal Consistency

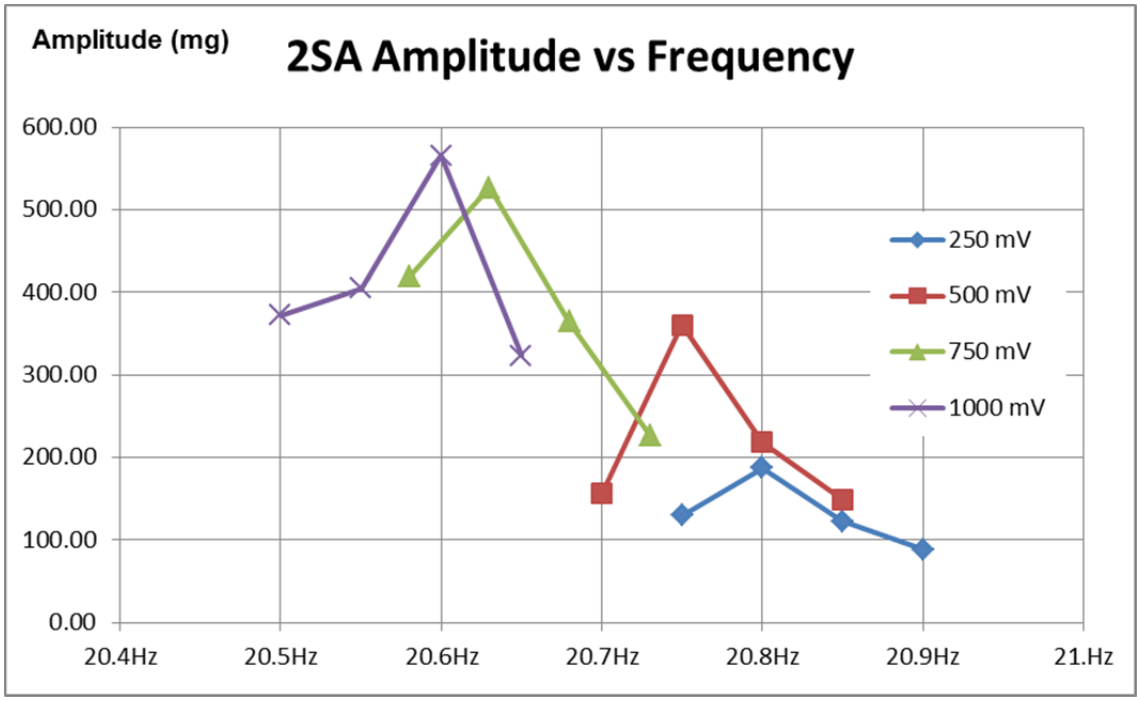

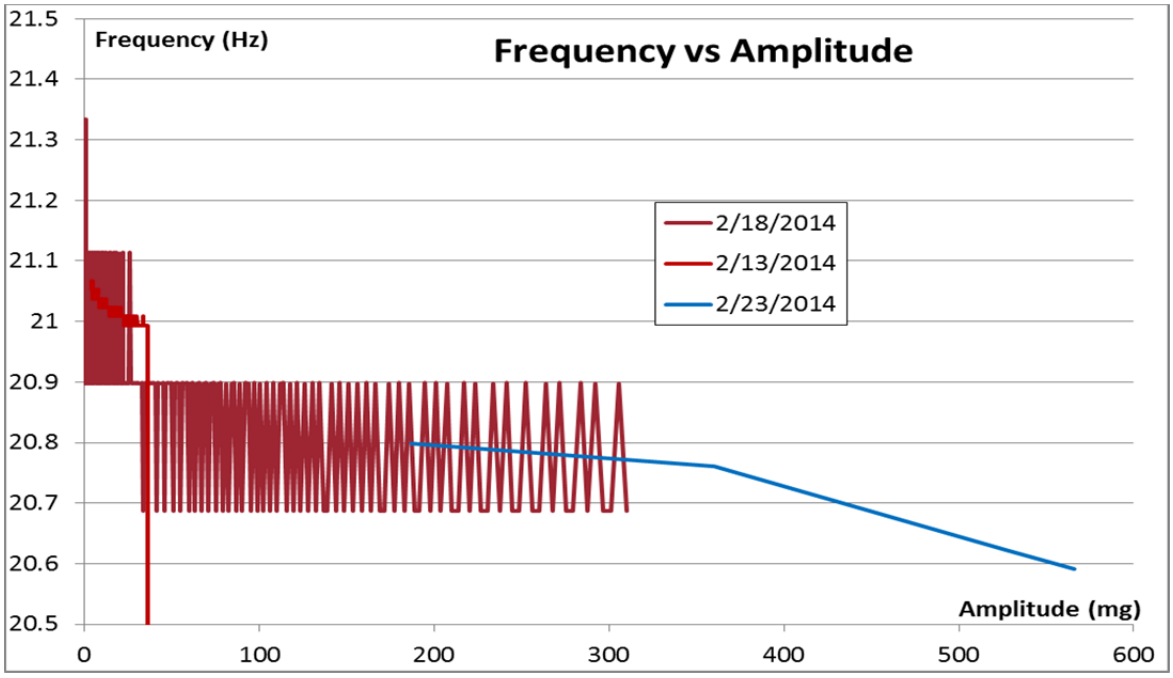

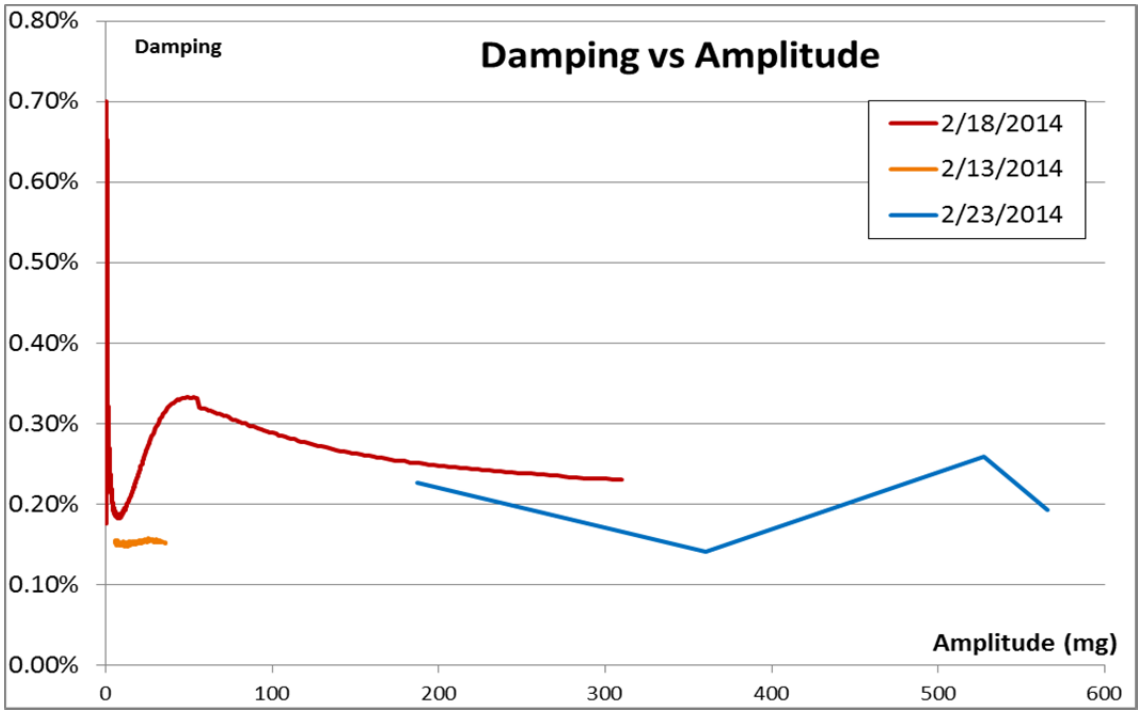

14.2.6 2T Modal Consistency

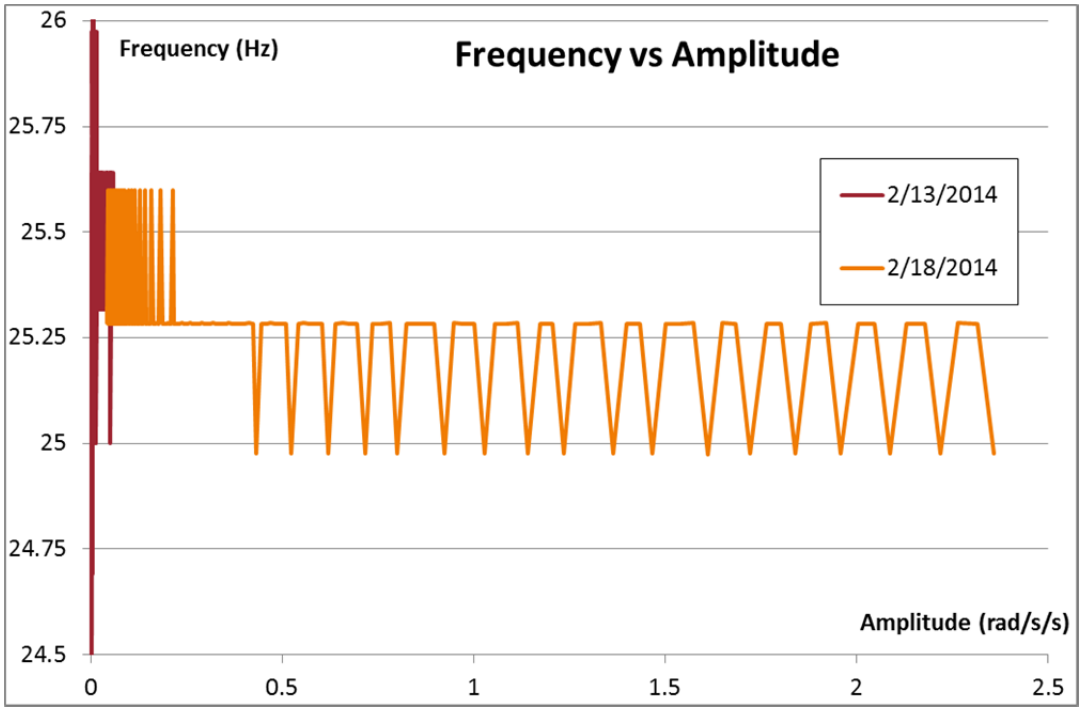

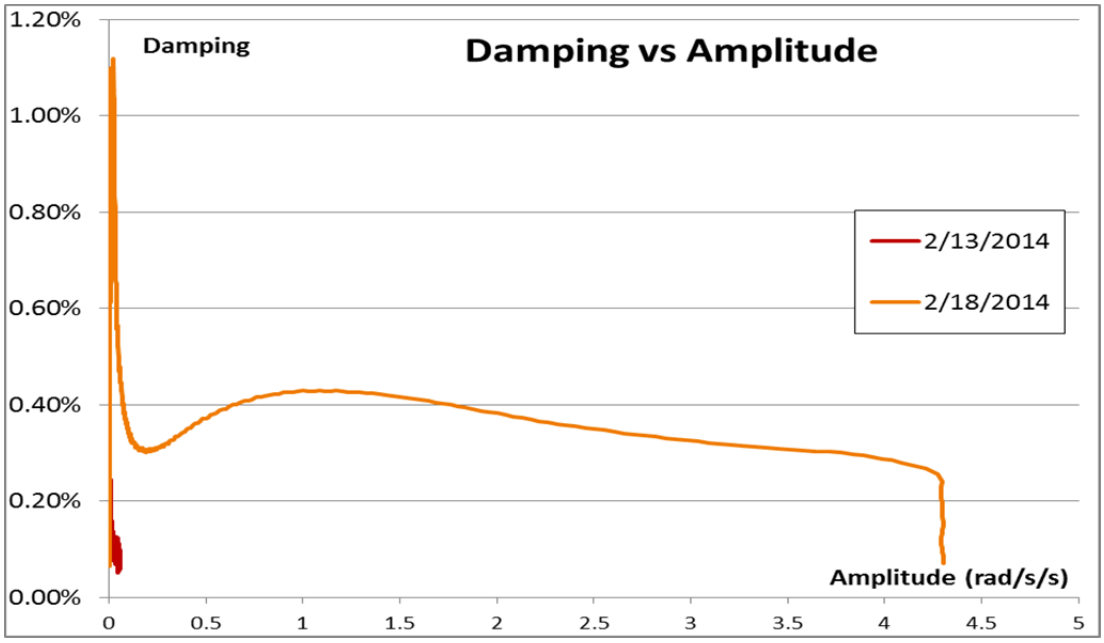

14.2.7 Modal Damping Estimation

Considering the variance in damping values that were measured through various testing amplitudes and procedures, a conservative estimate of the damping of each mode was determined as shown in the table below. This is important because in estimating the maximum safe shaker amplitude an overestimation of damping will underestimate the structure's resonance.

Mode	Damping
1WA	0.19%
1SA	0.30%
1T	0.28%
2WA	0.09%
2SA	0.18%
2T	0.11%

14.3 Comparative MAC Matrices

The full set of comparative MAC matrices is contained within this section. These were used to produce the metric values shown in section 9.5.

14.3.1 000 Configuration MAC Matrices with All ETABS Configurations

	Experimental (000)					
ETABS (000)	1WA	1SA	1T	2WA	2SA	2T
1WA	0.9972	0.0008	0.0001	0.0051	0.0001	0.0000
1SA	0.0008	0.9950	0.0028	0.0001	0.0040	0.0002
1T	0.0001	0.0027	0.9952	0.0007	0.0004	0.0001
2WA	0.0017	0.0000	0.0006	0.9941	0.0000	0.0000
2SA	0.0001	0.0012	0.0003	0.0000	0.9952	0.0003
2T	0.0000	0.0002	0.0010	0.0000	0.0003	0.9995

	Experimental (000)					
ETABS (L00)	1WA	1SA	1T	2WA	2SA	2T
1WA	0.9252	0.0007	0.0024	0.0779	0.0001	0.0087
1SA	0.0002	0.9944	0.0015	0.0025	0.0039	0.0000
1T	0.0157	0.0033	0.6357	0.2689	0.0004	0.0157
2WA	0.0582	0.0002	0.3594	0.6060	0.0001	0.0295
2SA	0.0002	0.0012	0.0001	0.0003	0.9949	0.0005
2T	0.0005	0.0002	0.0008	0.0446	0.0007	0.9456

	Experimental (000)					
ETABS (L0R)	1WA	1SA	1T	2WA	2SA	2T
1WA	0.8468	0.0008	0.0002	0.1588	0.0001	0.0000
1SA	0.0006	0.9936	0.0045	0.0003	0.0039	0.0000
1T	0.0000	0.0041	0.9554	0.0015	0.0004	0.0316
2WA	0.1524	0.0000	0.0013	0.8395	0.0000	0.0001
2SA	0.0001	0.0012	0.0005	0.0000	0.9948	0.0006
2T	0.0000	0.0002	0.0383	0.0000	0.0008	0.9677

	Experimental (000)					
ETABS (LFR)	1WA	1SA	1T	2WA	2SA	2T
1WA	0.8465	0.0009	0.0003	0.1589	0.0000	0.0000
1SA	0.0009	0.9503	0.0395	0.0002	0.0157	0.0041
1T	0.0000	0.0386	0.9066	0.0013	0.0000	0.0414
2WA	0.1525	0.0000	0.0010	0.8396	0.0001	0.0002
2SA	0.0001	0.0099	0.0031	0.0001	0.9602	0.0322
2T	0.0000	0.0001	0.0498	0.0000	0.0240	0.9220

	Experimental (000)					
ETABS (LF0)	1WA	1SA	1T	2WA	2SA	2T
1WA	0.9185	0.0024	0.0113	0.0758	0.0008	0.0061
1SA	0.0047	0.8366	0.1505	0.0040	0.0146	0.0057
1T	0.0113	0.1140	0.4986	0.2816	0.0000	0.0253
2WA	0.0651	0.0405	0.3269	0.5916	0.0051	0.0196
2SA	0.0000	0.0062	0.0089	0.0000	0.9390	0.0587
2T	0.0003	0.0000	0.0039	0.0472	0.0406	0.8845

	Experimental (000)					
ETABS (0F0)	1WA	1SA	1T	2WA	2SA	2T
1WA	0.9971	0.0006	0.0006	0.0051	0.0000	0.0000
1SA	0.0009	0.8351	0.1702	0.0001	0.0119	0.0092
1T	0.0001	0.1583	0.8099	0.0008	0.0006	0.0057
2WA	0.0017	0.0000	0.0006	0.9940	0.0000	0.0000
2SA	0.0001	0.0057	0.0104	0.0000	0.8563	0.1703
2T	0.0000	0.0000	0.0086	0.0000	0.1312	0.8147

14.3.2 L00 Configuration MAC Matrices with All ETABS Configurations

	Experimental (L00)					
ETABS (000)	1WA	1SA	1T	2WA	2SA	2T
1WA	0.9473	0.0000	0.0299	0.0094	0.0000	0.0071
1SA	0.0001	0.9981	0.0006	0.0000	0.0038	0.0000
1T	0.0102	0.0007	0.7749	0.1828	0.0000	0.0359
2WA	0.0386	0.0000	0.1498	0.8018	0.0006	0.0230
2SA	0.0000	0.0011	0.0000	0.0003	0.9945	0.0014
2T	0.0019	0.0000	0.0582	0.0034	0.0011	0.9225

	Experimental (L00)					
ETABS (L00)	1WA	1SA	1T	2WA	2SA	2T
1WA	0.9807	0.0001	0.0068	0.0017	0.0000	0.0156
1SA	0.0002	0.9981	0.0006	0.0000	0.0038	0.0000
1T	0.0058	0.0007	0.9330	0.0244	0.0000	0.0239
2WA	0.0014	0.0000	0.0418	0.9721	0.0004	0.0054
2SA	0.0000	0.0011	0.0000	0.0005	0.9951	0.0006
2T	0.0122	0.0000	0.0262	0.0011	0.0007	0.9446

	Experimental (L00)					
ETABS (L0R)	1WA	1SA	1T	2WA	2SA	2T
1WA	0.9145	0.0001	0.0333	0.0533	0.0000	0.0029
1SA	0.0002	0.9986	0.0002	0.0000	0.0038	0.0000
1T	0.0590	0.0003	0.8120	0.1271	0.0000	0.0013
2WA	0.0171	0.0000	0.1554	0.8184	0.0005	0.0074
2SA	0.0000	0.0011	0.0001	0.0003	0.9952	0.0006
2T	0.0039	0.0000	0.0062	0.0018	0.0006	0.9843

	Experimental (L00)					
ETABS (LFR)	1WA	1SA	1T	2WA	2SA	2T
1WA	0.9142	0.0008	0.0328	0.0536	0.0004	0.0020
1SA	0.0001	0.9759	0.0144	0.0000	0.0142	0.0045
1T	0.0595	0.0110	0.7930	0.1289	0.0033	0.0000
2WA	0.0170	0.0021	0.1555	0.8164	0.0027	0.0044
2SA	0.0000	0.0090	0.0077	0.0001	0.9409	0.0514
2T	0.0038	0.0015	0.0024	0.0019	0.0378	0.9359

	Experimental (L00)					
ETABS (LF0)	1WA	1SA	1T	2WA	2SA	2T
1WA	0.9754	0.0000	0.0144	0.0014	0.0021	0.0110
1SA	0.0015	0.8836	0.1109	0.0001	0.0131	0.0062
1T	0.0104	0.1022	0.8127	0.0298	0.0089	0.0090
2WA	0.0017	0.0038	0.0460	0.9661	0.0000	0.0054
2SA	0.0001	0.0058	0.0101	0.0012	0.9174	0.0819
2T	0.0103	0.0055	0.0128	0.0012	0.0573	0.8797

	Experimental (L00)					
ETABS (0F0)	1WA	1SA	1T	2WA	2SA	2T
1WA	0.9470	0.0041	0.0266	0.0095	0.0018	0.0037
1SA	0.0001	0.8879	0.1158	0.0000	0.0093	0.0114
1T	0.0104	0.0784	0.6923	0.1813	0.0147	0.0087
2WA	0.0388	0.0160	0.1325	0.8031	0.0097	0.0087
2SA	0.0000	0.0045	0.0159	0.0003	0.8165	0.2109
2T	0.0018	0.0110	0.0264	0.0035	0.1458	0.7515

14.3.3 L0R Configuration MAC Matrices with All ETABS Configurations

	Experimental (L0R)					
ETABS (000)	1WA	1SA	1T	2WA	2SA	2T
1WA	0.9271	0.0035	0.0001	0.0545	0.0001	0.0000
1SA	0.0034	0.9950	0.0003	0.0001	0.0037	0.0000
1T	0.0001	0.0003	0.9818	0.0007	0.0000	0.0245
2WA	0.0694	0.0000	0.0006	0.9448	0.0000	0.0000
2SA	0.0000	0.0010	0.0000	0.0000	0.9953	0.0010
2T	0.0000	0.0001	0.0171	0.0000	0.0008	0.9745

	Experimental (L0R)					
ETABS (L00)	1WA	1SA	1T	2WA	2SA	2T
1WA	0.9793	0.0030	0.0164	0.0006	0.0001	0.0013
1SA	0.0032	0.9956	0.0001	0.0001	0.0037	0.0000
1T	0.0127	0.0001	0.6762	0.2556	0.0000	0.0020
2WA	0.0030	0.0001	0.2957	0.7263	0.0001	0.0398
2SA	0.0000	0.0010	0.0000	0.0000	0.9957	0.0005
2T	0.0017	0.0001	0.0116	0.0174	0.0004	0.9563

	Experimental (L0R)					
ETABS (L0R)	1WA	1SA	1T	2WA	2SA	2T
1WA	0.9878	0.0035	0.0001	0.0104	0.0001	0.0000
1SA	0.0034	0.9953	0.0000	0.0001	0.0037	0.0001
1T	0.0001	0.0000	0.9986	0.0001	0.0000	0.0002
2WA	0.0087	0.0000	0.0002	0.9893	0.0000	0.0000
2SA	0.0000	0.0010	0.0000	0.0000	0.9959	0.0003
2T	0.0000	0.0001	0.0011	0.0000	0.0004	0.9994

	Experimental (L0R)					
ETABS (LFR)	1WA	1SA	1T	2WA	2SA	2T
1WA	0.9871	0.0037	0.0003	0.0104	0.0002	0.0000
1SA	0.0040	0.9704	0.0168	0.0001	0.0146	0.0031
1T	0.0002	0.0166	0.9723	0.0002	0.0026	0.0029
2WA	0.0087	0.0000	0.0003	0.9892	0.0001	0.0000
2SA	0.0000	0.0090	0.0066	0.0002	0.9441	0.0489
2T	0.0000	0.0002	0.0037	0.0000	0.0384	0.9451

	Experimental (L0R)					
ETABS (LF0)	1WA	1SA	1T	2WA	2SA	2T
1WA	0.9769	0.0183	0.0031	0.0006	0.0006	0.0006
1SA	0.0119	0.8668	0.1179	0.0004	0.0135	0.0049
1T	0.0081	0.0784	0.5764	0.2699	0.0042	0.0000
2WA	0.0018	0.0287	0.2868	0.7107	0.0060	0.0277
2SA	0.0001	0.0053	0.0118	0.0001	0.9180	0.0811
2T	0.0011	0.0022	0.0043	0.0183	0.0577	0.8857

	Experimental (L0R)					
ETABS (0F0)	1WA	1SA	1T	2WA	2SA	2T
1WA	0.9269	0.0028	0.0011	0.0546	0.0001	0.0001
1SA	0.0036	0.8808	0.1205	0.0001	0.0103	0.0090
1T	0.0001	0.1081	0.8598	0.0006	0.0128	0.0031
2WA	0.0694	0.0001	0.0004	0.9447	0.0000	0.0000
2SA	0.0000	0.0046	0.0145	0.0000	0.8224	0.2059
2T	0.0000	0.0033	0.0039	0.0000	0.1544	0.7820

14.3.4 LFR Configuration MAC Matrices with All ETABS Configurations

	Experimental (LFR)					
ETABS (000)	1WA	1SA	1T	2WA	2SA	2T
1WA	0.9972	0.0008	0.0001	0.0051	0.0001	0.0000
1SA	0.0008	0.9950	0.0028	0.0001	0.0040	0.0002
1T	0.0001	0.0027	0.9952	0.0007	0.0004	0.0001
2WA	0.0017	0.0000	0.0006	0.9941	0.0000	0.0000
2SA	0.0001	0.0012	0.0003	0.0000	0.9952	0.0003
2T	0.0000	0.0002	0.0010	0.0000	0.0003	0.9995

	Experimental (LFR)					
ETABS (L00)	1WA	1SA	1T	2WA	2SA	2T
1WA	0.9772	0.0012	0.0198	0.0010	0.0002	0.0013
1SA	0.0005	0.9880	0.0081	0.0026	0.0002	0.0000
1T	0.0169	0.0102	0.6577	0.2552	0.0026	0.0052
2WA	0.0030	0.0000	0.2908	0.7169	0.0002	0.0557
2SA	0.0004	0.0004	0.0000	0.0053	0.9364	0.0574
2T	0.0020	0.0002	0.0237	0.0186	0.0602	0.8808

	Experimental (LFR)					
ETABS (L0R)	1WA	1SA	1T	2WA	2SA	2T
1WA	0.9905	0.0009	0.0000	0.0101	0.0002	0.0000
1SA	0.0009	0.9897	0.0089	0.0001	0.0002	0.0000
1T	0.0000	0.0088	0.9880	0.0002	0.0027	0.0001
2WA	0.0084	0.0000	0.0001	0.9880	0.0001	0.0015
2SA	0.0002	0.0004	0.0029	0.0004	0.9356	0.0622
2T	0.0000	0.0002	0.0000	0.0012	0.0610	0.9363

	Experimental (LFR)					
ETABS (LFR)	1WA	1SA	1T	2WA	2SA	2T
1WA	0.9907	0.0007	0.0001	0.0101	0.0002	0.0000
1SA	0.0006	0.9953	0.0018	0.0001	0.0047	0.0020
1T	0.0000	0.0012	0.9961	0.0003	0.0001	0.0004
2WA	0.0084	0.0001	0.0003	0.9878	0.0005	0.0012
2SA	0.0002	0.0017	0.0001	0.0006	0.9892	0.0017
2T	0.0000	0.0010	0.0016	0.0010	0.0053	0.9947

	Experimental (LFR)					
ETABS (LF0)	1WA	1SA	1T	2WA	2SA	2T
1WA	0.9846	0.0031	0.0099	0.0010	0.0006	0.0008
1SA	0.0008	0.9245	0.0766	0.0016	0.0042	0.0030
1T	0.0108	0.0356	0.6212	0.2715	0.0005	0.0008
2WA	0.0018	0.0315	0.2793	0.7015	0.0081	0.0404
2SA	0.0009	0.0004	0.0054	0.0039	0.9860	0.0008
2T	0.0011	0.0049	0.0076	0.0202	0.0009	0.9540

	Experimental (LFR)					
ETABS (0F0)	1WA	1SA	1T	2WA	2SA	2T
1WA	0.9287	0.0007	0.0002	0.0555	0.0002	0.0000
1SA	0.0008	0.9366	0.0716	0.0000	0.0021	0.0067
1T	0.0001	0.0568	0.9181	0.0004	0.0058	0.0093
2WA	0.0700	0.0000	0.0007	0.9426	0.0005	0.0010
2SA	0.0004	0.0003	0.0048	0.0002	0.9743	0.0407
2T	0.0000	0.0056	0.0046	0.0014	0.0174	0.9420

14.3.5 LF0 Configuration MAC Matrices with All ETABS Configurations

	Experimental (LF0)					
ETABS (000)	1WA	1SA	1T	2WA	2SA	2T
1WA	0.9566	0.0005	0.0249	0.0057	0.0061	0.0004
1SA	0.0033	0.9622	0.0275	0.0073	0.0012	0.0001
1T	0.0060	0.0129	0.7363	0.2343	0.0050	0.0037
2WA	0.0258	0.0230	0.1984	0.7358	0.0026	0.0272
2SA	0.0010	0.0003	0.0009	0.0176	0.6283	0.3484
2T	0.0076	0.0005	0.0105	0.0023	0.3424	0.6339

	Experimental (LF0)					
ETABS (L00)	1WA	1SA	1T	2WA	2SA	2T
1WA	0.9823	0.0007	0.0068	0.0077	0.0062	0.0009
1SA	0.0005	0.9649	0.0074	0.0248	0.0012	0.0008
1T	0.0041	0.0129	0.9614	0.0048	0.0051	0.0018
2WA	0.0054	0.0204	0.0182	0.9615	0.0022	0.0033
2SA	0.0059	0.0002	0.0028	0.0000	0.6215	0.3695
2T	0.0017	0.0005	0.0031	0.0020	0.3492	0.6387

	Experimental (LF0)					
ETABS (L0R)	1WA	1SA	1T	2WA	2SA	2T
1WA	0.9084	0.0006	0.0227	0.0640	0.0061	0.0021
1SA	0.0005	0.9661	0.0226	0.0101	0.0012	0.0003
1T	0.0578	0.0106	0.7393	0.1742	0.0054	0.0079
2WA	0.0231	0.0215	0.2081	0.7364	0.0023	0.0079
2SA	0.0058	0.0002	0.0052	0.0129	0.6194	0.3583
2T	0.0043	0.0004	0.0008	0.0055	0.3511	0.6374

	Experimental (LF0)					
ETABS (LFR)	1WA	1SA	1T	2WA	2SA	2T
1WA	0.9082	0.0021	0.0193	0.0638	0.0059	0.0044
1SA	0.0004	0.9838	0.0002	0.0105	0.0080	0.0012
1T	0.0584	0.0001	0.7452	0.1766	0.0012	0.0123
2WA	0.0227	0.0077	0.2242	0.7338	0.0081	0.0029
2SA	0.0058	0.0034	0.0008	0.0120	0.7728	0.1772
2T	0.0044	0.0013	0.0086	0.0063	0.1927	0.8132

	Experimental (LF0)					
ETABS (LF0)	1WA	1SA	1T	2WA	2SA	2T
1WA	0.9763	0.0003	0.0109	0.0072	0.0094	0.0000
1SA	0.0007	0.9016	0.0772	0.0214	0.0084	0.0011
1T	0.0089	0.0582	0.9043	0.0076	0.0000	0.0000
2WA	0.0045	0.0302	0.0096	0.9611	0.0017	0.0060
2SA	0.0067	0.0032	0.0000	0.0000	0.8174	0.1400
2T	0.0029	0.0019	0.0011	0.0031	0.1526	0.8640

	Experimental (LF0)					
ETABS (0F0)	1WA	1SA	1T	2WA	2SA	2T
1WA	0.9563	0.0061	0.0165	0.0058	0.0051	0.0039
1SA	0.0031	0.9516	0.0430	0.0075	0.0040	0.0070
1T	0.0061	0.0365	0.7118	0.2327	0.0000	0.0000
2WA	0.0260	0.0001	0.2209	0.7370	0.0186	0.0061
2SA	0.0010	0.0004	0.0061	0.0176	0.9064	0.0370
2T	0.0077	0.0031	0.0001	0.0023	0.0597	0.9511

14.3.6 0F0 Configuration MAC Matrices with All ETABS Configurations

	Experimental (0F0)					
ETABS (000)	1WA	1SA	1T	2WA	2SA	2T
1WA	0.9965	0.0006	0.0009	0.0052	0.0003	0.0001
1SA	0.0002	0.8881	0.1114	0.0000	0.0013	0.0000
1T	0.0013	0.1104	0.8791	0.0012	0.0059	0.0020
2WA	0.0019	0.0000	0.0010	0.9931	0.0005	0.0000
2SA	0.0001	0.0001	0.0046	0.0003	0.7609	0.2345
2T	0.0001	0.0008	0.0030	0.0001	0.2311	0.7634

	Experimental (0F0)					
ETABS (L00)	1WA	1SA	1T	2WA	2SA	2T
1WA	0.9138	0.0007	0.0002	0.0912	0.0003	0.0082
1SA	0.0006	0.8912	0.0753	0.0247	0.0014	0.0016
1T	0.0225	0.1073	0.6145	0.1957	0.0062	0.0029
2WA	0.0626	0.0000	0.3066	0.6492	0.0006	0.0314
2SA	0.0001	0.0001	0.0021	0.0221	0.7540	0.2200
2T	0.0004	0.0007	0.0014	0.0170	0.2375	0.7359

	Experimental (0F0)					
ETABS (L0R)	1WA	1SA	1T	2WA	2SA	2T
1WA	0.8455	0.0006	0.0009	0.1594	0.0003	0.0000
1SA	0.0002	0.8959	0.0990	0.0000	0.0013	0.0034
1T	0.0006	0.1027	0.8697	0.0012	0.0063	0.0139
2WA	0.1537	0.0000	0.0004	0.8387	0.0005	0.0000
2SA	0.0000	0.0001	0.0224	0.0004	0.7524	0.2286
2T	0.0000	0.0007	0.0077	0.0002	0.2391	0.7540

	Experimental (0F0)					
ETABS (LFR)	1WA	1SA	1T	2WA	2SA	2T
1WA	0.8457	0.0003	0.0012	0.1592	0.0002	0.0000
1SA	0.0001	0.9582	0.0329	0.0000	0.0077	0.0002
1T	0.0005	0.0384	0.9343	0.0015	0.0010	0.0229
2WA	0.1536	0.0001	0.0007	0.8383	0.0007	0.0000
2SA	0.0000	0.0028	0.0099	0.0005	0.8860	0.0800
2T	0.0001	0.0003	0.0210	0.0004	0.1043	0.8969

	Experimental (0F0)					
ETABS (LF0)	1WA	1SA	1T	2WA	2SA	2T
1WA	0.9137	0.0001	0.0029	0.0898	0.0021	0.0055
1SA	0.0044	0.9589	0.0078	0.0224	0.0069	0.0001
1T	0.0126	0.0010	0.7122	0.2120	0.0005	0.0094
2WA	0.0689	0.0379	0.2757	0.6360	0.0072	0.0207
2SA	0.0003	0.0014	0.0003	0.0201	0.9070	0.0468
2T	0.0001	0.0007	0.0013	0.0196	0.0763	0.9174

	Experimental (0F0)					
ETABS (0F0)	1WA	1SA	1T	2WA	2SA	2T
1WA	0.9966	0.0002	0.0014	0.0052	0.0001	0.0001
1SA	0.0002	0.9972	0.0015	0.0000	0.0036	0.0032
1T	0.0012	0.0002	0.9938	0.0011	0.0000	0.0008
2WA	0.0019	0.0000	0.0010	0.9933	0.0003	0.0001
2SA	0.0001	0.0014	0.0000	0.0003	0.9823	0.0028
2T	0.0001	0.0010	0.0023	0.0001	0.0136	0.9930

14.3.7 Analysis with only fundamental modes

To investigate the impact of having fewer available modes, another analysis was completed with only information from the first mode in each direction (1WA, 1SA, 1T). This reflects the difficulty of measuring higher modes in real buildings that can lead to data set with fewer modes. This is completed by only inputting the MAC numbers for the first three modes into the prediction metric. The following table displays the prediction metrics of each configuration with this approach.

Mode Shape Analysis using only fundamental modes (1WA, 1SA, 1T)

	000	L00	L0R	LFR	LF0	0F0	Confidence
000	0.00006	0.13298	0.02346	0.02355	0.29996	0.11719	99.7%
L00	0.05189	0.00460	0.04256	0.05014	0.07003	0.12221	89.2%
L0R	0.00534	0.10529	0.00018	0.00207	0.20648	0.05987	96.5%
LFR	0.00510	0.11804	0.00040	0.00009	0.15211	0.01901	78.2%
LF0	0.07127	0.00228	0.07392	0.07008	0.02742	0.08711	91.7%
0F0	0.05172	0.17145	0.04794	0.02381	0.08313	0.00005	99.8%

The yellow cells indicate the correct configurations, and the orange cell represents a failure of the analysis. In examination of the LF0 configuration the metric incorrectly predicted the L00 configuration. This shows that having only the fundamental modes does degrade the accuracy of this approach slightly.

14.3.8 Analysis with only higher modes

Another set of analysis was completed with only the higher modes in each direction (2WA, 2SA, 2T). This is to allow for comparison between utilization of the fundamental modes versus use of the higher modes. The following table displays the prediction metrics of each configuration with this approach.

Mode Shape Analysis using only 2nd modes (2WA, 2SA, 2T)

	000	L00	L0R	LFR	LF0	0F0	Confidence
000	0.00004	0.15853	0.02576	0.02574	0.17020	0.10105	99.9%
L00	0.03998	0.00312	0.03304	0.03375	0.03043	0.15979	89.7%
L0R	0.00305	0.07708	0.00011	0.00987	0.08564	0.14494	96.3%
LFR	0.01862	0.08550	0.01579	0.00016	0.09150	0.00589	97.3%
LF0	0.51052	0.53213	0.52782	0.15470	0.09463	0.07017	25.8%
0F0	0.22150	0.23520	0.23110	0.04062	0.13389	0.00054	98.7%

The analysis metric correctly predicts 5 of 6 configurations when only examining the higher modes. This meets expectations of a slight loss in accuracy when limiting the amount of input data.

14.4 Final Frequency Sweep

This section contains figures displaying the frequency sweep data for each mode of each configuration. The title of the figure indicates the configuration as well as the mode being tested. The damping shown on each graph is calculated by the half power band method.

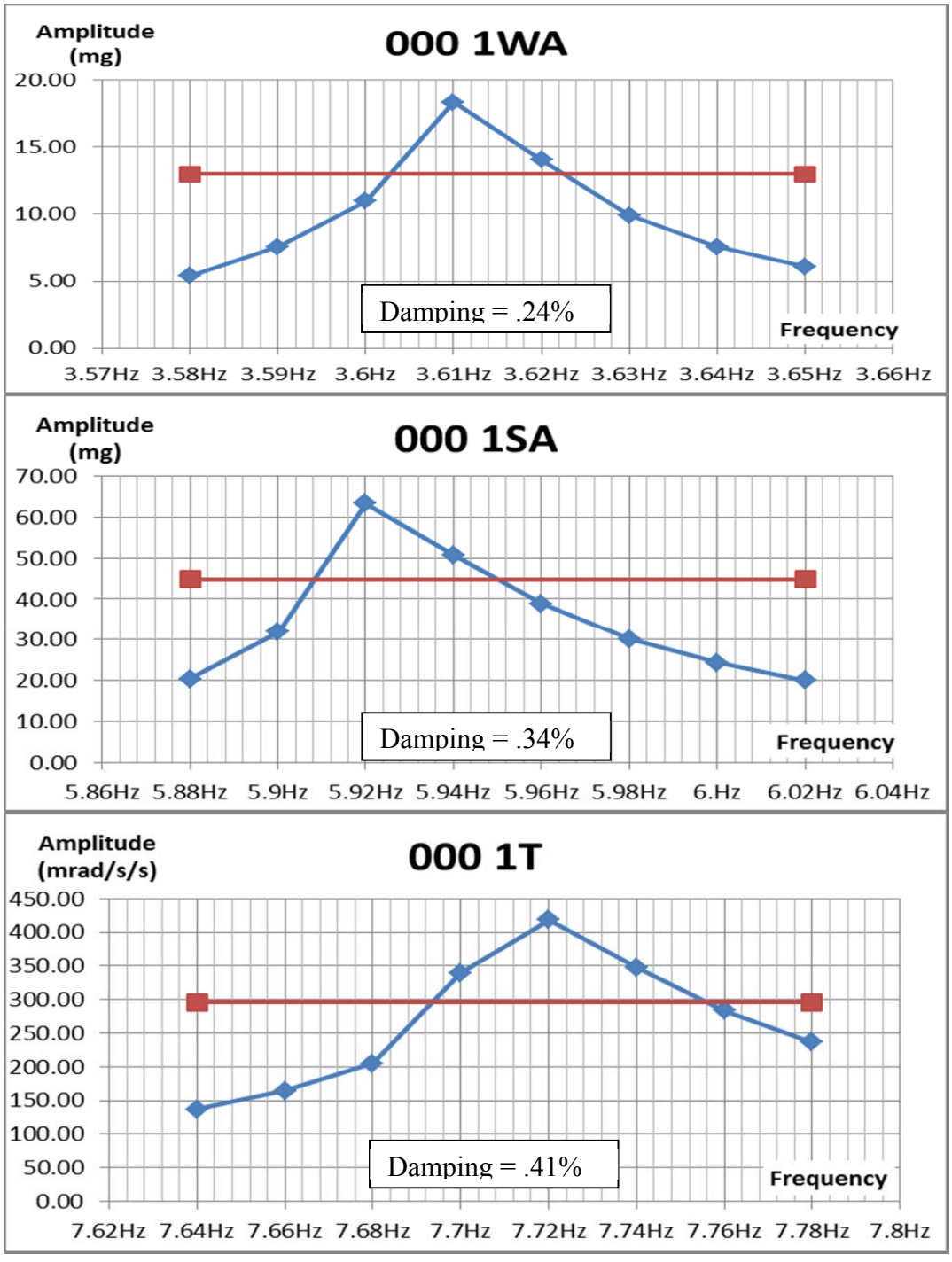
Amplitude (mg)
000 1WA
20.00
15.00
10.00
5.00
0.00
Damping = .24%
Frequency
3.57Hz 3.58Hz 3.59Hz 3.6Hz 3.61Hz 3.62Hz 3.63Hz 3.64Hz 3.65Hz 3.66Hz
Amplitude (mg)
000 1SA
70.00
60.00
50.00
40.00
30.00
20.00
10.00
0.00
Damping = .34%
Frequency
5.86Hz 5.88Hz 5.9Hz 5.92Hz 5.94Hz 5.96Hz 5.98Hz 6.Hz 6.02Hz 6.04Hz
Amplitude (mrad/s/s)
000 1T
450.00
400.00
350.00
300.00
250.00
200.00
150.00
100.00
50.00
0.00
Damping = .41%
Frequency
7.62Hz 7.64Hz 7.66Hz 7.68Hz 7.7Hz 7.72Hz 7.74Hz 7.76Hz 7.78Hz 7.8Hz

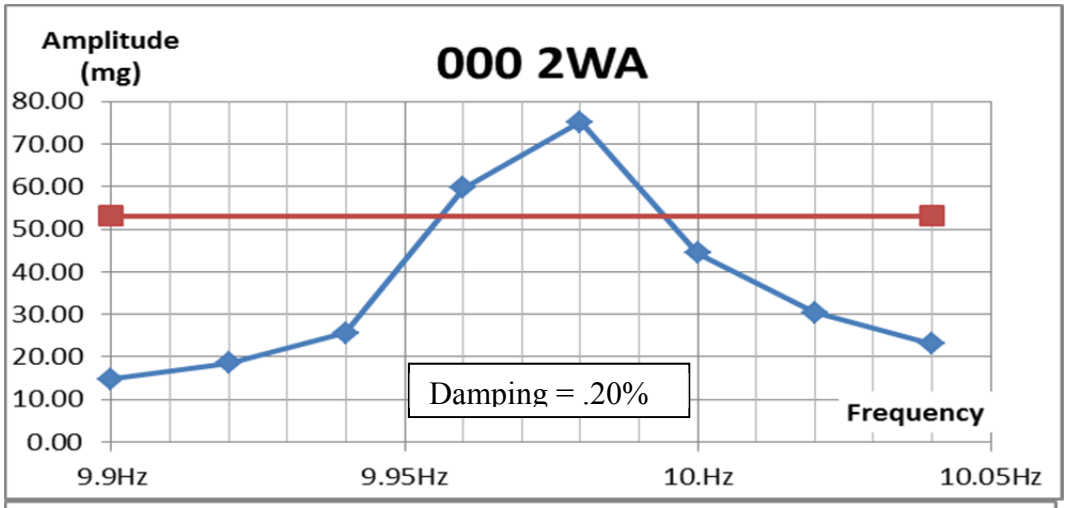
Amplitude (mg)
000 2WA
80.00
70.00
60.00
50.00
40.00
30.00
20.00
10.00
0.00
Damping = .20%
Frequency
9.9Hz
9.95Hz
10.Hz
10.05Hz

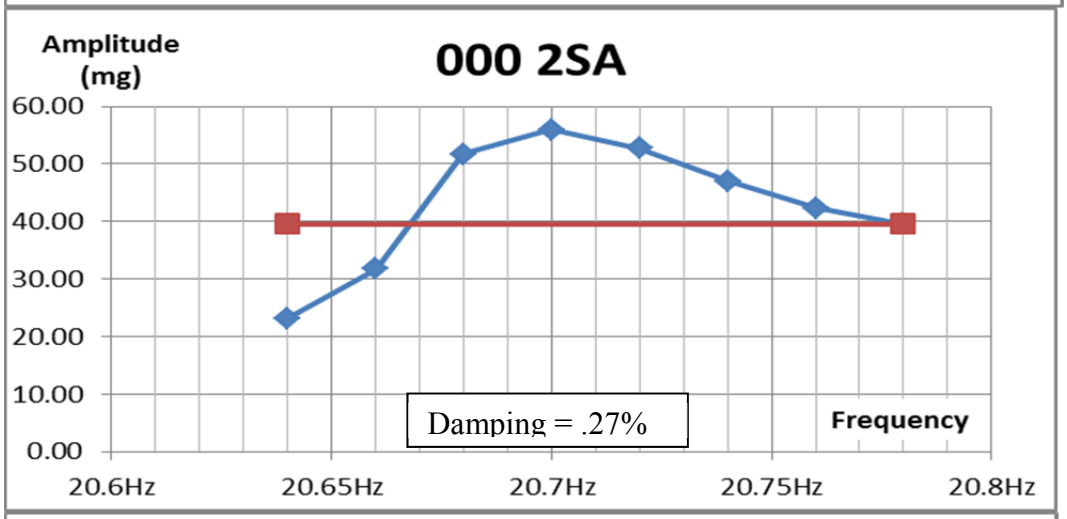
Amplitude (mg)
000 2SA
60.00
50.00
40.00
30.00
20.00
10.00
0.00
Damping = .27%
Frequency
20.6Hz
20.65Hz
20.7Hz
20.75Hz
20.8Hz

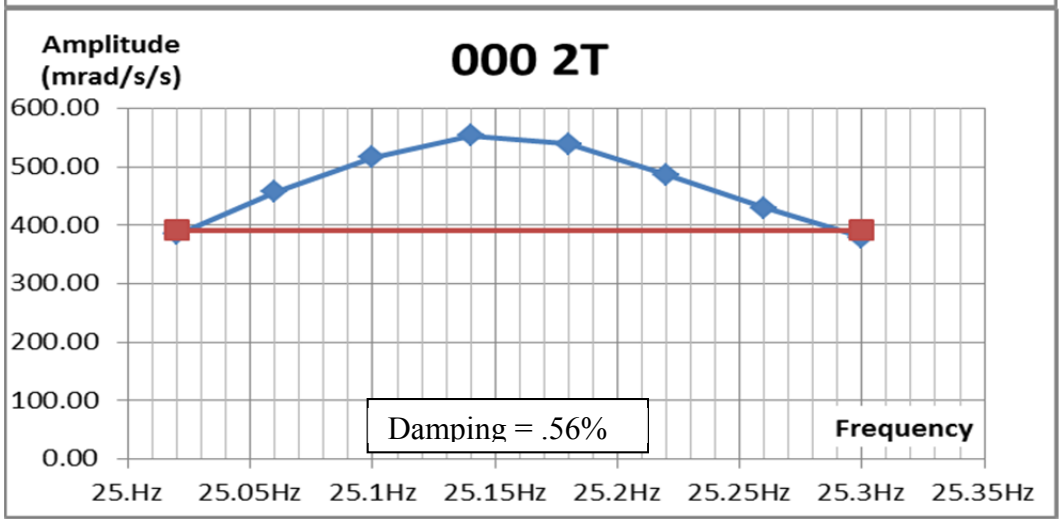
Amplitude (mrad/s/s)
000 2T
600.00
500.00
400.00
300.00
200.00
100.00
0.00
Damping = .56%
Frequency
25.Hz
25.05Hz
25.1Hz
25.15Hz
25.2Hz
25.25Hz
25.3Hz
25.35Hz

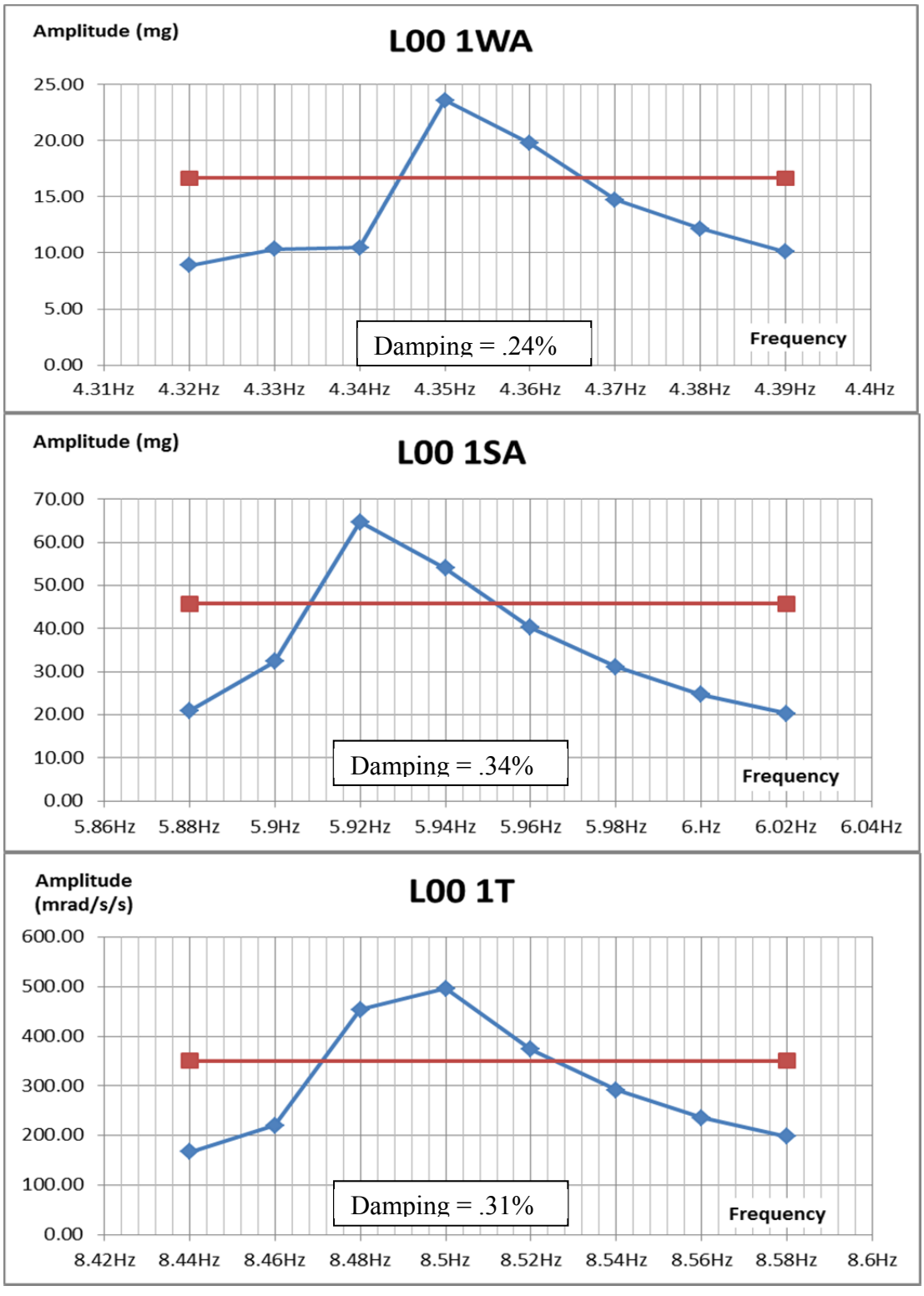
Amplitude (mg)
L00 1WA
25.00
20.00
15.00
10.00
5.00
0.00
4.31Hz
4.32Hz
4.33Hz
4.34Hz
4.35Hz
4.36Hz
4.37Hz
4.38Hz
4.39Hz
4.4Hz
Damping = .24%
Frequency
Amplitude (mg)
L00 1SA
70.00
60.00
50.00
40.00
30.00
20.00
10.00
0.00
5.86Hz
5.88Hz
5.9Hz
5.92Hz
5.94Hz
5.96Hz
5.98Hz
6.Hz
6.02Hz
6.04Hz
Damping = .34%
Frequency
Amplitude (mrad/s/s)
L00 1T
600.00
500.00
400.00
300.00
200.00
100.00
0.00
8.42Hz
8.44Hz
8.46Hz
8.48Hz
8.5Hz
8.52Hz
8.54Hz
8.56Hz
8.58Hz
8.6Hz
Damping = .31%
Frequency

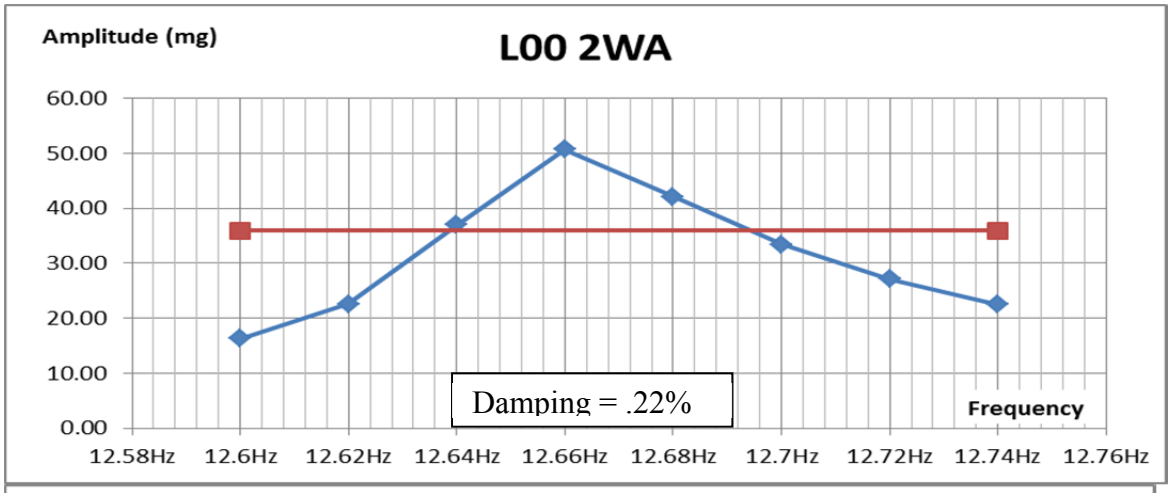
Amplitude (mg)
L00 2WA
60.00
50.00
40.00
30.00
20.00
10.00
0.00
Damping = .22%
Frequency
12.58Hz
12.6Hz
12.62Hz
12.64Hz
12.66Hz
12.68Hz
12.7Hz
12.72Hz
12.74Hz
12.76Hz

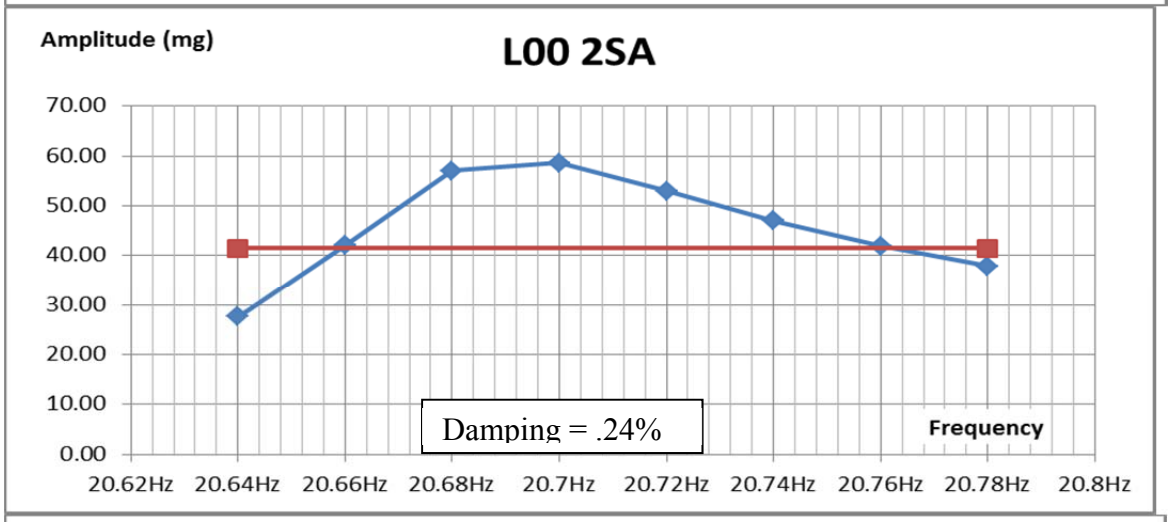
Amplitude (mg)
L00 2SA
70.00
60.00
50.00
40.00
30.00
20.00
10.00
0.00
Damping = .24%
Frequency
20.62Hz
20.64Hz
20.66Hz
20.68Hz
20.7Hz
20.72Hz
20.74Hz
20.76Hz
20.78Hz
20.8Hz

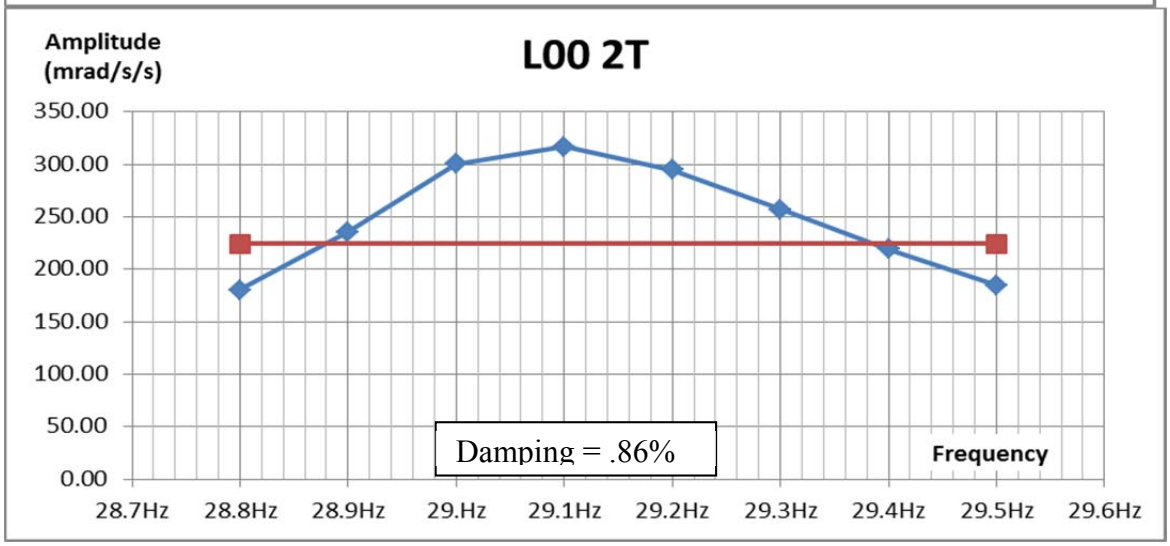
Amplitude (mrad/s/s)
L00 2T
350.00
300.00
250.00
200.00
150.00
100.00
50.00
0.00
Damping = .86%
Frequency
28.7Hz
28.8Hz
28.9Hz
29.Hz
29.1Hz
29.2Hz
29.3Hz
29.4Hz
29.5Hz
29.6Hz

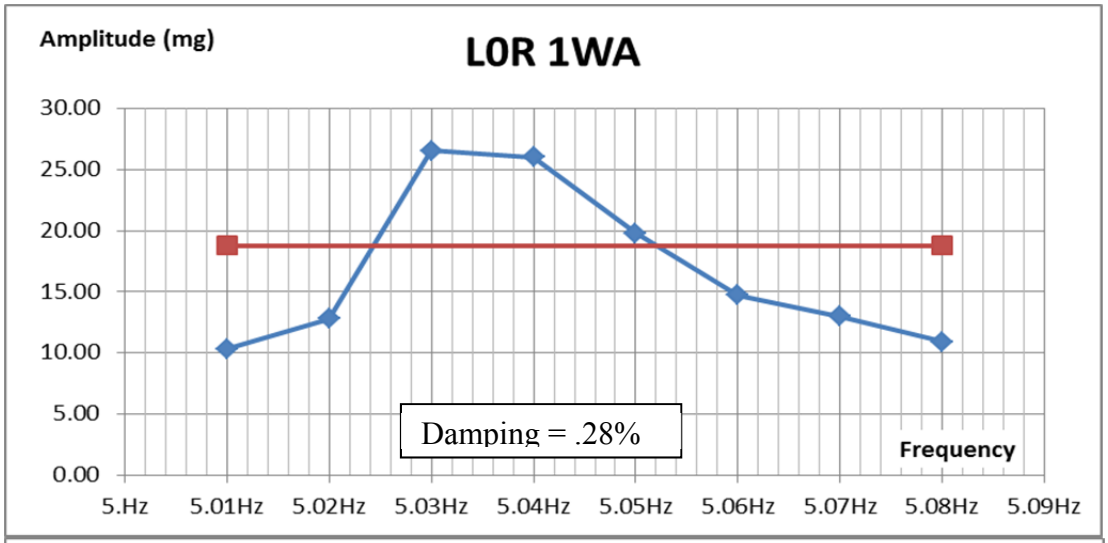
Amplitude (mg)
L0R 1WA
30.00
25.00
20.00
15.00
10.00
5.00
0.00
5.Hz
5.01Hz
5.02Hz
5.03Hz
5.04Hz
5.05Hz
5.06Hz
5.07Hz
5.08Hz
5.09Hz
Damping = .28%
Frequency

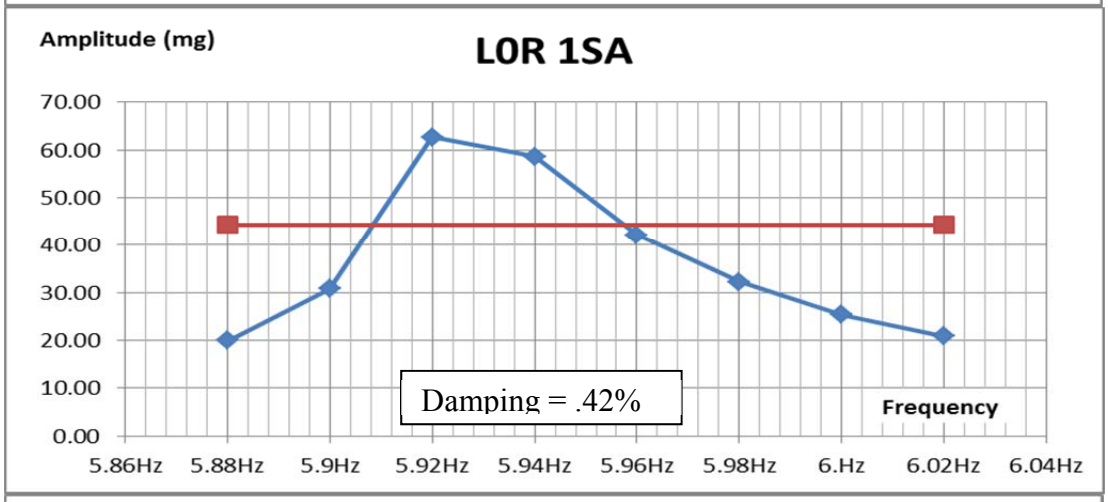
Amplitude (mg)
L0R 1SA
70.00
60.00
50.00
40.00
30.00
20.00
10.00
0.00
5.86Hz
5.88Hz
5.9Hz
5.92Hz
5.94Hz
5.96Hz
5.98Hz
6.Hz
6.02Hz
6.04Hz
Damping = .42%
Frequency

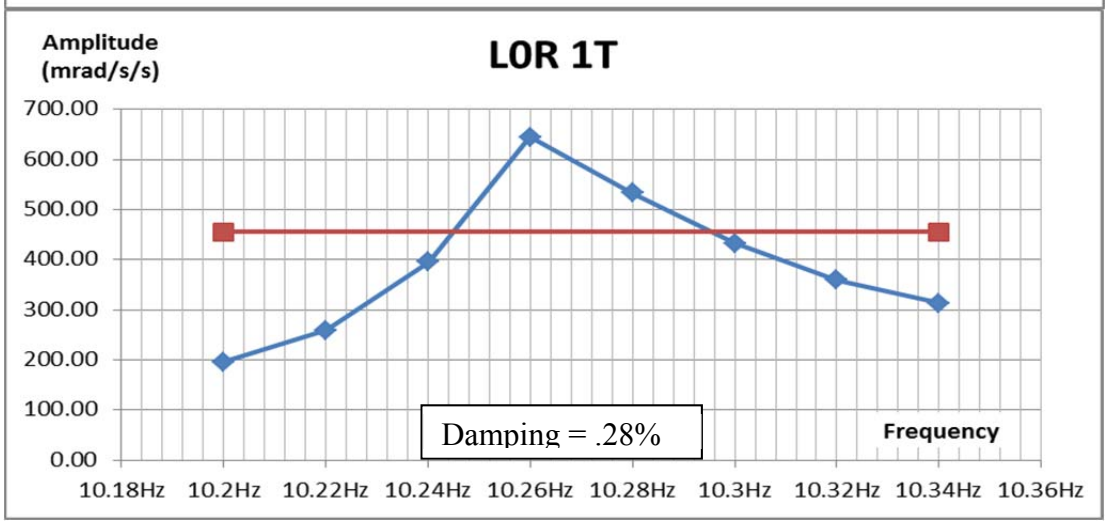
Amplitude (mrad/s/s)
L0R 1T
700.00
600.00
500.00
400.00
300.00
200.00
100.00
0.00
10.18Hz
10.2Hz
10.22Hz
10.24Hz
10.26Hz
10.28Hz
10.3Hz
10.32Hz
10.34Hz
10.36Hz
Damping = .28%
Frequency

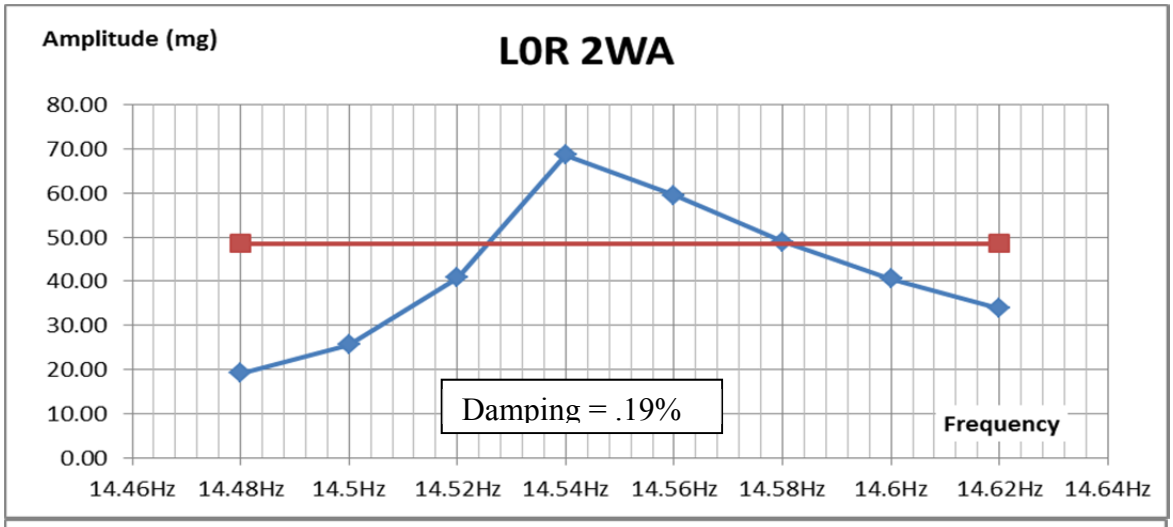
Amplitude (mg)
L0R 2WA
80.00
70.00
60.00
50.00
40.00
30.00
20.00
10.00
0.00
14.46Hz
14.48Hz
14.5Hz
14.52Hz
14.54Hz
14.56Hz
14.58Hz
14.6Hz
14.62Hz
14.64Hz
Damping = .19%
Frequency

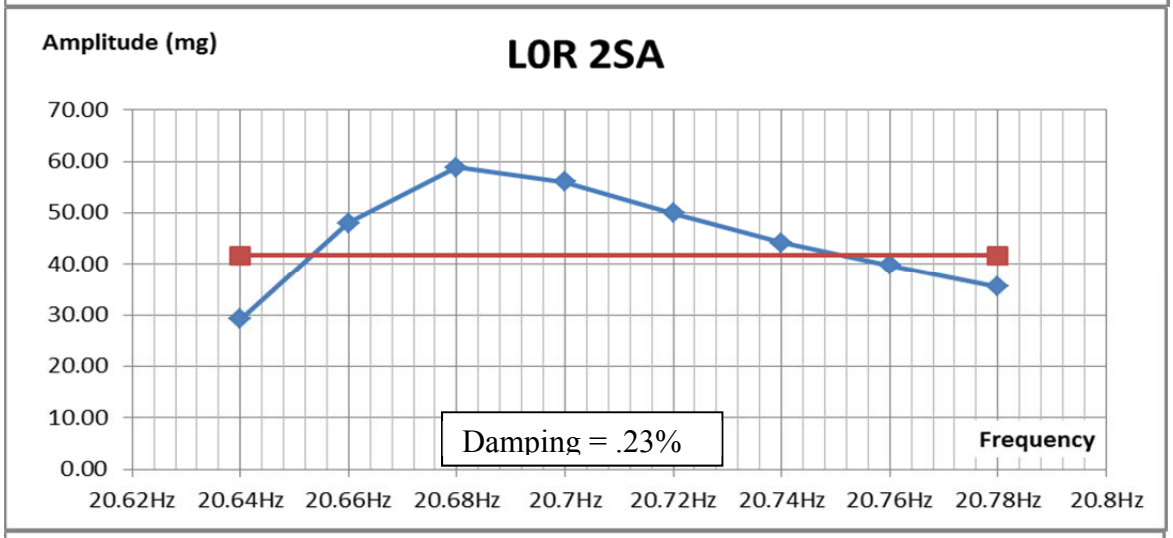
Amplitude (mg)
L0R 2SA
70.00
60.00
50.00
40.00
30.00
20.00
10.00
0.00
20.62Hz
20.64Hz
20.66Hz
20.68Hz
20.7Hz
20.72Hz
20.74Hz
20.76Hz
20.78Hz
20.8Hz
Damping = .23%
Frequency

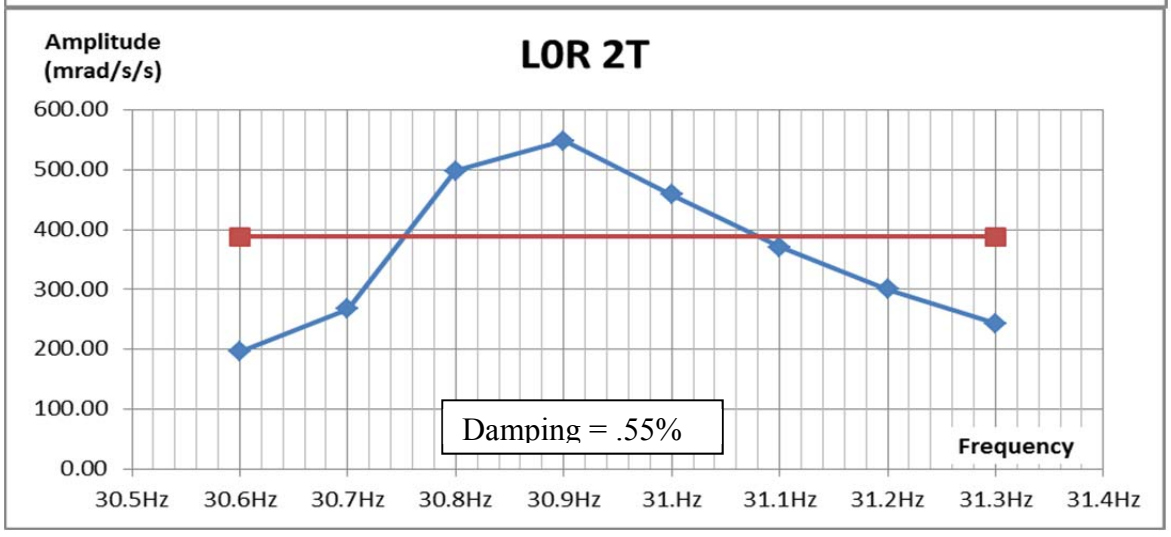
Amplitude (mrad/s/s)
L0R 2T
600.00
500.00
400.00
300.00
200.00
100.00
0.00
30.5Hz
30.6Hz
30.7Hz
30.8Hz
30.9Hz
31.Hz
31.1Hz
31.2Hz
31.3Hz
31.4Hz
Damping = .55%
Frequency

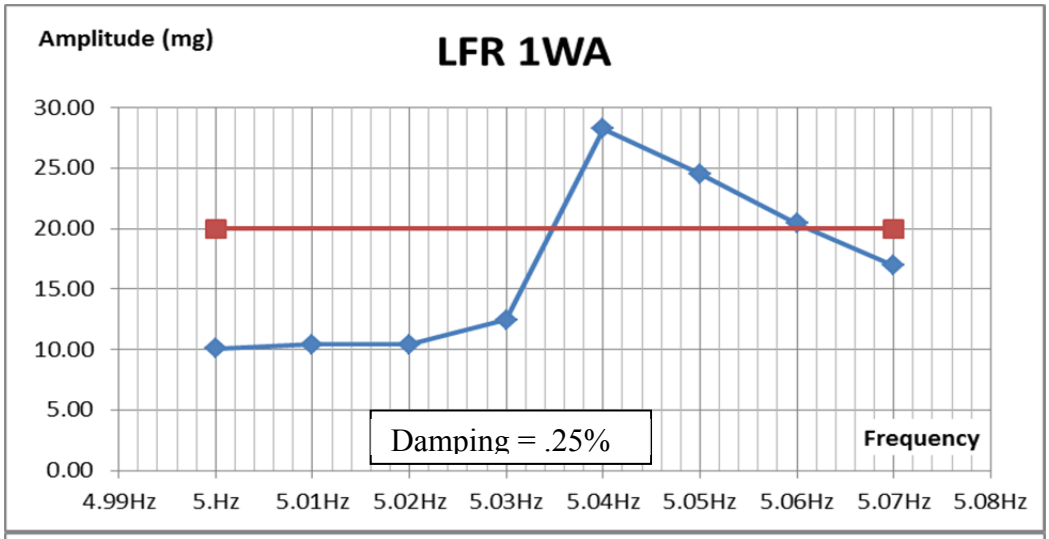
Amplitude (mg)
LFR 1WA
30.00
25.00
20.00
15.00
10.00
5.00
0.00
4.99Hz
5.Hz
5.01Hz
5.02Hz
5.03Hz
5.04Hz
5.05Hz
5.06Hz
5.07Hz
5.08Hz
Damping = .25%
Frequency

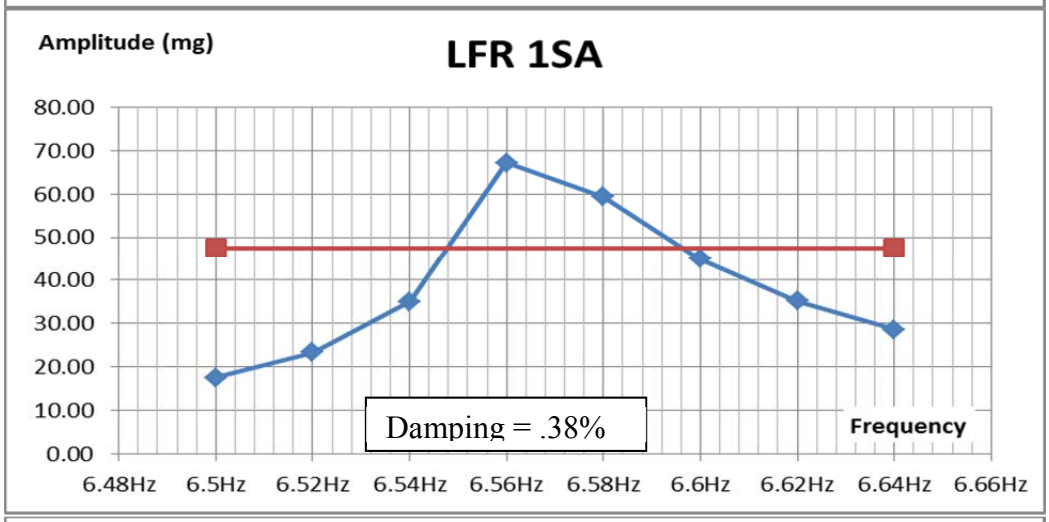
Amplitude (mg)
LFR 1SA
80.00
70.00
60.00
50.00
40.00
30.00
20.00
10.00
0.00
6.48Hz
6.5Hz
6.52Hz
6.54Hz
6.56Hz
6.58Hz
6.6Hz
6.62Hz
6.64Hz
6.66Hz
Damping = .38%
Frequency

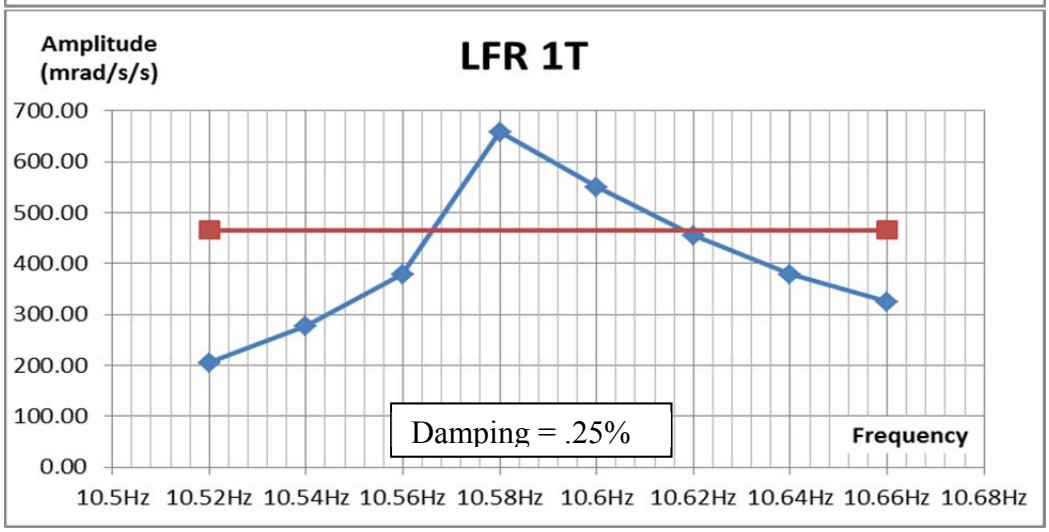
Amplitude (mrad/s/s)
LFR 1T
700.00
600.00
500.00
400.00
300.00
200.00
100.00
0.00
10.5Hz
10.52Hz
10.54Hz
10.56Hz
10.58Hz
10.6Hz
10.62Hz
10.64Hz
10.66Hz
10.68Hz
Damping = .25%
Frequency

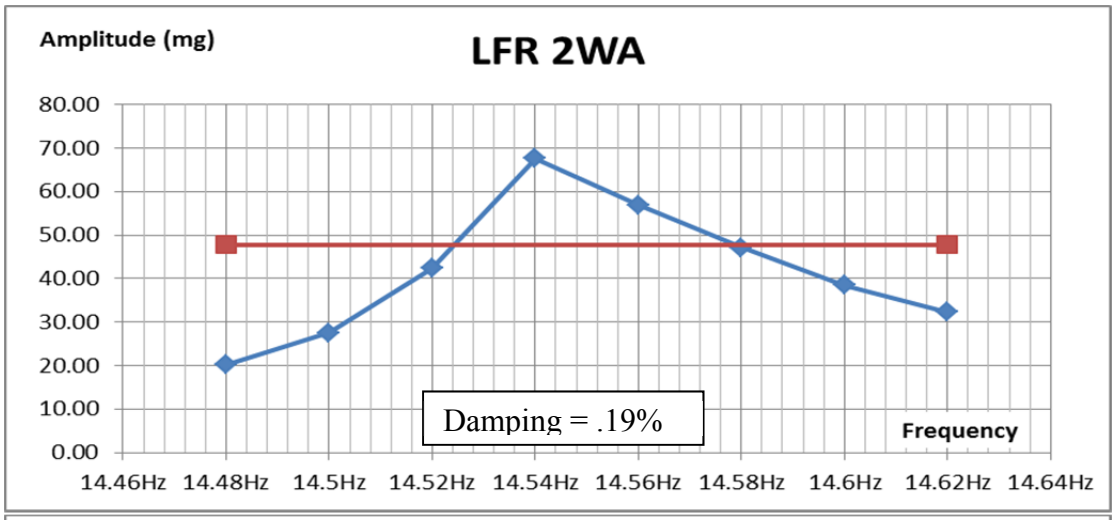
Amplitude (mg)
LFR 2WA
80.00
70.00
60.00
50.00
40.00
30.00
20.00
10.00
0.00
Damping = .19%
Frequency
14.46Hz 14.48Hz 14.5Hz 14.52Hz 14.54Hz 14.56Hz 14.58Hz 14.6Hz 14.62Hz 14.64Hz

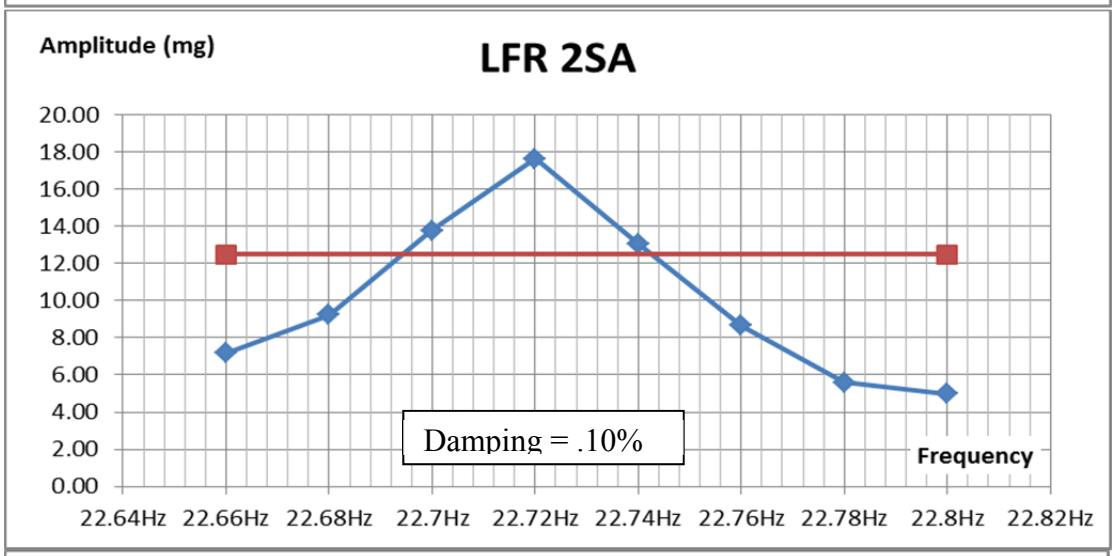
Amplitude (mg)
LFR 2SA
20.00
18.00
16.00
14.00
12.00
10.00
8.00
6.00
4.00
2.00
0.00
Damping = .10%
Frequency
22.64Hz 22.66Hz 22.68Hz 22.7Hz 22.72Hz 22.74Hz 22.76Hz 22.78Hz 22.8Hz 22.82Hz

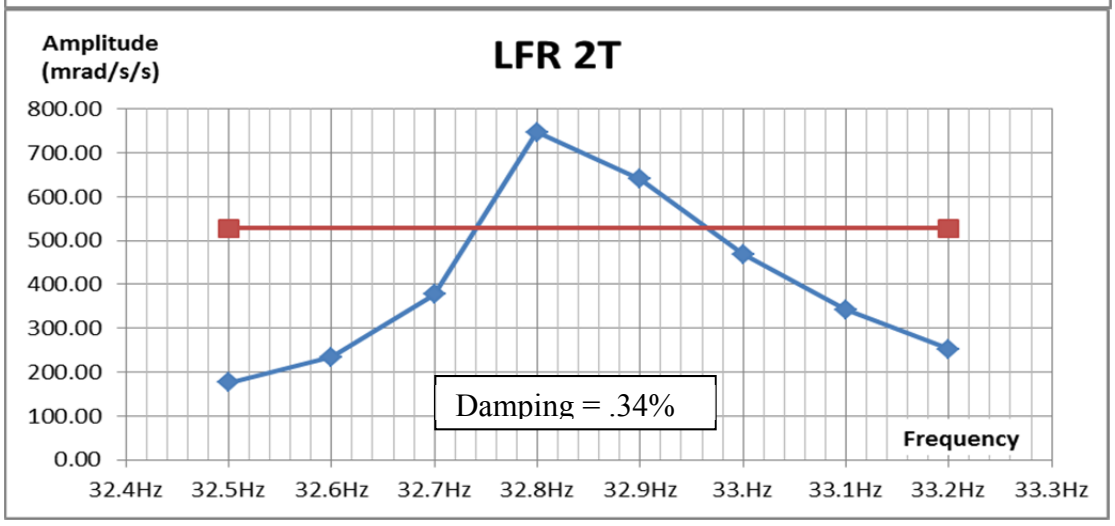
Amplitude (mrad/s/s)
LFR 2T
800.00
700.00
600.00
500.00
400.00
300.00
200.00
100.00
0.00
Damping = .34%
Frequency
32.4Hz 32.5Hz 32.6Hz 32.7Hz 32.8Hz 32.9Hz 33.Hz 33.1Hz 33.2Hz 33.3Hz

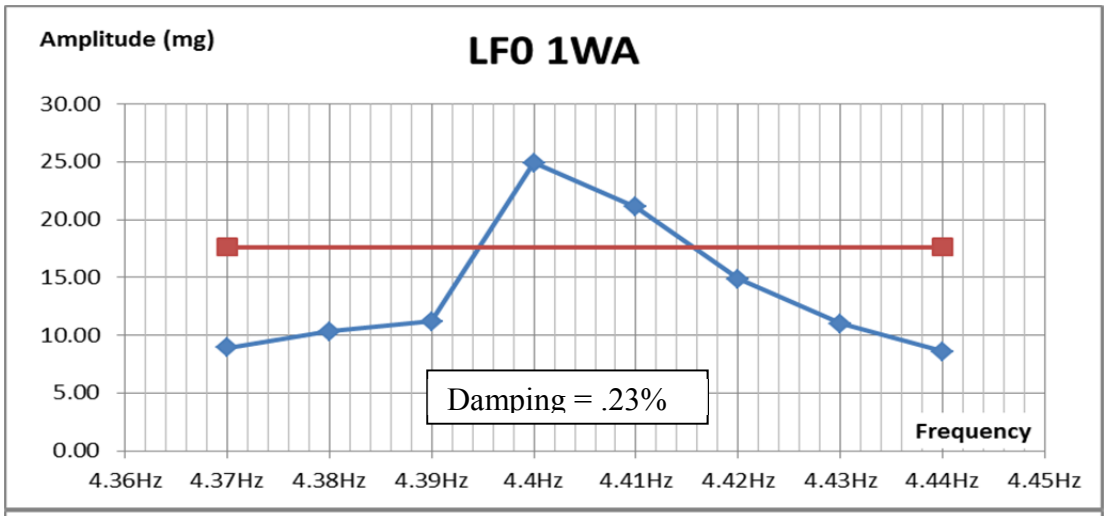
Amplitude (mg)
LF0 1WA
30.00
25.00
20.00
15.00
10.00
5.00
0.00
Damping = .23%
Frequency
4.36Hz
4.37Hz
4.38Hz
4.39Hz
4.4Hz
4.41Hz
4.42Hz
4.43Hz
4.44Hz
4.45Hz

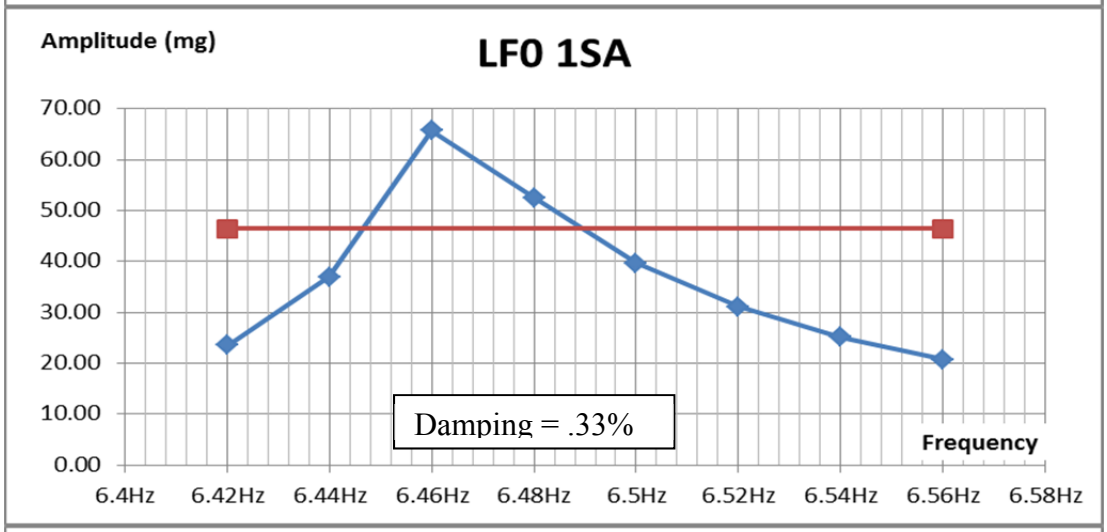
Amplitude (mg)
LF0 1SA
70.00
60.00
50.00
40.00
30.00
20.00
10.00
0.00
Damping = .33%
Frequency
6.4Hz
6.42Hz
6.44Hz
6.46Hz
6.48Hz
6.5Hz
6.52Hz
6.54Hz
6.56Hz
6.58Hz

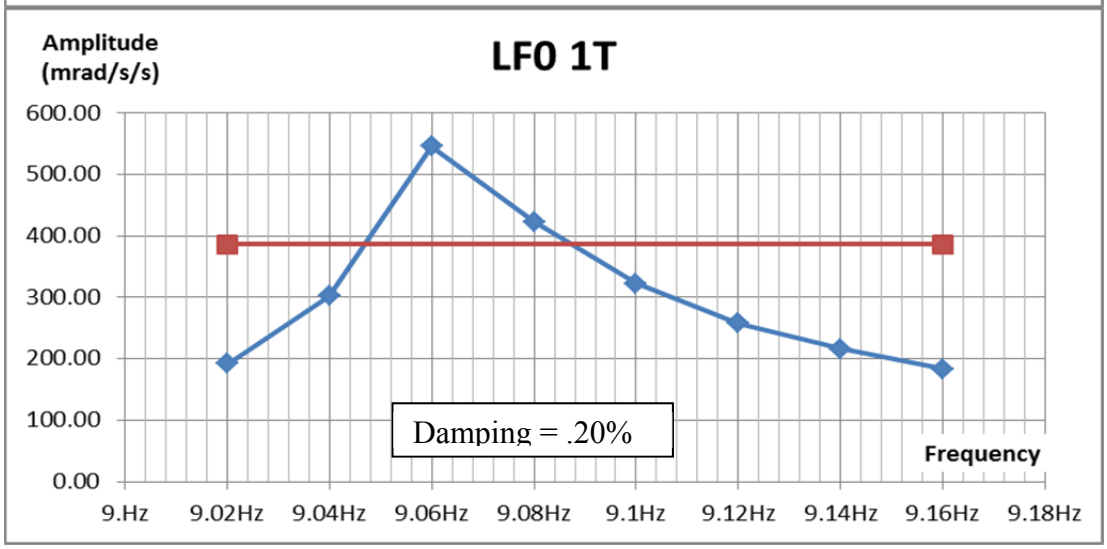
Amplitude (mrad/s/s)
LF0 1T
600.00
500.00
400.00
300.00
200.00
100.00
0.00
Damping = .20%
Frequency
9.Hz
9.02Hz
9.04Hz
9.06Hz
9.08Hz
9.1Hz
9.12Hz
9.14Hz
9.16Hz
9.18Hz

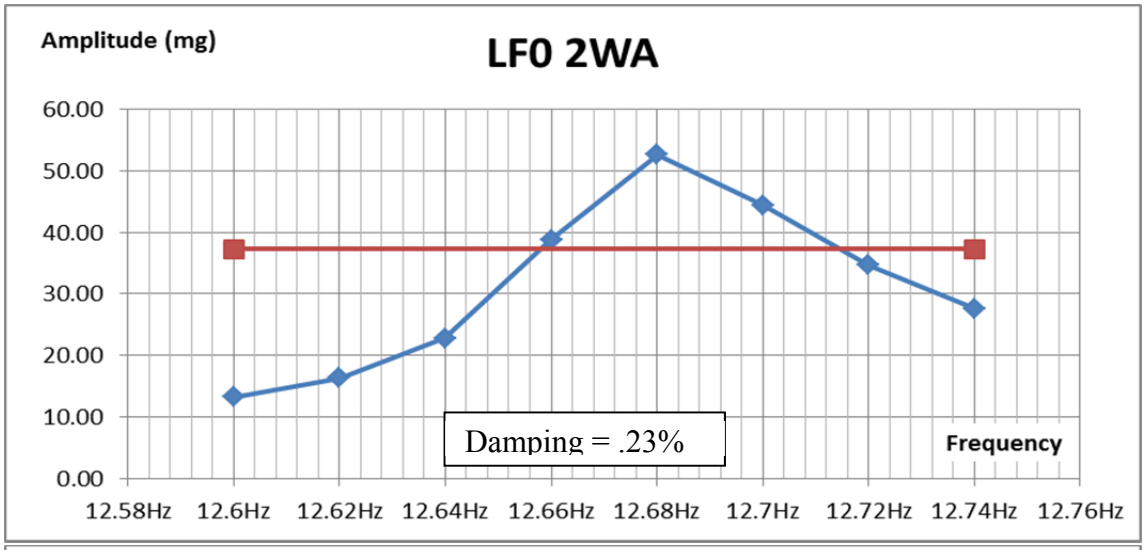
Amplitude (mg)
LF0 2WA
60.00
50.00
40.00
30.00
20.00
10.00
0.00
12.58Hz
12.6Hz
12.62Hz
12.64Hz
12.66Hz
12.68Hz
12.7Hz
12.72Hz
12.74Hz
12.76Hz
Damping = .23%
Frequency

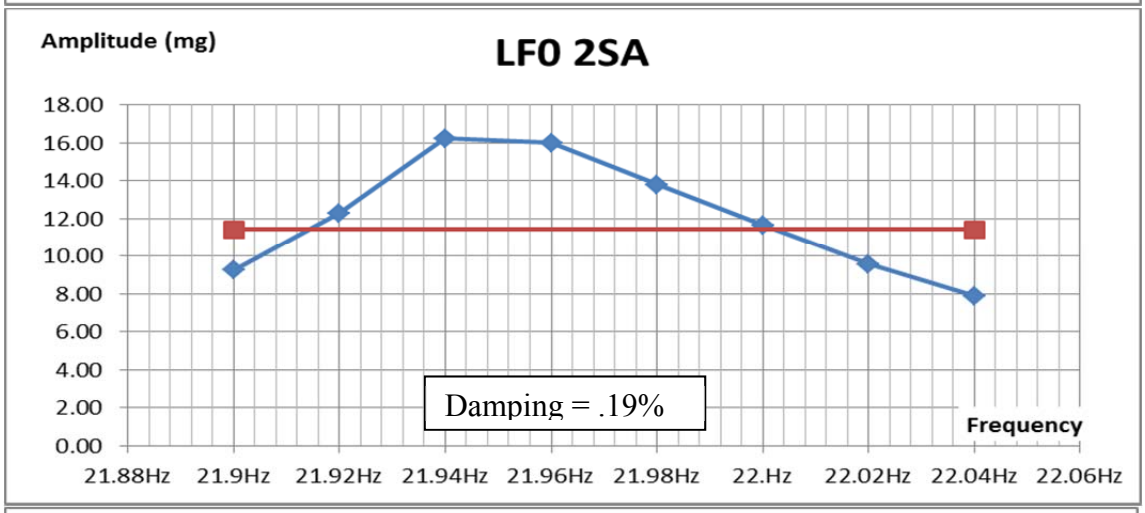
Amplitude (mg)
LF0 2SA
18.00
16.00
14.00
12.00
10.00
8.00
6.00
4.00
2.00
0.00
21.88Hz
21.9Hz
21.92Hz
21.94Hz
21.96Hz
21.98Hz
22.Hz
22.02Hz
22.04Hz
22.06Hz
Damping = .19%
Frequency

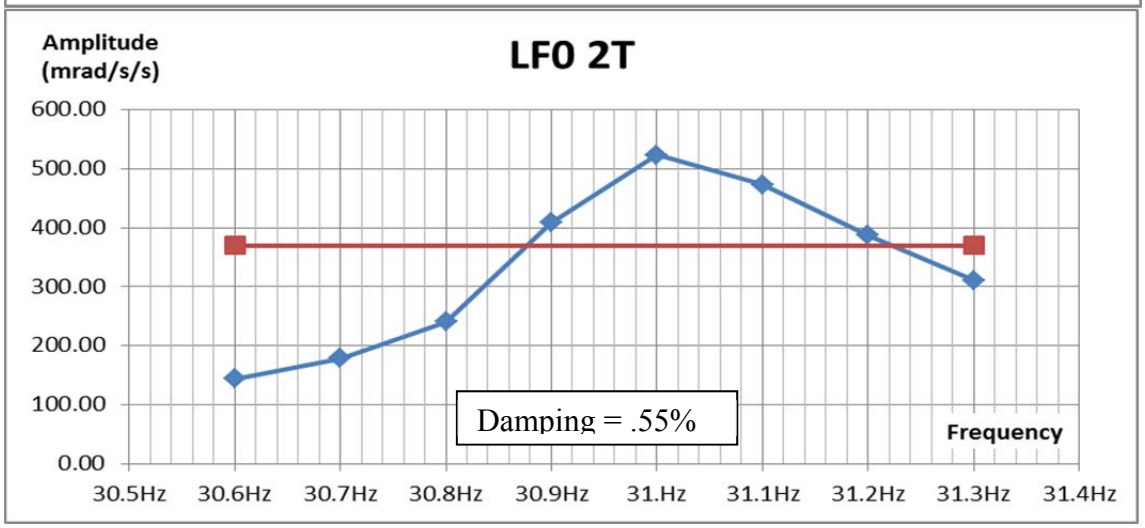
Amplitude (mrad/s/s)
LF0 2T
600.00
500.00
400.00
300.00
200.00
100.00
0.00
30.5Hz
30.6Hz
30.7Hz
30.8Hz
30.9Hz
31.Hz
31.1Hz
31.2Hz
31.3Hz
31.4Hz
Damping = .55%
Frequency

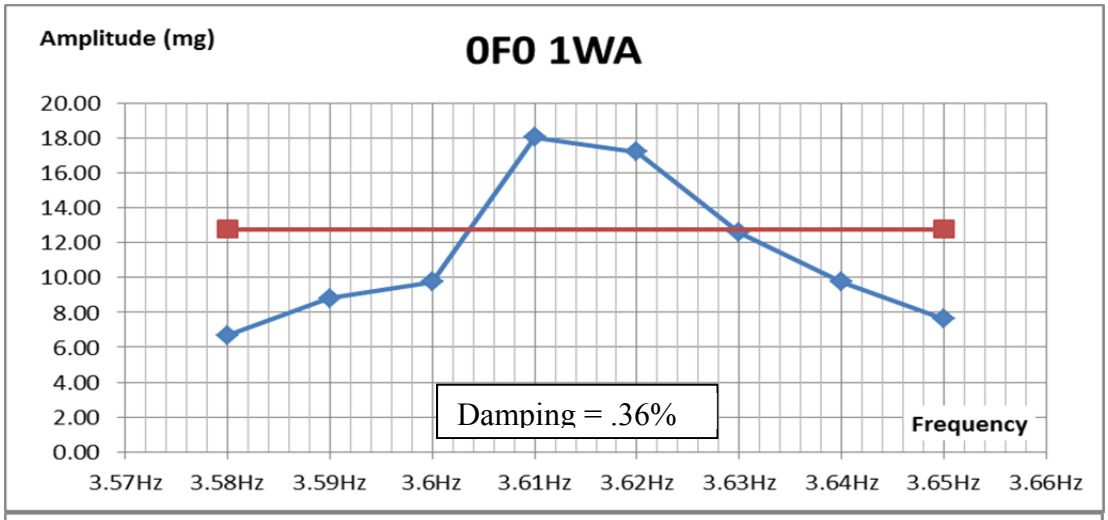
Amplitude (mg)
0F0 1WA
20.00
18.00
16.00
14.00
12.00
10.00
8.00
6.00
4.00
2.00
0.00
3.57Hz
3.58Hz
3.59Hz
3.6Hz
3.61Hz
3.62Hz
3.63Hz
3.64Hz
3.65Hz
3.66Hz
Damping = .36%
Frequency

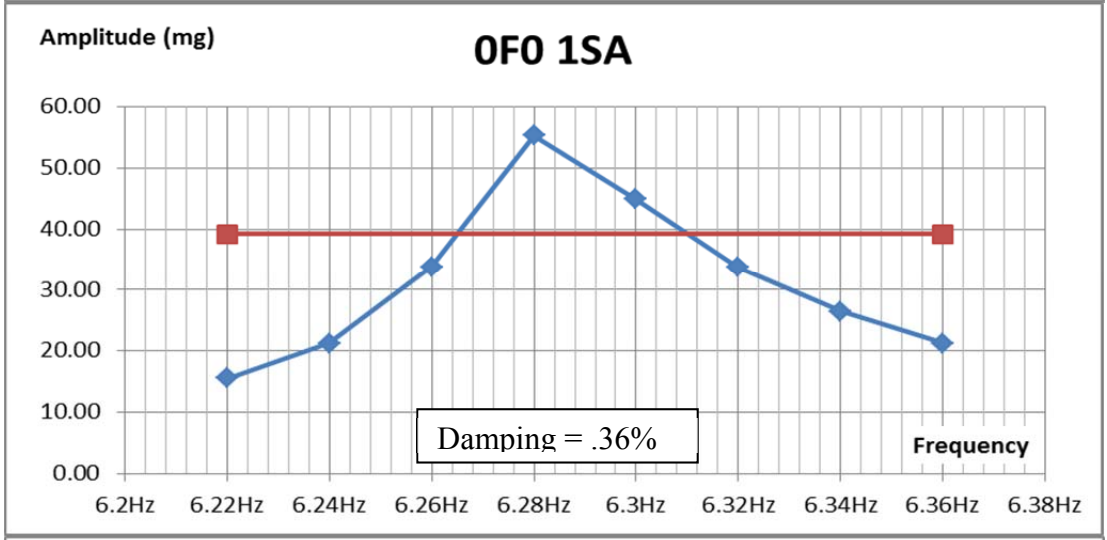
Amplitude (mg)
0F0 1SA
60.00
50.00
40.00
30.00
20.00
10.00
0.00
6.2Hz
6.22Hz
6.24Hz
6.26Hz
6.28Hz
6.3Hz
6.32Hz
6.34Hz
6.36Hz
6.38Hz
Damping = .36%
Frequency

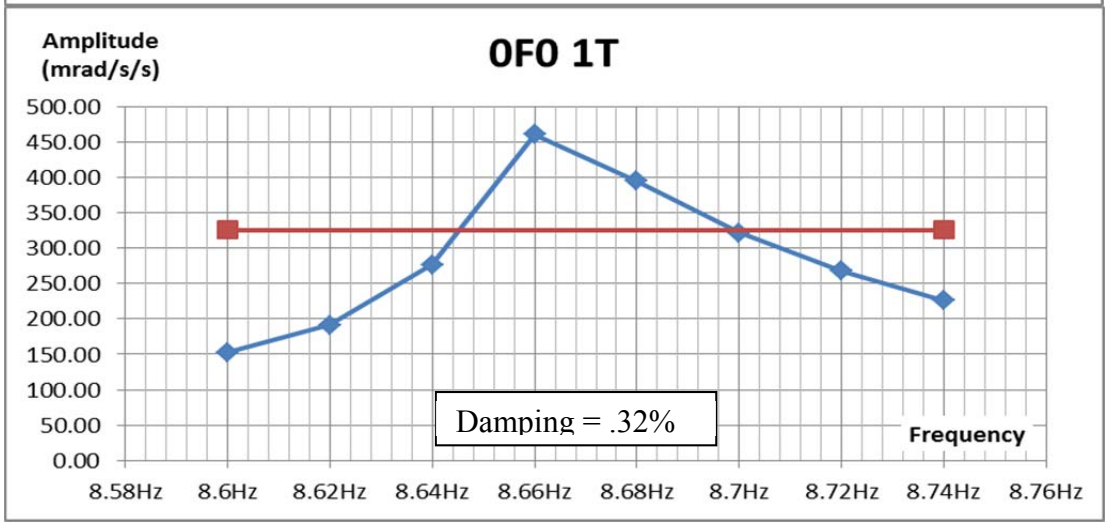
Amplitude (mrad/s/s)
0F0 1T
500.00
450.00
400.00
350.00
300.00
250.00
200.00
150.00
100.00
50.00
0.00
8.58Hz
8.6Hz
8.62Hz
8.64Hz
8.66Hz
8.68Hz
8.7Hz
8.72Hz
8.74Hz
8.76Hz
Damping = .32%
Frequency

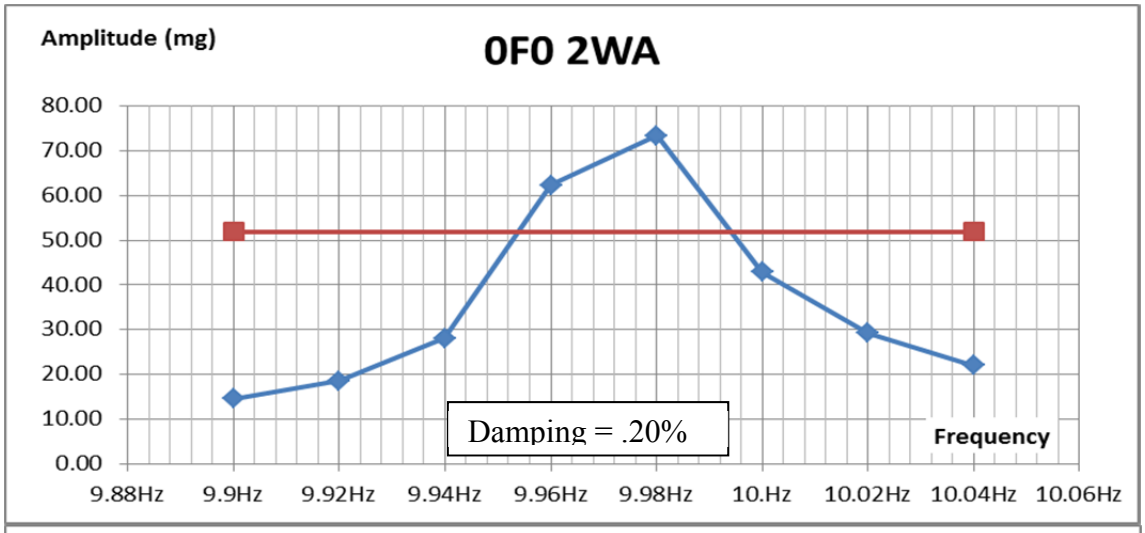
Amplitude (mg)
0F0 2WA
80.00
70.00
60.00
50.00
40.00
30.00
20.00
10.00
0.00
9.88Hz
9.9Hz
9.92Hz
9.94Hz
9.96Hz
9.98Hz
10.Hz
10.02Hz
10.04Hz
10.06Hz
Damping = .20%
Frequency

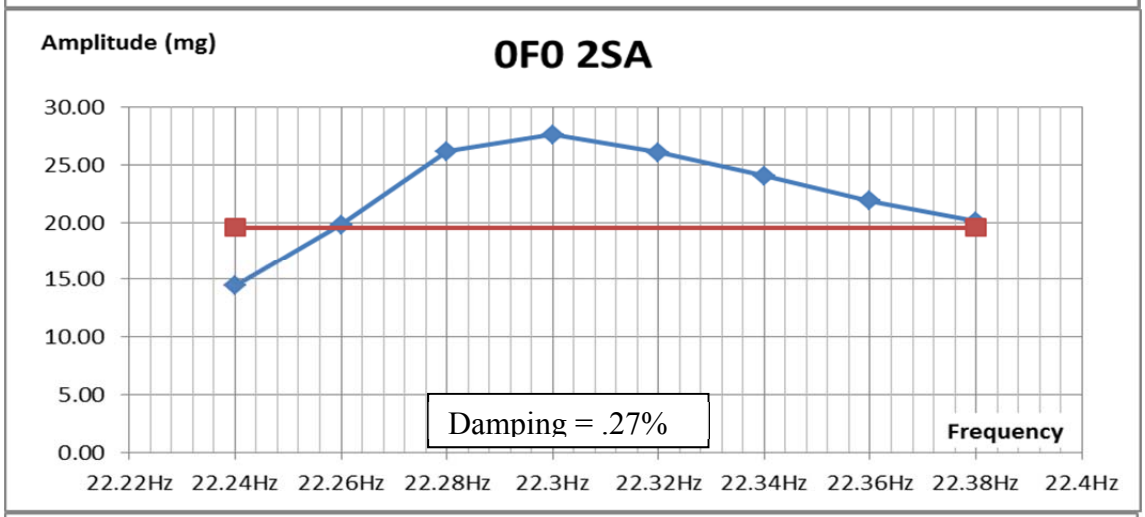
Amplitude (mg)
0F0 2SA
30.00
25.00
20.00
15.00
10.00
5.00
0.00
22.22Hz
22.24Hz
22.26Hz
22.28Hz
22.3Hz
22.32Hz
22.34Hz
22.36Hz
22.38Hz
22.4Hz
Damping = .27%
Frequency

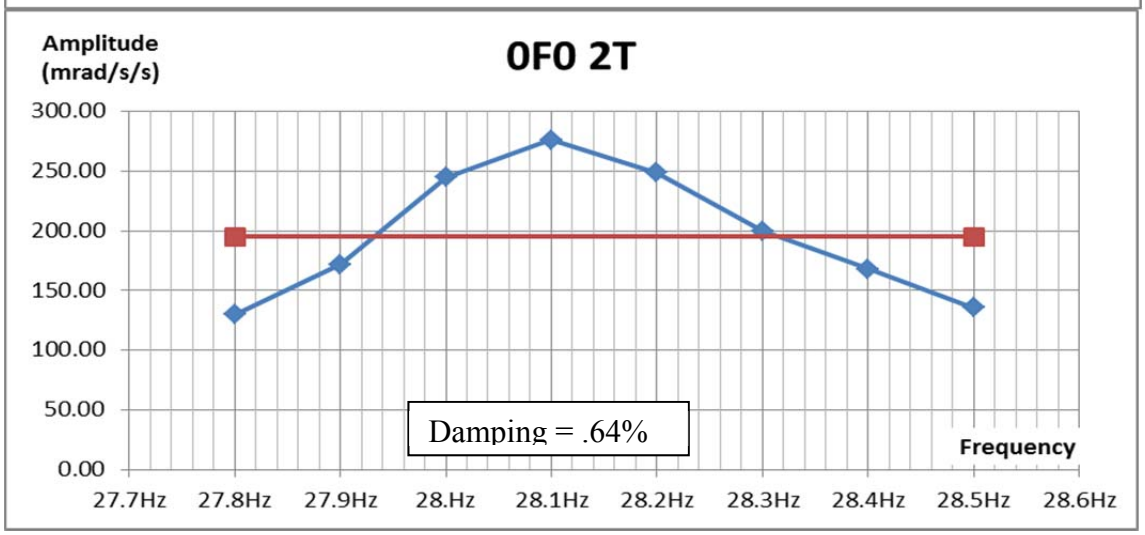
Amplitude (mrad/s/s)
0F0 2T
300.00
250.00
200.00
150.00
100.00
50.00
0.00
27.7Hz
27.8Hz
27.9Hz
28.Hz
28.1Hz
28.2Hz
28.3Hz
28.4Hz
28.5Hz
28.6Hz
Damping = .64%
Frequency

14.5 Hand Calculations of Safe Acceleration Levels

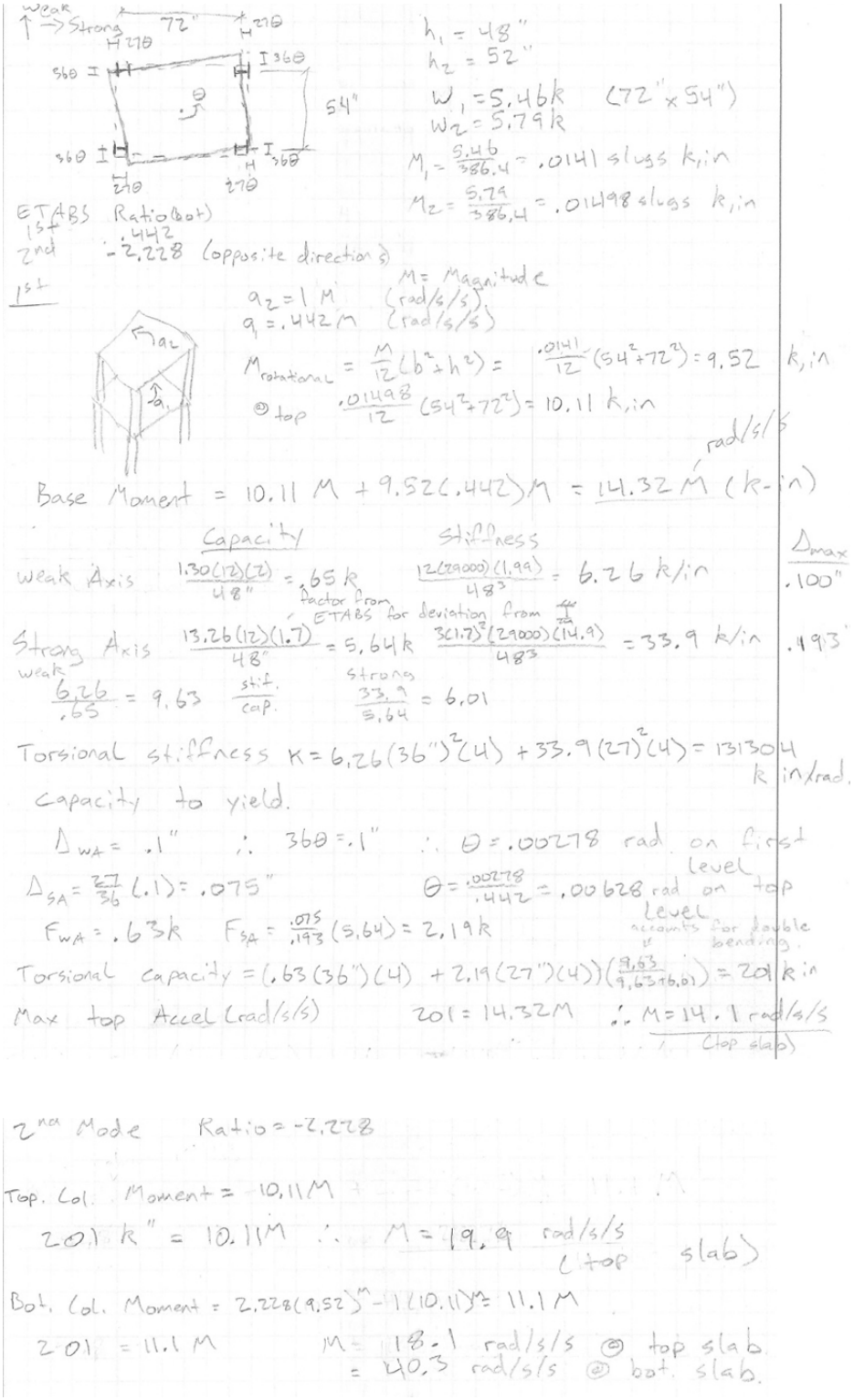

Mode 1 Weak Axis Maximum Excitation

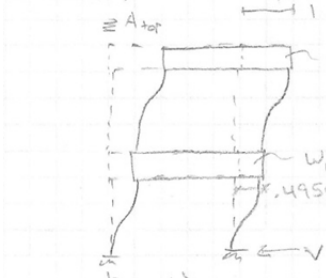

*Ignores damping force (conservative)

$V = A_{top}(w_2 + .4959 w_1) = 8.498 A_{top}$ (g)

$V_{max} = 1.372$ (from strength calcs based on fixed-fixed column)

$\frac{1.372}{8.498} = .161$ $A_{top\,max} = .161\,g = 161.\,mg$ 4% under ETABS

Mode 4 Weak Axis Maximum Excitation

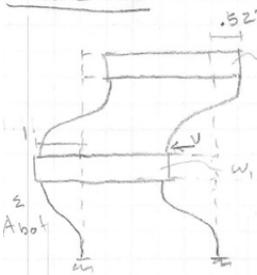

$V = A_{bot}(.523 w_2) = 3.028 A_{bot}$ (g)

$V_{max} = 2.47 \therefore A_{bot} = .8163 = 816\,mg$

11% over ETABS

Mode 2 Strong Axis Maximum Excitation

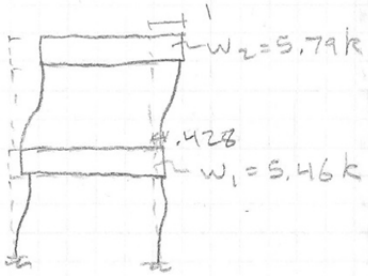

$V = A_{top}(W_2 + .428(W_1)) = 8.127\ A_{top}$

$V_{max} = 13.99\ k$ (from strength calcs based on fixed-fixed)

$\therefore A_{top} = 1.721\ g = 1721\ mg$

8% below ETABS

Mode 5 Strong Axis Maximum Excitation

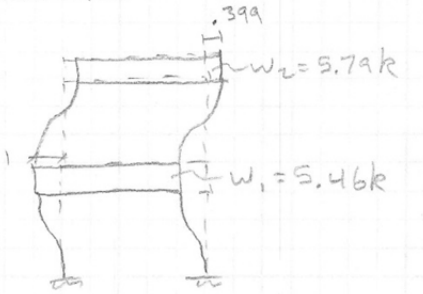

$V = A_{bot} * (.601(5.46)) = 3.28\ A_{bot}$ (W_2)

$V_{max} = 27.97(.9) = 25.17k$ (↑ estimate due to deviation from fixed fixed.)

$A_{bot} = 7.675\ g = 7675\ mg$

1.% below ETABS

LIST OF NOMENCLATURE

FVT – Forced Vibration Testing, this is done by exciting a particular mode, and recording the mode shapes of the structure.

MAC – Modal Assurance Criterion compares two mode shapes and provides a metric of correlation between the two vectors.

Measurement Locations (See section 6.1.6 for diagrams showing these locations)

TWA: Translational measurement at the top level of the structure in the weak axis direction at the center of mass.

TSA: Translational measurement at the top level of the structure in the strong axis direction at the center of mass.

TTOR: Rotational measurement at the top level of the structure at the center of mass.

BWA: Translational measurement at the bottom level of the structure in the weak axis direction at the center of mass.

BSA: Translational measurement at the bottom level of the structure in the strong axis direction at the center of mass.

BTOR: Rotational measurement at the bottom level of the structure at the center of mass.

Mode Names

1WA: First mode of oscillation in the weak axis direction of the structure.

1SA: First mode of oscillation in the strong axis direction of the structure.

1TA: First mode of oscillation in the torsional direction of the structure.

2WA: Second mode of oscillation in the weak axis direction of the structure.

2SA: Second mode of oscillation in the strong axis direction of the structure.

2TA: Second mode of oscillation in the torsional direction of the structure.

Modal Contamination – The degree to which one mode has participated in the collection of another mode, see section 5.1.3 for details on this calculation.

Modal Force – The dot product of the force vector and the mode shape. This is a measurement of how much a unique force will excite a particular mode.

Modal Sweeping – A process used to make modes orthogonal to each other, see section 5.1.2 for details on this calculation.

MWMAC – Mass Weighted Modal Assurance Criterion is a modified version of MAC.

REO – Rigid End Offsets, these are used in the analytical model to capture the increased stiffness of the column to beam connection.

Shaker – A machine used to vibrate back and forth and excite the structure.